Passive Damping in Stiffened Structures Using Viscoelastic Polymers

Naveed Ahmad

Dissertation submitted to the faculty of the
Virginia Polytechnic Institute and State University
in partial fulfillment of the requirements for the degree of

Doctor of Philosophy
in
Engineering Mechanics

Rakesh K. Kapania, Chair
Muhammad R. Hajj
Saad A. Ragab
Surot Thangjitham
Kamal B. Rojiani

March 25, 2016
Blacksburg, Virginia

Keywords: Passive Damping, Finite Element, Viscoelasticity, Modal Strain Energy, Free Vibration, Constrained Layer damping, Integrally Stiffened Plates, Stepped Plates, Adhesively Bonded Plates

Passive Damping in Stiffened Structures Using Viscoelastic Polymers

Naveed Ahmad

Abstract

Noise and vibration suppression is an important aspect in the design process of structures and machines. Undesirable vibrations can cause fatigue in a structure and are, therefore, a risk to the safety of a structure. One of the most effective and widely used methods of mitigating these unwanted vibrations from a system is passive damping, by using a viscoelastic material. This dissertation will primarily focus on constrained layer passive damping treatments in structures and the investigation of associated complex modes. The key idea behind constrained damping treatment is to increase damping as affected by the presence of a highly damped core layer vibrating mainly in shear. Our main goal was to incorporate viscoelastic material in a thick stiffened panel with plate-strip stiffeners, to enhance the damping characteristics of the structure.

First, we investigated complex damped modes in beams in the presence of a viscoelastic layer sandwiched between two elastic layers. The problem was solved using two approaches, (1) Rayleigh beam theory and analyzed using the principle of virtual work, and (2) by using 2D plane stress elasticity based finite-element method. The damping in the viscoelastic material was modeled using the complex modulus approach. We used FEM without any kinematic assumptions for the transverse shear in both the core and elastic layers. Moreover, numerical examples were studied, by including complex modulus in the base and constraining layers. The loss factor was calculated by modal strain energy method, and by solving a complex eigenvalue problem. The efficiency of the modal strain energy method was tested for different loss factors in the core layer. Complex mode shapes of the beam were also examined in the study, and a comparison was made between viscoelastically damped and non-proportionally damped structures.

Secondly, we studied the free vibration response of an integrally stiffened and/or stepped

plate. The stiffeners used here were plate-strip stiffeners, unlike the rib stiffeners often investigated by researchers. Both plate and stiffeners were analyzed using the first-order shear deformation theory. The deflections and rotations were assumed as a product of Timoshenko beam functions, chosen appropriately according to the given boundary conditions. Unlike Navier and Levy solution techniques, the approach used here can also be applied to fully clamped, free and cantilever supported stiffened plates. The governing differential equations were solved using the Rayleigh-Ritz method. The development of the stiffness and the mass matrices in the Ritz analysis was found to consume a huge amount of CPU time due to the recursive integration of Timoshenko beam functions. An approach is suggested to greatly decrease this amount of CPU time, by replacing the recursive integration in a loop structure in the computer program, with the analytical integration of the integrand in the loop. The numerical results were compared with the exact solutions available in the literature and the commercially available finite-element software ABAQUS®. Some parametric studies were carried out to show the influence of certain important parameters on the overall natural frequencies of the stiffened plate.

Finally, we investigated the damped response of an adhesively bonded plate employing plate-strip stiffeners, using FSDT for both the plate and stiffeners. The problem was analyzed using the principle of virtual work. At first, we did not consider damping in the adhesive in order to validate our code, by comparing our results with those available in the literature as well as with the results obtained using ABAQUS® 3D model. The results were found to be highly satisfactory. We also considered the effect of changing the stiffness of the adhesive layer on the vibration of the bonded system. As a second step, we included damping in the stiffened structure using complex modulus approach, a widely used technique to represent the rheology of the viscoelastic material. We observed an overall increase in the natural frequencies of the system, due to the damping provided by the viscoelastic material. Moreover, it was noticed that when the thickness of the adhesive layer is increased, the natural frequencies and loss factor of the stiffened structure decrease. A viscoelastic material with high loss factor and small thickness will be a perfect design variable to obtain overall high damping in the structure.

Passive Damping in Stiffened Structures Using Viscoelastic Polymers

Naveed Ahmad

General Audience Abstract

Noise and vibration are often a concern in many engineering applications such as aircraft, spacecraft, automobiles, ships, trains and civil structures. Noise suppression is desirable for comfort and the well-being of passengers; whereas undesirable vibration can cause damage to a structure. Unfortunately, the materials used to construct an aircraft or an automobile, can not suppress vibration on their own and we need soft materials, such as viscoelastic polymers, to mitigate vibration from a structure. The main focus of this dissertation was to use these soft viscoelastic materials to suppress vibration and noise with a minimal increase in the overall weight of the structure. Nowadays, there is an increased demand for an overall reduction of the weight of the structures, for efficient performance and low fuel consumption. Structures with varying thickness are analyzed in this work to save material, decrease the overall weight, strengthen the structure in appropriate locations, and increase the vibration natural frequencies to avoid resonance. Moreover, adhesive bonding is utilized to connect various parts by using soft viscoelastic materials to reduce the vibration of the structures.

Dedicated to

My Parents, Brother & Sister

Acknowledgments

First of all, I am grateful to Almighty Allah, for giving me the strength to complete this milestone.

This research work would not have been possible without the constant help, support and guidance from my advisor, Dr. Rakesh K. Kapania. I am thankful from the core of my heart to Dr. Kapania, for being kind and patient with me during the period of my Ph.D. program. I am also grateful to Dr. Muhammad R. Hajj for his support, help and care throughout the Ph.D. studies. I would also like to thank Dr. Saad Ragab, Dr. Surot Thangjitham, and Dr. Kamal B. Rojiani, for serving on my committee and for their help, valuable input and comments. I would like to thank Dr. Sameer B. Mulani for guiding and helping me in the early days of my graduate studies. I am indebted to Late Christa Thomas for giving me the opportunity to work as a graduate assistant in the Department of Physics, Virginia Tech. I would also like to recognize and thank Ms. Lisa Smith for her prompt help in all the documentation and accommodations.

Moreover, I would like to thank my best friend, roommate and office mate Dr. Arshad Mehmood, for constantly pushing and helping me during my studies, and the laughs and fun, we had together. I had a great time in Blacksburg and enjoyed every bit with my friends Dr. Zaka Ullah Zahid, Dr. Abdul Hafeez, Dr. Zeshan Hyder, Adarsh K. Chaurasia, and last but not the least Umar Kalim. In the end, I would like to thank University of Engineering and technology, Peshawar, Pakistan, for the financial support during my graduate studies.

Contents

List of Figures

List of Tables

Chapter 1

Introduction

1.1 Structural Vibration and Damping

Structure-borne noise and vibration are often a concern in many engineering applications such as aircraft, spacecraft, automobiles, ships, trains and civil structures. A variety of sources is expected to contribute to the structure-borne vibration and noise in an aircraft structure. The turbulent airflow over the fuselage and wings is the main sources of noise in the aircraft cabin, followed by the jet noise from aircraft engines and the air-conditioning system [1, 2]. The flow over the aircraft fuselage eventually contribute to the structural vibration of the stiffened panels in the fuselage; the turbulent boundary layer thickness grows from 13mm to 30cm from the airplane flight deck to the back of the airplane, respectively [2].

Aircraft engine and its rotating parts produce an imbalance, and hence produce harmonic excitations, that are transferred to the aircraft through engine mounts. In order for the aircraft to reach the desired altitude, high engine thrust is utilized which imparts high-frequency loading on the aircraft structure adjacent to the location where the engine is mounted [3]. Similarly, an aircraft experiences dynamic loads during takeoff and landing; especially during landing, high impact loads are expected along with wing tip deflection [3]. One important phenomenon, which should be considered in obtaining the dynamic response of a structure, called flutter, the instability caused by the fluid-structure interaction. Flutter is a self-induced oscillatory phenomenon, which takes place due to the coupling between aerodynamic forces and natural modes of vibration of the structure, that increase in amplitude

over time [4].

Mellert et al. [5] reported the physiological and psychological impact of noise and vibration on health, comfort and performance of the crew members during long flights. Nowadays, passenger comfort and overall satisfaction are directly related to the quality of the product, with lesser issues with noise and vibration. Moreover, undesirable vibrations can cause fatigue in a structure and are, therefore, a risk to the safety of a structure. Hence, mitigation of vibration and noise are very important to avoid failures due to fatigue and flutter. Extensive literature is available on the free and forced vibration of aircraft structures. This dissertation will primarily focus on the damping of vibration and noise in the sandwich and stiffened structures.

Structural damping can be broadly divided into two categories i.e., passive vibration control and active vibration control [6]. A third category called semi-active vibration control also exists, which is a combination of both active and passive damping [2, 7], but is generally categorized under the broad term active damping. Active vibration damping utilizes sensors to measure the amplitude of vibration, actuators to produce an opposite force to resist the amplitude, and controllers to manage the force produced by the actuators. An external source of energy is normally required to power actuators, which adds extra weight to the structure. Piezoelectric ceramics (PZT) are widely used as sensors and actuators on opposite sides of the base structure to provide damping in the structure. Moreover, active control can be achieved to reduce noise in a structure such as an aircraft fuselage, by using speakers, actuators and microprocessors to produce an out of phase signal to cancel the noise [2].

Passive vibration damping mechanism involves the use of absorbers, barriers and silencers; such as viscous dampers, viscoelastic layers and tuned mass dampers [7]; which provide damping by converting the excessive mechanical vibrational energy into heat. In the category of energy absorbing materials as a mean of passive damping, viscoelastic materials have shown significant efficiency for vibration mitigation and the application of these materials can alter the mode shapes and increase the natural frequencies of the structure and are, therefore, widely used in the industry and have been extensively studied in the published literature.

Viscoelastic materials possess both elastic and viscous properties. Many polymeric materials exhibit internal damping due to the rearrangement of long chain molecules when the

material undergoes deformation. The term damping refers to the loss of energy from a system during each cycle. When a viscoelastic material is deformed, the long chain molecules are stretched and then retract back, when stress is removed, to their original position slowly as compared to pure elastic materials. This slow response opposes the next cycle of vibration [8]. These materials are highly dependent on the working temperature and frequency, and their damping characteristics change under different temperature and frequency ranges. Damping from viscoelastic materials can be efficiently obtained when deformed under shear [9]. Semi-active control, on the other hand, uses materials, whose properties can be changed in real time; such as electro-rheological and magneto-rheological materials, as well as a combination of viscoelastic and piezoelectric material [2, 7].

1.2 Types of Surface Damping Treatments

The damping during cyclic deformation in metals, such as aluminum and steel, is almost negligible and thus, we need materials with higher inherent damping, such as viscoelastic materials, to control the vibration and sound transmission in structures. But unfortunately, the stiffness of viscoelastic polymer based materials is small and thus, they can not be used as a standalone structure member. In order to change the dynamic behavior of a structure and to damp the structure-borne noise and vibration, the viscoelastic material can be applied to the structure in two ways; unconstrained or free layer damping and constrained layer damping. The two methods differ in the way a viscoelastic material is employed to the original structure. Unconstrained damping is applied to the system by spraying viscoelastic material on one or both sides of the base structure, on the other hand, in constrained treatment; the viscoelastic material is sandwiched between two elastic faces. The base and constraining layers can be of different materials. In the unconstrained damping treatment, the viscoelastic material is subjected to extensional deformation during cyclic deformation, whereas in constrained layer damping, the material is subjected to shear deformation. Figure 1.1 and 1.2 depicts the damping mechanism and structural arrangement of both constrained and unconstrained layer passive treatments, respectively.

Constrained layer damping has an advantage over unconstrained layer damping. Nashif,

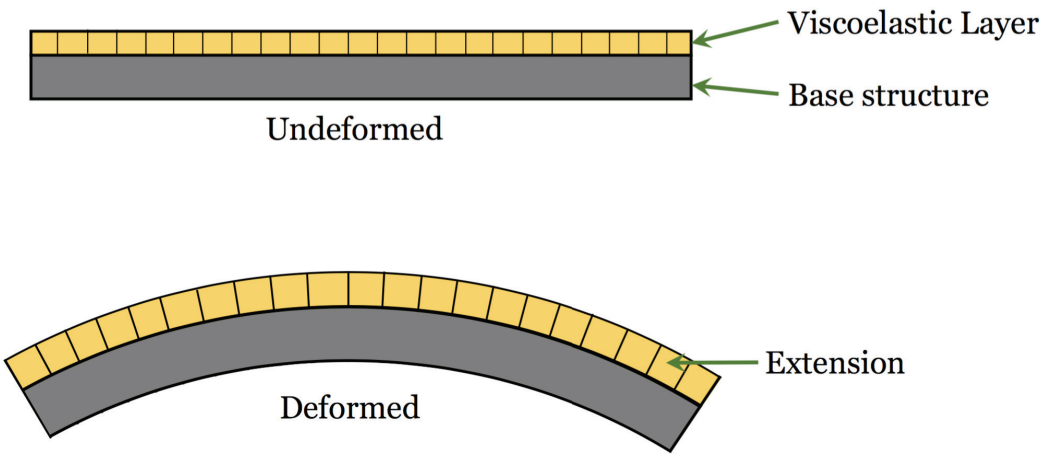

Figure 1.1: Damping Mechanism and Configuration of Free Viscoelastic Passive Layer Damping Treatment

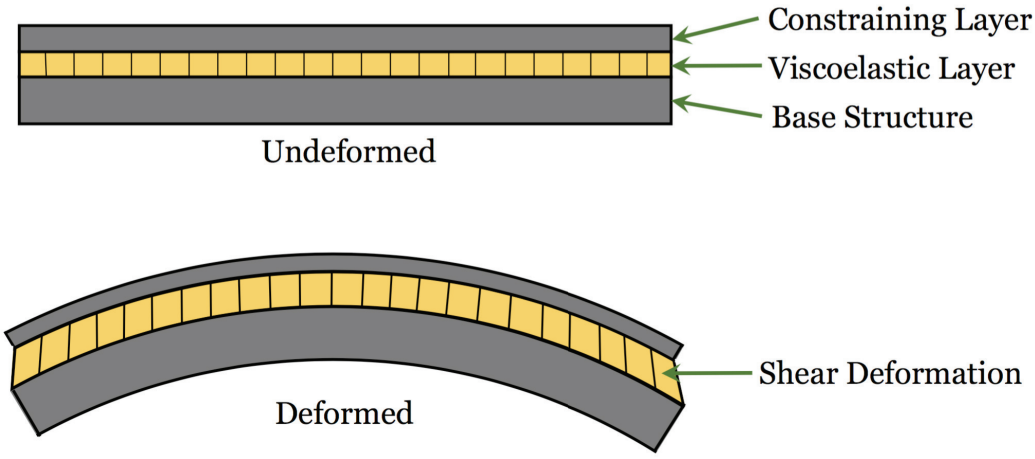

Figure 1.2: Damping Mechanism and Configuration of Constrained Viscoelastic Passive Layer Damping Treatment

Jones and Henderson [8] reported that in the optimal working temperature regime, the viscoelastic material operates with an optimal modulus, and this is the reason due to which the constrained viscoelastic layer dissipates maximum energy. Moreover, they concluded that the energy dissipation in constrained damping treatment is highly dependent on the viscoelastic core layer thickness, modulus and thickness of the constraining layer as well as the vibration frequency. Sun and Lu [9] considered that this added advantage of constrained layer is due to the high difference in the moduli of the elastic and core layers. Hu et al. [10]reported this advantage due to the difference between in-plane displacements of the base and constraining elastic layers and the low stiffness of the core viscoelastic layer.

However, it should be noticed that the efficiency of constrained layer treatment is linked with complexities in the modeling procedure [8]. In the category of constrained layer damping, treatments in which the base and the constraining elastic layers have same thickness and stiffness, are considered to provide maximum damping due to high shear deformation [11]. One other advantage of using passive viscoelastic surface damping treatments is that they can be applied to existing in-use structural and machine components. Baz and Ro [12] used a Lead zirconate titanate (PZT) piezoelectric ceramic layer to replace the metallic constraining layer on top of the viscoelastic material, to incorporate active damping in constrained layer damping, and this method of surface damping treatment is now called active constrained layer damping. PZT layer was used to enhance the damping characteristic of the viscoelastic layer. We will only consider constrained layer passive damping treatment in this dissertation.

1.3 Modeling the Rheological Behavior of Viscoelastic materials

1.3.1 Classical Spring and Dashpot Models

As pointed out earlier, that the viscoelastic materials possess both elastic and viscous material properties. The simplest way to model elastic properties is by using a spring, and for viscous properties, a dashpot. The two basic models used are known as the Maxwell and Kelvin-Voigt models, with spring and dashpot in series and parallel, respectively. In order to accurately

model the rheology of viscoelastic materials, a combination of Maxwell and Kelvin-Voigt models are used to construct the standard linear model (also known as Zener model), Bürgers model and the generalized Maxwell model. A detailed review of these models can be found in books by Nashif, Jones and Henderson [8], and Sun and Lu [9], and a recent review paper by Zhou et.al [13]. Composite materials have internal damping because the matrix material is usually made from polymers, and, thus, same viscoelastic damping models are used in modeling damping in composites [14]. These simplistic models are not able to accurately represent the damping mechanism in viscoelastic materials, because the damping is dependent on frequency, operating temperature and amplitude [13]. An improvement can be made by using Prony series, with experimentally determined time constants; although this method needs more terms in the series and a lot of testing to get a good estimate of viscoelastic properties [14].

1.3.2 Complex Modulus Approach

In the classical models, we start with a time-domain formulation and then convert it into the frequency domain to represent the viscoelastic response of the material. The parameters involved in the frequency domain formulation of the classical models, to represent viscoelastic behavior, are obtained by curve-fitting the experimental data. The empirical data corresponding to the deformation of viscoelastic materials, is usually available in the frequency domain. Complex modulus approach is an exactly opposite approach to classical models, in which the equations of motion are based in the frequency domain so that the experimental data can be directly incorporated into the model [8]. The complex modulus representation of a viscoelastic material is given as follows [6, 8, 9]:

$$E^* = E^{'}(\omega) + iE^{''}(\omega) \tag{1.1}$$

$$E^* = E^{'}(\omega)\left[1 + i\eta(\omega)\right] \tag{1.2}$$

$$\eta = \frac{E^{''}}{E^{'}} \tag{1.3}$$

whereas an asterisk $()^*$ in the superscript denotes a complex quantity throughout this dissertation. The real part of the complex modulus, $\mathrm{E}^{'}$, is called the storage modulus and represents the elastic property of the viscoelastic materials. On the other hand, the imaginary

part of the complex modulus, $E^{''}$, is called the loss modulus, which represents the viscous property of the viscoelastic material. The ratio of the imaginary to the real part of complex modulus is called the loss factor (η) of the viscoelastic material, which represent the amount of energy dissipated in the viscoelastic material during cyclic deformation in the form of heat [15]. Both the storage modulus and the loss factor in the complex modulus are frequency depended. However, we have to use Fourier transform in order to obtain the transient response of a structure, as the equations of motion are modeled in the frequency domain in the complex modulus approach. Similarly, the shear modulus corresponding to a viscoelastic material is given as:

$$G^* = G^{'}(\omega) + iG^{''}(\omega) \tag{1.4}$$

$$G^* = G^{'}(\omega)\left[1 + i\eta(\omega)\right] \tag{1.5}$$

$$\eta = \frac{G^{''}}{G^{'}} \tag{1.6}$$

The loss factor (η) obtained from equations 1.3 and 1.6 is the same for a viscoelastic material [9]. The complex modulus can be assumed constant for a finite bandwidth of the frequency without compromising on the accuracy of the response of the structure [14].

1.4 Literature Review

Extensive literature is available on damping of structural vibrations and noise by employing a viscoelastic layer sandwiched between two elastic layers. These types of sandwich structures are frequently used in the aerospace industry [2, 16], and provide an effective mean of dissipating the noise and vibrational energy by using a soft and heavily damped viscoelastic material [17, 18]. The main idea behind this type of structures is that damping can be obtained due to highly damped shear vibrations in the viscoelastic core layer, sandwiched between two elastic layers.

1.4.1 Beam Models for Constrained Layer Damping

Kerwin [19] introduced the theory for damping of flexural waves in sandwich viscoelastic layered structures. Mead and Marcus [20], and DiTaranto [21] followed the work by Kerwin

to investigate damping in structures utilizing viscoelastic core layers. Mead and Marcus presented an analytical solution for determining the loss factor of such structures and derived a sixth order differential equation in terms of the transverse displacement; whereas, DiTaranto derived a sixth order differential equation in terms of the longitudinal displacement. The transverse shear strain is not considered in the elastic layers.

Rikards [22] and Barkanov [23] used beam elements to calculate the frequency and loss factors. Rikards used four superelements with third-order approximation, each element having 8 nodes and 20 degrees of freedom, with same transverse displacement through the thickness of the beam. Barkanov used four elements with 61 degrees of freedom to model a sandwich beam having different materials for the base and constraining layer. Rikards and Barkanov [24] used the method of complex eigenvalues and the QR-algorithm to solve the complex eigenvalue problem and reported that these methods need more computation time as compared to the problem without damping.

Most of the previous work did not consider longitudinal and rotary inertias in the core. Rao and Nakra [25] considered these inertias in their work for both plates and beams having constrained layers. But they reported that while these inertias do not play a vital role when we consider homogeneous beams vibrating at low frequencies, these can be of significant importance if interest is in very high frequencies. For unsymmetric beams, these inertias have to be considered even for low frequencies due to inherent coupling between in-plane and transverse vibrations. Rao [26] reported the optimal design of a three-layered sandwich beam which can lead to the maximum loss factor by using different shear parameters and geometrical properties. Lall, Asnani and Nakra [27] worked on partially covered sandwich beams.

Fasana and Marchesiello [28] used the Rayleigh-Ritz method for constrained layer beams. They followed the work by Rao and Nakra [25] by including the longitudinal and rotation inertias in the core layer. They used simple polynomials as admissible functions for different boundary conditions. Singhvi and Kapania [29] reported the limitations of employing simple polynomials over trigonometric and other orthogonal functions. They showed that as the number of terms using simple polynomials is increased, the mass and stiffness matrices become computationally singular especially for higher modes but, on the other hand, orthogonal

functions do not suffer from such limitations.

Sainsbury and Zhang [30] used the Galerkin element method for analyzing the damped sandwich beams. Most of the work, available in the literature for analyzing structural damping using viscoelastic core, considers a linear relation for the variation of axial displacement through the thickness, but Bhimaraddi [31] used non-linear variation to employ non-uniform shear stress variation through the thickness. He concluded that this theory is suitable for structures having thick core layers. Use of higher order finite element helps in a better approximation of the damping ratios. Imaino and Harrison [32] showed that by using the *p*-version finite element method we can get good estimates of damping, especially for sandwich structures with lower core moduli.

Hu et al. [10] reviewed the classical and higher-order theories to model sandwich structures as well as the Zig-Zag models and concluded that all these theories include shear deformation in the kinematic formulation by using some assumptions. They also reported that higher-order theories make a great effort to implement, but do not give better results as compared to the first-order shear deformation theory, in view of 3D elasticity equations. Sanliturk and Koruk [33] developed a composite finite element with damping capability, employing rotational degrees of freedom.

1.4.2 Implementing Viscoelastic Damping in Finite-Element Formulation

Johnson and Kienholz [34] used NASTRAN commercial software for the three-dimensional finite element analysis. They used quadrilateral or triangular plate elements for modeling the face layers and a solid element to model the core layer. Modal strain energy method was first used by Johnson and Kienholz [34] to calculate the loss factor from undamped real eigenmodes. Soni and Bogner [35] used MAGNA-D finite element computer program to solve the problem of damped sandwich structures using shell elements. Kosmatka and Liguore [36] reported the use of finite element analysis for constrained layer damping, and a comparison between different methods used to calculate the damped response. Haftka and Kapania [37] studied the discrepancies of complex eigenvalues, due to modeling errors, to study the sensitivity of damped response of structures. These discrepancies were found between the experimental and analytical mode shapes and natural frequencies.

Various time domain models have been used in the literature, in connection with the frequency and temperature dependent viscoelastic material damping, and have been successfully employed in the finite element formulation. These models include modal strain energy (MSE), Golla-Hughes-McTavish (GHM), fractional Calculus and anelastic displacement field (ADF) method. The MSE method has been used extensively in literature as well as commercially, to include viscoelastic properties in the finite element analysis. This method will be explained in the next section.

Bagley and Torvik [38] modeled the frequency dependent viscoelastic material using a fractional derivative and four model parameters. This model can be used in conjunction with frequency domain as well as time domain analysis. An important feature of this model is that it can be used with materials showing weak frequency dependence, by incorporating a small number of model parameters, over a wide frequency rang [16].

Golla and Hughes [39] made use of experimentally measured constants called mini-oscillators terms, dependent on the viscoelastic material, through which damping can be introduced in the constitutive relations of the system. The governing equations of motion of the system are developed in the Laplace domain and included in the finite element analysis using Ritz method. By using dissipation coordinates and Laplace transform, the problem is transformed into the time-domain. McTavish extended the Golla-Hughes model for linear viscoelastic structures and called this method Golla-Hughes-McTavish model (GHM) [40].

The anelastic displacement field (ADF) method is another way of representing viscoelastic behavior. Lesieutre and Bianchini [41] developed this model, based on augmenting thermodynamic field (ATF), in which the modulus is divided into two parts, first is the elastic part and the second is the anelastic part which encompasses the dissipation in the viscoelastic material. ATF is a material damping method based on time-domain continuum model. ATF model is considered as a 1-D model but Lesieutre and Bianchini [41] extended this work to a 3-D generalized model based on ADF. Liu and Ewing [42] reported that the inclusion of GHM, fractional calculus and ADF is still very inconvenient because of the need to use dissipation coordinates in the commercially available software, although the results obtained through these methods are more accurate than the commercially used Modal strain energy method and allow large damping analysis.

Rao [2] reported the applications of the viscoelastic materials in the aircraft industry. A spacer material with high shear stiffness and an extremely small bending stiffness, with slots to lower the weight, is used along with viscoelastic layer to enhance its damping properties and provide shear deformation at lower modes; as the viscoelastic material alone does not provide sufficient damping due to reduced shear in the lower modes [2]. Rao [2] reported that nowadays stand-off dampers are used, instead of damping tapes in the fuselage of the aircraft, to reduce the overall weight of the structure from 15% to 25% with equivalent damping. Moreover, lightweight acoustic tile type dampers are employed with hat stringers in certain aircraft, to provide damping in the skin, and different type of viscoelastic material is used in frames than in stringers and skin, due to the difference in the operating temperatures [2].

Lima et al. [43] used an improved Craig-Bampton condensation method along with the substructuring method, also known as the component mode synthesis (CMS) method, for model reduction of large and complex structures incorporating a frequency and temperature dependent viscoelastic material. Due to the frequency and temperature dependence of the viscoelastic material, the eigenvalue problem becomes non-linear, so the study was aimed to obtain the dynamic behavior of complex viscoelastically damped structures in a cost and time-efficient manner. In the CMS method, the structure is divided into different components called substructures, that are analyzed and condensed separately by using Ritz normal vectors, selected on the basis of interface boundary conditions. Residual static vectors, based on external loads and forcing functions induced by material damping, were used to improve the Craig-Bampton Transformation method. As a result of using this technique, the dofs of the system were reduced efficiently even in the presence of viscoelastic damping treatment and stiffeners in the system.

Cao, Hua and Zhang [44] considered the effect of constrained layer damping on acoustic radiation from stiffened cylindrical shells, by applying Sanders thin shell theory, for possible application in submarines and torpedoes. Stationary phase method was used to find an analytical expression for the far-field sound pressure. The effect of a change in parameters such as damping ratio and thickness of the viscoelastic material, thickness of the constraining layer and different loads were considered for the study. It should be noted that here full coverage was considered as opposed to partial coverage. It was observed that the constrained

layer damping had a good impact on decreasing the surface and far-field sound pressure in the medium frequency range but, on the other hand, the effect was minimal in the low-frequency range due to the reduced change in radial deformation. The effect of an increase in the thickness of the constraining layer was manifested by a decrease in the far-field sound pressure, approximately in almost every frequency band. The sound pressure due to the axial and circumferential stresses was lowered by using the constrained layer damping treatment.

Boucher et al. [45] investigated the damping enhancement in a honeycomb structure by filling it with a viscoelastic material. Prior to this study, it was reported in the literature that the material inserted into the voids of the honeycomb structure can alter the damping characteristics of the structure. The main objective of this study was to find the location and percentage of viscoelastic material inserted into the void, with minimal increase in density, using analytical, FE and topological optimization methods. It was concluded from the study that the damping is affected by the geometry and loading modes of the void in the honeycomb structure. A viscoelastic ligament in the middle of the cell was proved to be efficient in the case of in-plane axial deformation. Moreover, it was clearly shown that partial filling was a much better option as compared to completely filled voids on the basis of density.

Zhou et al. [46] analyzed the free flexural vibration of a periodically stiffened thin steel plate using simplified super element method, by combining Floquet-Bloch's theorem and super element method. The voids between the stiffeners were filled with damped viscoelastic material. The element is called super element because it contains dofs for both the elastic and viscoelastic layers. It is difficult and time-consuming to use super element technique to model a frequency dependent viscoelastic material. This disadvantage is removed by using the simplified super element method, which also makes the calculations easy for a complex structure. The basic aim of this work was to improve the vibration characteristics of a structure in the low-to-medium frequency range. The structure was investigated with and without viscoelastic material. It was noticed that the damping ratio of the viscoelastic material affects the frequency band gap significantly, especially in the low-to-medium frequency range. An increase in the density of viscoelastic material had a poor effect on the band gap. It was concluded that the viscoelastic material and its damping ratio shift the low band gap to a lower frequency.

Panda and Ray [47] investigated the dynamic response of a geometrically nonlinear functionally graded (FG) plate under changing thermal conditions, with active constrained layer (ACLD) patches. Damping from the patch is enhanced by combining the passive viscoelastic layer and active piezoelectric patch, the piezoelectric patch acts as a constraining layer to produce shear in the viscoelastic material as well as enhance damping by using its piezoelectric properties. The constraining patch used in this study is a new form of the piezoelectric material called piezoelectric fiber reinforced composite (PFRC), in which the piezoelectric coefficient is increased by applying electric field normal to the fibers. The piezoelectric fibers were used parallel to the neutral axis of the plate to achieve active damping due to in-plane stretching of the fibers. A power law distribution was utilized to represent the temperature dependent material properties of the FG plate in the thickness direction, whereas the poisons ratio was assumed to be constant on the entire plate. Golla-Hughes-McTavish (GHM) method was used to model the rheology of the viscoelastic material in the time-domain, and a 3D FE model based on FSDT was employed to model the functionally graded plate. It was reported that enhanced damping of the FG plate with active patches utilizing PFRC was obtained as compared to the case of using only passive damping. It was concluded that the ACLD treatment was more effective in controlling the non-linear geometric vibration of the FG plate as compared to the linear vibration control of the FG plate. An enhancement in damping characteristics of the FG plate was observed when the ACLD patch is attached to the softer side of the functionally graded material.

Balamurugan and Narayanan [48] developed a 9-noded isoparametric piezoelectric shell element with 5 elastic dofs at each node and one electric degree of freedom for each piezoelectric layer; while a 3-noded isoparametric beam element with 3 dofs at each node was utilized for the stiffener. Due to the interaction between plate/shell and the stiffener displacements and rotations, modeling of the stiffened structures become more complex. This complexity is dealt in this study by constraining the stiffener displacement fields to the shell displacement fields, thus giving the flexibility to place the stiffener anywhere on the shell. Linear-quadratic regulator controller was used for the active vibration control. Stiffened panel with laminated stiffeners in the x and y-directions with distributed piezoelectric sensors and actuators, were investigated to obtain the static and dynamic response of the structure. It was noticed that

the frequency increases and amplitude decreases for the stiffened structure as compared to the unstiffened structure. It was also reported that some of the modes were missed during the analysis, due to the cancelation of the voltage across fully covered PZT sensors and actuators. Moreover, the control effectiveness is reduced in the case of the stiffened plate as compared to that of the unstiffened plate, for a given Linear-quadratic regulator control parameter.

Mohammadi and Sedaghati [49] investigated the vibration response and optimization of sandwich cylindrical panels in the presence of electro-rheological fluid material to enhance the damping characteristics of viscoelastic material; as viscoelastic damping changes with temperature and damping is usually very less with lower excitation. As opposed to complete active vibration techniques, electro-rheological fluids (semi-active material) does not require a large setup for attenuation and its lesser density makes it superior to magneto-rheological (MG) materials [49]. In this study, both electro-rheological fluid and unconstrained viscoelastic layer were used to suppress excessive vibrational energy, the main reason after using viscoelastic material was to seal the electro-rheological fluid. The sandwich structure was modeled using FE with a 4-noded shell element with 20 dofs per layer, which amount to 40 dofs for the entire sandwich element as the core dofs can be determined using base and constraining layer. The optimization problem was performed with four variables; such as optimum number and distribution of the unconstrained viscoelastic and constrained electro-rheological fluid patches, electric field intensity, and thickness ratios of treating layers. Finite element model was combined with the genetic algorithm to approximately obtain optimum global variables; these values were then used as the starting point for sequential quadratic programming. It was concluded from the analysis that for some boundary conditions, the sandwich panel partially treated with electro-rheological fluids provides better damping performance compared with that of fully treated structure.

Shivakumar, Ashok and Ray [50] applied the same methodology used for the geometrically non-linear analysis of FG plate with ACLD patches utilizing piezoelectric fiber reinforced composite by Panda and Ray [47], to determine the geometrically non-linear transient response of a laminated composite cylindrical panel with piezoelectric fiber reinforced composite patches. First-order shear deformation theory and von Kármán type nonlinear strain-displacement relations were used to model the 3D finite element model. Both symmetric and anti-symmetric

laminated cylindrical panels were considered in the study. The active constrained layer damping patches were found to be effective in damping the geometrically nonlinear transient vibrations of the cylindrical panel for both the symmetric and anti-symmetric cases. The geometrically nonlinear vibrations of the panel were mitigated better with an increase in the shallowness angle.

Kattimani and Ray [51] investigated the geometrically nonlinear vibration of a smart laminated magneto-electro-elastic doubly curved shell with active constrained layer damping (ACLD) patches utilizing 1-3 piezoelectric composite (PZC) as the constraining layer. 1-3 PZC is made of piezoelectric ceramic fibers in an epoxy matrix; where 1-3 refers to the continuous orientation of the fiber in one direction out of 3-dimensions. Vertical and oblique reinforced 1-3 PZC were investigated in the study. The constrained viscoelastic layer was modeled using Golla-Hughes-McTavish (GHM) method in time domain. Magneto-electro-elastic (MEE) is a new category of smart laminated composites made of piezoelectric (P) and magnetostrictive (M) materials also known as multiferroic composites, with the ability to convert energy between mechanical, electrical and magnetic energies. Two different sequences of layers were investigated in this study i.e., P/M/P and M/P/M. The MEE substrate with the ACLD patch was modeled using 3D finite element, by a layerwise shear deformation theory and geometric nonlinearity was modeled using von Kármán type nonlinear strain-displacement relations. A simple velocity feedback controller was employed for the active vibration control of the shell. A significant improvement in the damping of geometrically nonlinear vibrations, for both P/M/P and M/P/M doubly curved shells, was noticed as compared to the passive damping. Parabolic shells provided more damping than the hyperbolic shells given the same geometric and material properties. MEE substrate with vertically reinforced 1-3 PZC layer and the central ACLD patch showed promising results than the other scenarios considered.

Sharma et al. [52] investigated the transient response of a laminated piezoelectric composite shell, in order to replace the commonly used lead zirconate titanate (PZT) with lead-free piezoelectric materials such as $(K_{0.475}Na_{0.475}Li_{0.05})(Nb_{0.92}Ta_{0.05}Sb_{0.03})O_3$ (KNLNTS), and $0.885(Bi_{0.5}Na_{0.5})TiO_3$–$0.05(Bi_{0.5}K_{0.5})TiO_3$–$0.015(Bi_{0.5}Li_{0.5})TiO_3$–$0.05BaTiO_3$ (BNKLBT). Lead zirconate titanate (PZT) has been successfully used in many applications and exten-

sively tested by various researchers, because of its excellent piezoelectric properties, but unfortunately, it has the drawback of not being environmentally friendly and its toxic nature. The vibrational response was calculated using FE with 9-node degenerate elements and employing first order shear deformation theory (FSDT), whereas linear piezoelectric theory was used for modeling the piezoelectric layers. The effect of the adhesive was not considered in the study. The fuzzy logic controller was used in the analysis and its performance was found better than proportional and proportional-derivative controllers. It was found that a combination of PZT-sensor and KNLNTS-actuator was efficient in damping the vibration of the cylindrical shell than a PZT-sensor and PZT-actuator. However, BNKLBT-sensor and KNLNTS-actuator combination was not as effective as the other two sensor-actuator systems considered.

1.5 Frequency and Loss Factor Calculation

After following any of the procedures discussed above, we can come up with a system of equations, which we can write in matrix form as:

$$\mathbf{M}\ddot{\mathbf{x}} + \mathbf{K}^*\mathbf{x} = 0 \tag{1.7}$$

1.5.1 Method of Complex Eigenvalues

By looking at Eq. 1.7, we see that the stiffness matrix is complex, because of the inclusion of complex shear and Young's moduli. We can solve this equation by the usual approach, we generally solve a real eigenvalue problem, but in this case, we will get complex eigenvalues and eigenvectors. Johnson and Kienholz [34] reported that the complex modes we get are orthogonal in nature and we can get uncoupled equations of motion. They also found that this method costs three times more than the corresponding undamped eigenvalue problem. Kosmatka and Liguore [36] too found this method to be more accurate but at the same time more computationally expensive because of the complex form of the problem. This method assumes displacements to be harmonic in nature [22] and to be of the form:

$$x^* = x_0^* e^{i\omega^* t} \tag{1.8}$$

where ω^* is the complex frequency and x_0^* is complex eigenvector. For free vibration, we can write Eq. 1.7 as:

$$(-\lambda^* M + K^*)\, x_0^* = 0 \tag{1.9}$$

where $\lambda^* = (\omega^*)^2$ is complex eigenvalue. By solving the above system of equations, we get complex eigenvalues and complex frequencies for the damped structure:

$$\lambda^* = \lambda + i\lambda' \tag{1.10}$$

$$\omega^* = \omega + i\omega' \tag{1.11}$$

The loss factor η_n corresponding to each frequency can be obtained by the following ratio [22]:

$$\eta_n = \frac{\lambda'_n}{\lambda_n} \tag{1.12}$$

where λ_n and λ'_n are the real and imaginary parts of the complex eigenvalue, λ_n^*, respectively. It is also possible to calculate the loss factor from the complex frequencies ω^* [22], as follows

$$\eta = 2 \arctan \frac{\omega'}{\omega} \tag{1.13}$$

where ω and ω' are real and imaginary parts of the complex frequency, ω^*, respectively.

1.5.2 The Modal Strain Energy Method

Johnson and Kienholz [34] used this method with NASTRAN, a commercially available software, to determine the modal loss factor. The main idea behind this method is that one does not have to solve the complex eigenvalue problem, the lost factor can be found from the undamped real modes. We can use these undamped modes to obtain energy dissipated in the damped structure. Rikards [22] reported that this method is an approximate method and for small damping the difference between undamped frequencies and modes, and damped frequencies and modes is relatively small. This will save us time and computational cost provided that the modal coupling is negligible [36]. Moreover, this method assumes that the damping in elastic layers is very small as compared to damping in the viscoelastic layer [34]. We will use this method only with the plane stress case. By using the real undamped modes,

we can calculate the energy dissipated, ΔU, in one cycle of steady state vibrations and elastic strain energy, U, using [22]:

$$\Delta U = \pi x_{0_n}^T K' x_{0_n}; \quad U = \frac{1}{2} x_{0_n}^T K x_{0_n} \tag{1.14}$$

Where, K is the real and K' is the imaginary part of the complex stiffness matrix K^* and n denotes the n^{th} mode. Now the loss factor can be calculated from the relation [22]:

$$\eta_n = \frac{\Delta U}{2\pi U} = \frac{x_{0_n}^T K' x_{0_n}}{x_{0_n}^T K x_{0_n}} \tag{1.15}$$

MSE is based on the assumption that damped, and undamped mode shapes of the sandwich structure are identical, and the natural frequency predictions of the sandwich structure are independent of the damping level [33, 53]. MSE method has some limitations because of the inherent assumption of similar mode shapes. The method of Complex eigenvalues (MCE) has also been used frequently in the literature. Rikards and Barkanov [24] used MCE and reported that this method needs more computation time as compared to the problem without damping.

Koruk and Sanliturk [54] reviewed both MSE and MCE methods, and concluded that complex eigenvalue method gives accurate results at the expense of huge CPU time; on the other hand, MSE is computationally efficient but better accuracy is not obtained for highly damped structures, although, the qualitative predictions of MSE are quite acceptable. We will investigate the ability of MSE method to predict the overall loss factor corresponding to different core loss factors, and compare it with MCE and published analytical results. Koruk and Sanliturk [53] reported that the accuracy of MSE method is strongly dependent on the mean angle (mode shape complexity factor) of the complex eigenmodes. For the mean angle, less than 5%, the error in the loss factor prediction by MSE was only 3%. Koruk and Sanliturk [55] used MSE method, because of its computational efficiency, to optimize general viscoelastically damped structures.

1.6 Research Objectives

Constrained layer damping is widely studied in the literature, and is an effective tool to mitigate vibrational energy and noise. In most of the work available in the literature, the

authors used either different beam theories or finite element with multi-degree-of-freedom beam elements. In defining these beam theories and beam elements, different assumptions are made, such as shear is neglected in the face layers and the shear strain is treated as a linear function in the thickness coordinate. There is a need to investigate constrained layer damping without any kinematic assumptions both in the elastic and viscoelastic layers, to understand the kind of effects viscoelastic material provide in terms of damping.

Stiffened structures have been extensively studied in the published literature to avoid critical frequencies and provide local stiffness to the structure. In these structures, no adequate consideration is given to the damping in the material. These stiffened panels as well as the stepped plates are widely used in the aerospace, ship and automobile industries; and investigation of damping can greatly help in controlling vibration and noise, general safety and consumer experience. More specifically, the stepped plates are used in wind tunnels to accurately determine the aeroelastic effect of the aircraft. Although, rib-type stiffeners can alter the response of a structure to external excitations by providing appropriate stiffness, but it is difficult to incorporate enough quantity of viscoelastic material to achieve high damping due to the small cross-sectional area of the rib stiffeners. In view of this, we wanted to investigate the response of a thick plate structure with adhesively bonded plate-type stiffeners. In this way, we will be able to add more damping to the system utilizing viscoelastic material. As a first step, we wanted to investigate the response of an integrally stiffened plate with plate-strip stiffeners and/or stepped plate, without considering viscoelastic damping, for different boundary conditions. And finally to study the effect of including high damping viscoelastic material between plate and stiffeners, to improve the damping characteristic of the stiffened plate.

1.7 Research Contributions

The main contributions of this dissertation are as follows:

1. Investigation of complex modes in damped sandwich beams

    - Complex modes in a damped sandwich beam were studied for various beam configurations. All the layers in the sandwich structure were modeled using 2D elements

in the normal direction without any kinematic assumptions, and transverse shear strains were introduced in both the elastic and core layers.

- Simple trigonometric functions were used with the principle of virtual work, to analyze constrained layer damped sandwich beam, modeled using Rayleigh beam theory.
- The efficiency of the modal strain energy method was tested for different loss factors in the core layer.
- Complex mode shapes of the beam were studied and a comparison was made between viscoelastically and viscously damped structures.

2. Vibration response of integrally stiffened plates

- Freely vibrating integrally stiffened thick plate with plate-strip stiffeners was analyzed using the first-order shear deformation theory (FSDT).
- There was a need to analyze integrally stiffened/stepped plates with any possible combination of boundary conditions, unlike the Navier and Levy's type solutions and, hence, static Timoshenko beam functions were used to study fully clamped, free and cantilever supported stiffened plates.
- A CPU time reduction technique was developed and used to decrease the amount of CPU time, by avoiding the recursive integration in a loop structure in the computer program, with the analytical integration of the integrand in the loop, thus saving a considerable amount of time.
- Effect of varying some important parameters on the overall frequency of the integrally stiffened structure was also investigated.
- Mode shapes of a cantilever supported plate with viscous dampers at the corners were studied at different times during cyclic oscillations.

3. Investigation of damping in an adhesively bonded plate

- The damped response of an adhesively bonded stiffened thick plate with plate-strip stiffeners was investigated utilizing FSDT for both plate and stiffener.

- The effect of a change in the stiffness of the adhesive layer on the overall natural vibration response of the bonded stiffened structure was investigated.
- The damping characteristics of the stiffened structure were tested for different kinds of viscoelastic material and variation of the adhesive thickness.

These contributions will be discussed in the following chapters.

Chapter 2

Viscoelastic Damped Sandwich Beams

2.1 Introduction

In this chapter, free vibration response of sandwich beams with a core viscoelastic layer is investigated with an effort to understand the behavior of complex modes and their impact on structural response. Simple trigonometric functions are used as admissible functions in a principle of virtual work formulation to obtain the damped response, and the convergence rate of these functions is compared with simple polynomial functions. The principle of virtual work is used along with the Rayleigh beam theory, by including the longitudinal and rotational inertias in the formulation. Rayleigh beam theory is an extension of Euler-Bernoulli beam theory, that includes the rotary inertias of the beam in the kinetic energy formulation [56]. In most of the work available in the literature, the authors used either different beam theories or finite element with multi degree-of-freedom beam elements. In defining these beam theories and beam elements, different assumptions are made, such as shear is neglected in face layers. In this work, an investigation is made on the use of plane stress elasticity based finite element formulation to get improved natural frequencies and loss factor estimates. In this procedure, no kinematic assumptions are considered in the face as well as core layers. All the layers are modeled using 2D elements in the normal direction, and transverse shear strains are

introduced both in elastic and core layers. Moreover, an effect on the damped response of the sandwich structure from using 4-noded as well as 9-noded rectangular elements is investigated. The frequency and loss factor is calculated for each mode using both the method of complex eigenvalues and the modal strain energy method. The efficiency of the modal strain energy method is tested for different loss factors in the core layer. Additionally, numerical examples are studied, where both the base and constraining layers are also damped. Complex mode shapes of the beam are studied and a comparison is made between viscoelastically and viscously damped structures. This work was presented in 54th AIAA Structural Dynamics and Materials (SDM) Conference [57] and was subsequently published in the Journal of Advances in Aircraft and Spacecraft Science [58].

2.2 Principle of Virtual Work

2.2.1 Strain and Kinetic Energies

The assumptions made in this study, for the damped structure shown in Fig. 2.1, are as follows,

1. The face and core layers are assumed to be homogenous and isotropic.
2. Planes perpendicular to the middle plane before bending remains plane after deformation.
3. Normal stresses and extension in the core layer are neglected.
4. All displacements and rotations are considered small.
5. All three layers undergo same deflection.
6. The longitudinal displacements in the layers change linearly through the thickness (Fig. 2.1)
7. Along the interface, no slip condition and continuity of displacements is considered.

The displacement field for the faces can be written as:

$$Face\ 1: \quad u = u_1 - zw', \tag{2.1}$$

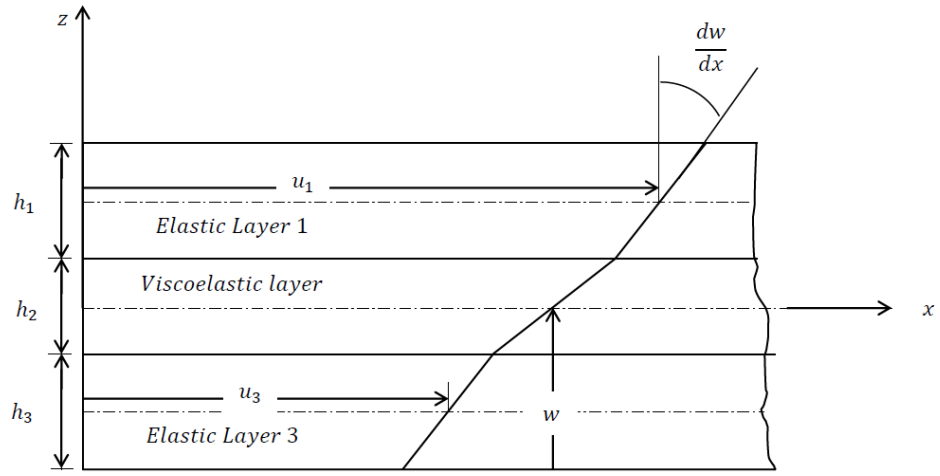

Figure 2.1: Schematic for Damped Structure

$$Face\ 3: \quad u = u_3 - zw' \tag{2.2}$$

where w is the deflection of the beam and u_1 and u_3 are the longitudinal displacements (at middle surfaces) in layers 1 and 3, respectively. The strain-displacement and constitutive relations for the three layers are as follows [28],

$$Face\ 1: \quad \epsilon^1_{xx} = u_1' - zw'' \tag{2.3}$$

$$Core \quad : \quad \gamma_{xz} = \frac{(u_1 - \frac{h_1}{2}w') - (u_3 + \frac{h_3}{2}w')}{h_2} - w', \tag{2.4}$$

$$Face\ 3: \quad \epsilon^3_{xx} = u_3' - zw'', \tag{2.5}$$

$$Face\ 1: \quad \sigma^1_{xx} = E_1(u_1' - zw'') \tag{2.6}$$

$$Core \quad : \quad \tau_{xz} = G^* \left[\frac{(u_1 - \frac{h_1}{2}w') - (u_3 + \frac{h_3}{2}w')}{h_2} - w' \right] \tag{2.7}$$

$$Face\ 3: \quad \sigma^3_{xx} = E_3(u_3' - zw'') \tag{2.8}$$

where $(\,)'$ represent the derivative with respect to x, σ and ϵ are the longitudinal stress and strain in the face layers, τ and γ are the shear stress and strain in the core layer, respectively. An asterisk denotes a complex quantity throughout this paper; for example $G^* = G(1 + i\eta)$

is the complex shear modulus with η as loss factor of the core. One can also include the damping in the face layers, which are usually considered elastic, by using complex Young's moduli [28], as we will see in one of the numerical examples, Example 3.

We can write the virtual work done by the internal stresses as:

$$\delta W_i = \int_V [\sigma^1_{xx}\delta\epsilon^1_{xx} + \sigma^3_{xx}\delta\epsilon^3_{xx} + \tau_{xz}\delta\gamma_{xz}]dV \tag{2.9}$$

$$\begin{aligned}\delta W_i = \int_0^L [&E_1A_1u_1'\delta u_1' + E_1I_1w''\delta w'' + E_3A_3u_3'\delta u_3' + E_3I_3w''\delta w'' \\ &+ \frac{G_2^*A_2}{h_2^2}[u_1\delta u_1 + u_3\delta u_3 - u_1\delta u_3 - u_3\delta u_1 + C^2w'\delta w' \\ &+ C(u_3\delta w' + \delta u_3w' - u_1\delta w' - \delta u_1w')]]dx\end{aligned} \tag{2.10}$$

where $C = (h_1 + h_3)/2 + h_2$, A is the cross sectional area and I is the moment of inertia.

Furthermore, by using d'Alembert's principle, the virtual work due to the inertial forces, including the longitudinal and rotary inertias, can be written as:

$$\begin{aligned}\delta W_{inertial} = \int_0^L [&\rho_1 \int_{A_1} (\ddot{u}_1 - z\ddot{w}')\delta(u_1 - zw')dA_1 \\ &+ \rho_3 \int_{A_3} (\ddot{u}_3 - z\ddot{w}')\delta(u_3 - zw')dA_3 + \rho\ddot{w}\delta w]dx\end{aligned} \tag{2.11}$$

where $\rho = \rho_1A_1 + \rho_2A_2 + \rho_3A_3$ and ρ_1, ρ_2, ρ_3 are the densities of layer 1, 2, and 3, respectively. In the absence of external forces, we can write by using Eqs. 2.10 and 2.11, the principle of virtual work as:

$$\begin{aligned}\int_0^L [&E_1A_1u_1'\delta u_1' + E_1I_1w''\delta w'' + E_3A_3u_3'\delta u_3' + E_3I_3w''\delta w'' + \frac{G_2^*A_2}{h_2^2}\{u_1\delta u_1 \\ &+ u_3\delta u_3 + C^2w'\delta w' - u_1\delta u_3 - \delta u_1u_3 + C(u_3\delta w' + \delta u_3w' - u_1\delta w' - \delta u_1w')\} \\ &- \omega^2[\rho w\delta w + \rho_1A_1u_1\delta u_1 + \rho_3A_3u_3\delta u_3 + \frac{w'\delta w'}{12}(\rho_1A_1h_1^2 + \rho_3A_3h_3^2)]]dx = 0\end{aligned} \tag{2.12}$$

In the above equation, we have assumed the harmonic vibrations of u and w.

2.2.2 Admissible Functions

We can express the displacements as a sum of admissible functions:

$$w(x) = \sum_{i=1}^{n} a_i \phi_i(x), \quad u_1(x) = \sum_{i=1}^{n} b_i \psi_i(x), \quad u_3(x) = \sum_{i=1}^{n} c_i \psi_i(x) \tag{2.13}$$

where n is the number of modes. It should be noted that coefficients, the so-called generalized co-ordinates, **a**, **b** and **c** are arbitrary as well as independent from each other. Putting these displacement functions in Eq. 2.12 and separating the coefficients of $\delta\mathbf{a}$, $\delta\mathbf{b}$ and $\delta\mathbf{c}$ and equating them to zero, we can get the following set of equations:

$$\delta a_j : \quad \int_0^L [E_1 I_1 a_i \phi_i'' \phi_j'' + E_3 I_3 a_i \phi_i'' \phi_j'' + \frac{G_2 A_2}{h_2^2}\{C^2 a_i \phi_i' \phi_j' + C(c_i \psi_i \phi_j' - b_i \psi_i \phi_j'\} - \omega^2[\rho a_i \phi_i \phi_j + \frac{a_i \phi_i' \phi_j'}{12}(\rho_1 A_1 h_1^2 + \rho_3 A_3 h_3^2)]]dxdt = 0 \tag{2.14}$$

$$\delta b_j : \quad \int_0^L [E_1 A_1 b_i \psi_i' \psi_j' + \frac{G_2 A_2}{h_2^2}\{b_i \psi_i \psi_j - c_i \psi_i \psi_j - C a_i \phi_i' \psi_j\} - \omega^2 \rho_1 A_1 b_i \psi_i \psi_j]dx = 0 \tag{2.15}$$

$$\delta c_j : \quad \int_0^L [E_3 A_3 c_i \psi_i' \psi_j' + \frac{G_2 A_2}{h_2^2}\{c_i \psi_i \psi_j - b_i \psi_i \psi_j + C a_i \phi_i' \psi_j\} - \omega^2 \rho_3 A_3 c_i \psi_i \psi_j]dx = 0 \tag{2.16}$$

The above equations can be written in the matrix form as:

$$K^* \mathbf{x} = \lambda \mathbf{M} \mathbf{x} \tag{2.17}$$

where $\lambda = \omega^2$ and $x = [a_j, b_j, c_j]^T$. The stiffness matrix is complex because of the inclusion of complex shear modulus and complex Young's modulus.

We used trigonometric functions as admissible functions. For the simply supported case:

$$\phi_i(x) = \sin\left(\frac{i\pi x}{L}\right), \quad \psi_i(x) = 1 - \cos\left(\frac{(2i-1)\pi x}{2L}\right), \mathrm{i} = 1, 2, 3....\mathrm{n} \tag{2.18}$$

For the cantilever boundary conditions:

$$\phi_i(x) = 1 - \cos\left(\frac{(2i-1)\pi x}{2L}\right), \;\; \psi_i(x) = 1 - \cos\left(\frac{(2i-1)\pi x}{2L}\right), \text{i} = 1, 2, 3....\text{n} \tag{2.19}$$

2.3 Elasticity Solution (The Plane-Stress Case)

The governing equations of motion are:

$$\frac{\partial \sigma_{xx}}{\partial x} + \frac{\partial \tau_{xz}}{\partial z} = \rho \frac{\partial^2 u}{\partial t^2} \tag{2.20}$$

$$\frac{\partial \tau_{xz}}{\partial x} + \frac{\partial \sigma_{zz}}{\partial z} = \rho \frac{\partial^2 w}{\partial t^2} \tag{2.21}$$

where, u and w are the displacements in the x and z-direction, respectively, as shown in Fig. 2.2. We assumed that every layer is isotropic, so the stress-strain relation can be written as:

$$\begin{Bmatrix} \sigma_{xx} \\ \sigma_{zz} \\ \tau_{xz} \end{Bmatrix} = \begin{bmatrix} C_{11} & C_{12} & 0 \\ C_{12} & C_{22} & 0 \\ 0 & 0 & C_{66} \end{bmatrix} \begin{Bmatrix} \epsilon_{xx} \\ \epsilon_{zz} \\ 2\epsilon_{xz} \end{Bmatrix} \tag{2.22}$$

The square matrix in the above equation will be complex because of complex shear and Young's moduli for the core layer. This matrix will also be complex for the constraining layers when we will consider complex Young's modulus in the constraining layers. The strain-displacement relations are given as:

$$\epsilon_{xx} = \frac{\partial u}{\partial x}, \;\; \epsilon_{zz} = \frac{\partial w}{\partial z}, \;\; 2\epsilon_{xz} = \frac{\partial u}{\partial z} + \frac{\partial w}{\partial x} \tag{2.23}$$

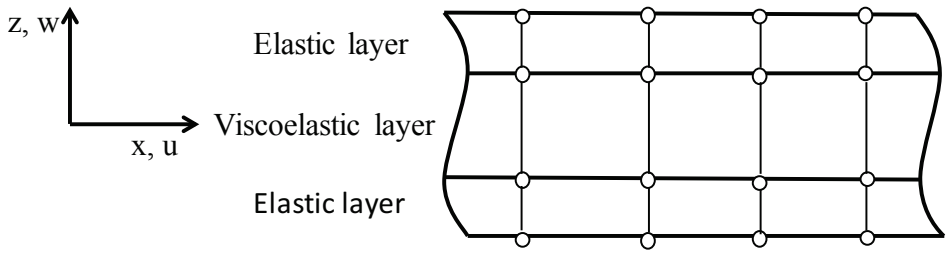

Figure 2.2: Schematic of Partial Sandwich Beam with 4-Noded Elements in Face and Core Layers

By substituting Eqs. 2.22 and 2.23 into Eqs. 2.20 and 2.21, we obtain the following two equations:

$$\frac{\partial}{\partial x}\left(C_{11}\frac{\partial u}{\partial x}+C_{12}\frac{\partial w}{\partial z}\right)+\frac{\partial}{\partial z}\left(C_{66}\frac{\partial u}{\partial z}+C_{66}\frac{\partial w}{\partial x}\right) = \rho\frac{\partial^2 u}{\partial t^2} \tag{2.24}$$

$$\frac{\partial}{\partial x}\left(C_{66}\frac{\partial u}{\partial z}+C_{66}\frac{\partial w}{\partial x}\right)+\frac{\partial}{\partial z}\left(C_{12}\frac{\partial u}{\partial x}+C_{22}\frac{\partial w}{\partial z}\right) = \rho\frac{\partial^2 w}{\partial t^2} \tag{2.25}$$

Deriving the weak form and using the test function, we obtain [59],

$$\begin{bmatrix} [M] & [0] \\ [0] & [M] \end{bmatrix}\begin{Bmatrix} \{\ddot{u}\} \\ \{\ddot{w}\} \end{Bmatrix}+\begin{bmatrix} [K^{11}] & [K^{12}] \\ [K^{12}]^T & [K^{22}] \end{bmatrix}\begin{Bmatrix} \{u\} \\ \{w\} \end{Bmatrix}=0 \tag{2.26}$$

where,

$$u \approx \sum_{i=1}^{n} u_i^e \psi_i^e(x,y); \qquad K_{ij}^{11}=\int_{\Omega^e} t\left(C_{11}\frac{\partial\psi_i}{\partial x}\frac{\partial\psi_j}{\partial x}+C_{66}\frac{\partial\psi_i}{\partial z}\frac{\partial\psi_j}{\partial z}\right)dxdz$$

$$w \approx \sum_{i=1}^{n} a_i^e \psi_i^e(x,y); \qquad K_{ij}^{12}=\int_{\Omega^e} t\left(C_{12}\frac{\partial\psi_i}{\partial x}\frac{\partial\psi_j}{\partial z}+C_{66}\frac{\partial\psi_i}{\partial z}\frac{\partial\psi_j}{\partial x}\right)dxdz$$

$$M_{ij}=\int_{\Omega^e}\rho t\psi_i\psi_j dxdz; \qquad K_{ij}^{22}=\int_{\Omega^e} t\left(C_{66}\frac{\partial\psi_i}{\partial x}\frac{\partial\psi_j}{\partial x}+C_{22}\frac{\partial\psi_i}{\partial z}\frac{\partial\psi_j}{\partial z}\right)dxdz$$

The stiffness matrix will be complex. We used bilinear quadrilateral and biquadratic elements along the length and thickness of each layer.

2.4 Results

First, we used the principle of virtual work (PVW) to compare our results with Fasana and Marchesiello [28] to validate our code. Fasana and Marchesiello also used a similar method to solve their problem but they used simple polynomials as admissible functions. We used trigonometric functions and found that we can get a good estimate of lower frequencies and the loss factors with lesser number of modes. Fasana and Marchesiello, used 20 modes and we only used 4 modes to get the results with required accuracy as can be seen in Table 2.1. Of course, we will have to use higher modes for better approximating the higher frequencies. The material and geometrical properties used for this beam were; $h_1 = 0.5$mm; $h_3 = 5$mm; $E_1 = E_3 = 207$GPa; $\eta_1 = \eta_3 = 0$; $h_2 = 2.5$mm; $G_2 = 4$MPa; $\eta_2 = 0.38$; $L = 242.5$mm.

Table 2.1: Modal Frequencies and Loss Factors for a Simply-Supported Sandwich Beam

	Mode number	1	2	3	4
Present study $n = 4$	ω_n (rad/s)	1206	4638	10345	18318
	η_n (%)	3.57	1.07	0.50	0.28
Present study $n = 8$	ω_n (rad/s)	1206	4639	10345	18318
	η_n (%)	3.56	1.07	0.50	0.28
Present study $n = 12$	ω_n (rad/s)	1206	4639	10345	18318
	η_n (%)	3.57	1.07	0.50	0.28
Present study $n = 20$	ω_n (rad/s)	1206	4639	10345	18318
	η_n (%)	3.56	1.07	0.50	0.28
Fasana and Marchesiello [28] $n = 20$	ω_n (rad/s)	1204	4631	10328	18278
	η_n (%)	3.43	1.07	0.5	0.28

2.4.1 Example 1: Sandwich Beam with Pure Elastic Face Layers

We modeled simply-supported and cantilever beams with the same material properties as used by Rikards [22], namely, C2A and A2A, respectively. The C2A properties are given as $h_1 = h_3 = 3$mm; $E_1 = E_3 = 45.54$GPa; $\rho_1 = \rho_3 = 2040$ kg/m^3; $\nu_1 = \nu_3 = 0.33$; $\eta_1 = \eta_3 = 0$; $h_2 = 3$mm; $E_2 = 0.0159$GPa; $\rho_1 = 1200$kg/m^3; $\nu_2 = 0.45$; $\eta_2 = 1$; $b(width) = 15$mm; $L = 270$mm.

The A2A properties are given as $h_1 = h_3 = 1$mm; $E_1 = E_3 = 45.54$GPa; $\rho_1 = \rho_3 = 2040$ kg/m^3; $\nu_1 = \nu_3 = 0.33$; $\eta_1 = \eta_3 = 0$; $h_2 = 1$mm; $E_2 = 0.000057$GPa; $\rho_1 = 1200$kg/m^3; $\nu_2 = 0.5$; $\eta_2 = 1$; $b(width) = 15$mm; $L = 300$mm. The face layers are considered completely elastic, i.e., without complex Young's modulus. The core layer is considered viscoelastic with complex shear modulus in which the loss factor η does not change with frequency.

We investigated the first three natural frequencies for the simply supported case and fundamental frequency for the cantilever beam using the principle of virtual work (PVW) and using plane stress elasticity with 1200 bilinear quadrilateral (4-noded) and 300 biquadratic (9-noded) elements. Frequency results are shown in Table 2.2 and the resulting loss factor

results are shown in Table 2.3.

We compared our results with Rikards [22], who used four superelements with third-order approximation, each element having 8 nodes and 20 degrees of freedom. Rikards used both the method of complex eigenvalues (MCE) as well as the modal strain energy method (MSE) to calculate the frequencies and loss factors. He also reported analytical results based on the sixth order theory derived by Mead and Marcus [20]. Our results are closer to the analytical values reported by Rikards, than those obtained by Rikards himself.

The frequencies predicted by MCE are a bit higher than undamped frequencies but on the other hand the loss factors predicted by MSE are lower than those predicted by MCE. Loss factors obtained using 300 biquadratic elements are higher than using 1200 bilinear quadrilateral elements but for the natural frequencies opposite is the case. Convergence of the first frequency for a simply-supported sandwich beam with four and nine noded elements is shown in Fig. 2.3. It is noted that by using a high degree of approximation for the elasticity based FEM, we can get better estimates of the frequencies that are close to the analytical results given by Rikards.

The CPU time for using MCE was 350 seconds as compared to 10 seconds for MSE for the simply supported case. The CPU time was calculated using 1200 quadrilateral elements. The reason for difference in time between the two methods is that we have to solve the entire complex eigenvalue problem in MCE for getting the first three loss factors and frequencies, on the other hand MSE solved for only first three loss factors and we need to solve only the undamped real eigenvalue problem.

First six mode shapes for the simply-supported (S-S) beam using the principle of virtual work are shown in Fig. 2.4 with real and imaginary parts. It is seen that the imaginary part changes with respect to the real part from one mode to another, signifying the role of damping in each mode. Moreover, the mode shapes for both u_1 and u_3 were exactly the same because of the same thickness and material used.

Table 2.2: Natural Frequencies (rad/s) of Simply-Supported and Cantilever Sandwich Beams

Mode	Method of complex eigenvalues				Modal strain energy method			Analytical [22]
	PVW	4 Node	9 Node	Rikards [22]	4 Node	9 Node	Rikards [22]	
	Simply-supported beam							
1	904.42	910.75	897.49	1001	850.91	836.00	924	878
2	2488.96	2544.06	2466.83	2723	2491.33	2410.91	2574	2458
3	4948.08	5066.12	4870.07	5256	5015.35	4818.51	4839	4927
	Cantilever beam							
1	91.87	97.24	91.59	91.6	91.05	85.22	85.2	85.3

Table 2.3: Loss Factor of Simply-Supported and Cantilever Sandwich Beams

Mode	Method of complex eigenvalues				Modal strain energy method			Analytical [22]
	PVW	4 Node	9 Node	Rikards [22]	4 Node	9 Node	Rikards [22]	
	Simply supported beam							
1	0.57	0.48	0.50	0.38	0.54	0.55	0.45	0.55
2	0.34	0.32	0.34	0.30	0.33	0.35	0.34	0.34
3	0.20	0.20	0.20	0.20	0.20	0.21	0.29	0.20
	Cantilever beam							
1	0.43	0.38	0.42	0.42	0.45	0.50	0.5	0.47

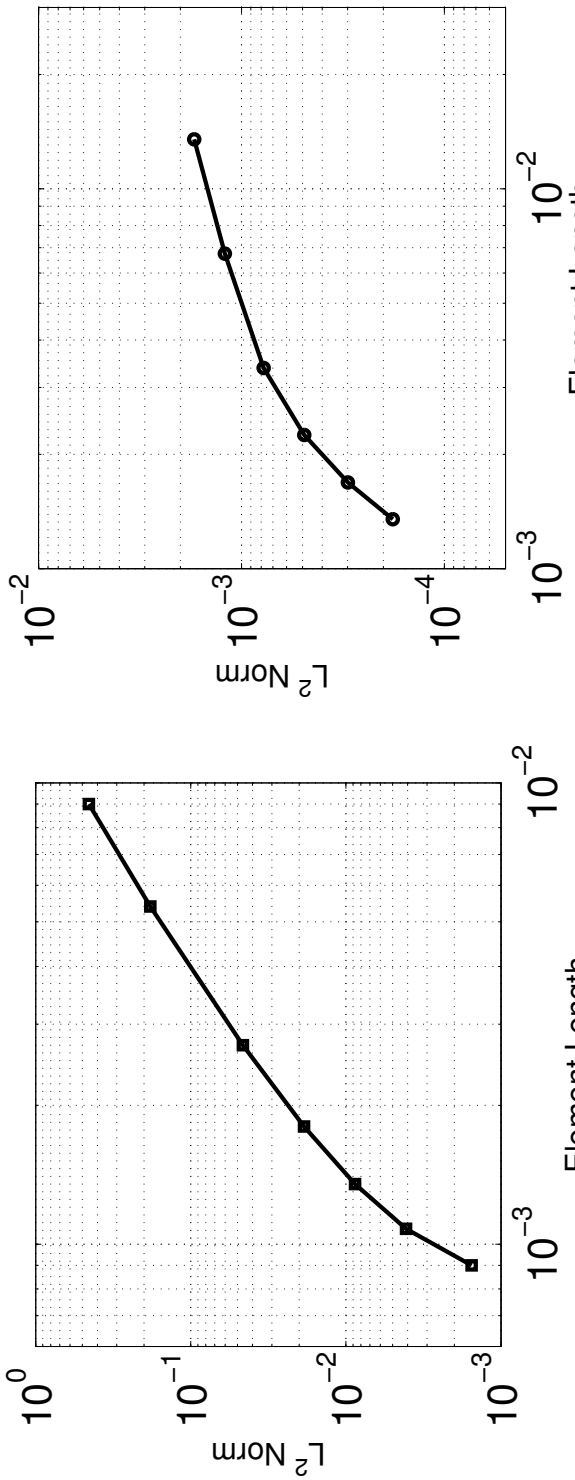

(a) Convergence using 4 Nodes

(b) Convergence using 9 Nodes

Figure 2.3: Convergence Plot for Sandwich Beam with Pure Elastic Faces

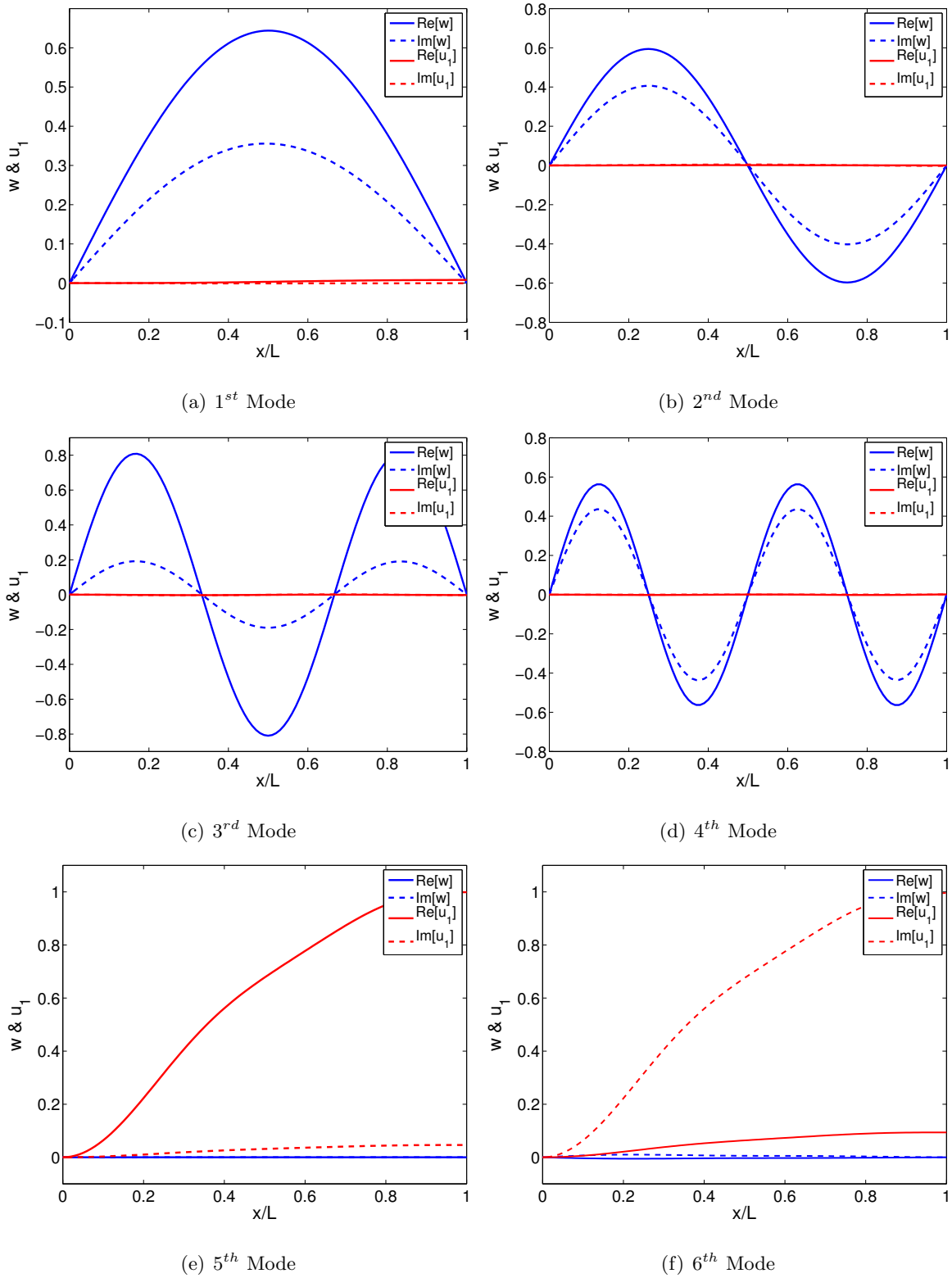

(a) 1^{st} Mode

(b) 2^{nd} Mode

(c) 3^{rd} Mode

(d) 4^{th} Mode

(e) 5^{th} Mode

(f) 6^{th} Mode

Figure 2.4: The Real and Imaginary Parts of Mode Shapes for S-S Sandwich Beam with Pure Elastic Layers

Table 2.4: Natural Frequencies (Hz) for First Three Modes of the Cantilever Beam with Different Core Loss Factors

η_c	PVW	MSE	MSE [60]	MCE	MCE [60]	ANM [61]	Analytical [62]
0.1	64.6	64.1	64.1	64.1	64.1	64.2	64.1
	296.7	296.5	296.6	296.6	296.6	296.9	296.4
	744.6	743.8	744.3	743.8	744.4	745.5	743.7
0.6	66.2	64.1	64.1	65.7	65.5	65.6	65.5
	299.9	296.5	296.6	299.8	299.1	299.5	298.9
	747.1	743.8	744.3	746.4	746.2	747.3	745.5
1	68.4	64.1	64.1	67.8	67.4	67.5	67.4
	304.8	296.5	296.6	304.7	303	303.3	302.8
	751.6	743.8	744.3	750.8	749.4	750.4	748.6
1.5	71.1	64.1	64.1	70.4	69.9	70	69.9
	312.3	296.5	296.6	312.3	309.1	309.4	308.9
	759.8	743.8	744.3	759.0	755.2	756.2	754

2.4.2 Example 2: Cantilever Sandwich Beam with Different Core Loss Factors

We modeled a cantilever beam with pure elastic face layers with material properties given as $h_1 = h_3 = 1.524$mm; $E_1 = E_3 = 69$GPa; $\rho_1 = \rho_3 = 2766$ kg/m^3; $\nu_1 = \nu_3 = 0.3$; $\eta_1 = \eta_3 = 0$; $h_2 = 0.127$mm; $E_2 = 0.001794$GPa; $\rho_1 = 968.1$kg/m^3; $\nu_2 = 0.3$; $\eta_2 = 1$; $b(width) = 12.7$mm; $L = 177.8$mm, for various core layer loss factors. We assumed that the complex stiffness is constant and does not change with frequency and thus it leads to a linear complex eigenvalue problem [60]. This problem has been extensively studied in the literature [11, 16, 60–62].

We investigated the first three frequencies and the corresponding loss (η_b) factors for the cantilever beam using the principle of virtual work with 12 modes and the FEM elasticity method with 300 elements. Natural frequencies (Hz) are shown in Table 2.4 and the loss factor ratios (η_b/η_c) for the beam are shown in the Table 2.5 for different core loss factors

(η_c). It was noted that for this example, which is a relatively short beam as compared to the example considered above, the results obtained by using 9 node FEM plane stress elements are better than using PVW method. The difference is much pronounced in the calculation of fundamental frequency and the corresponding loss factor.

Table 2.5: Loss Factor for First Three Modes of the Cantilever Beam with Different Core Loss Factors

η_c	PVW	MSE	MSE [60]	MCE	MCE [60]	ANM [61]	Analytical [62]
0.1	0.292	0.283	0.283	0.281	0.281	0.281	0.282
	0.242	0.242	0.243	0.242	0.242	0.242	0.242
	0.154	0.154	0.154	0.154	0.154	0.153	0.154
0.6	0.256	0.283	0.283	0.246	0.246	0.246	0.246
	0.232	0.242	0.243	0.232	0.232	0.232	0.232
	0.153	0.154	0.154	0.152	0.152	0.152	0.153
1	0.212	0.283	0.283	0.202	0.202	0.202	0.202
	0.217	0.242	0.243	0.217	0.217	0.217	0.218
	0.150	0.154	0.154	0.150	0.150	0.150	0.150
1.5	0.162	0.283	0.283	0.153	0.153	0.153	0.153
	0.197	0.242	0.243	0.197	0.197	0.197	0.197
	0.146	0.154	0.154	0.146	0.145	0.145	0.146

Moreover, it is evident from the results that modal strain energy method cannot be used with structures which have a high loss factor as predicted by Johnson [34] and reported by Bilasse, Daya and Azrar [60]. The MSE approach underestimates the frequencies and overestimates the loss factors for the beams with a high core loss factor. Our results for the MSE were closed to those reported by Bilasse, Daya and Azrar [60].

We also compared our results from the plane stress finite element formulation with Daya and Potier-Ferry [61], who assumed plane strain conditions with 1226 degree of freedom over the beam. The frequency and loss factors estimates were in good agreement. Daya and Potier-Ferry [61] devised a new numerical method, for solving the nonlinear complex

eigenvalue problem, called Asymptotic numerical method (ANM) by using a perturbation technique. Our results calculated by using MCE were closed to ANM, because there was no nonlinearity in this example and complex stiffness was considered constant. The results obtained by using method of complex eigenvalues were in good agreement with Soni [62], who reported the analytical results obtained by using sixth order differential equation.

Table 2.6: Natural Frequencies (rad/s) for Sandwich Beam with Damped Face Layers

	MCE			MSE		
	PVW	4 Node	9 Node	4 Node	9 Node	Barkanov [23]
Simply-Supported	190.50	191.45	179.51	183.71	171.10	183.40
	562.01	621.00	561.03	611.33	549.75	577.90
	1141.86	1288.30	1140.00	1281.45	1131.77	1170.30
	1942.91	2211.53	1937.36	2206.45	1931.38	1999.90
	2969.66	3391.79	2955.79	3387.02	2950.57	3101.30
Cantilever	73.98	77.26	72.87	74.92	70.38	71.6
	344.49	377.90	344.47	369.05	334.79	335.2
	839.95	942.05	838.92	931.18	826.17	820.8
	1529.71	1740.59	1525.82	1733.20	1516.84	1504.6
	2447.26	2803.87	2438.15	2798.05	2431.04	2415.1

2.4.3 Example 3: Sandwich Beam with Damped Face Layers

We modeled simply supported and cantilever beam, with the following material and geometric properties, as used by Barkanov [23]. $h_1 = 1.5$mm; $E_1 = 69$GPa; $\rho_1 = 2760$ kg/m^3; $\nu_1 = 0.32$; $\eta_1 = 0.033$; $h_2 = 0.5$mm; $E_2 = 0.00176$GPa; $\rho_1 = 980$kg/m^3; $\nu_2 = 0.49$; $\eta_2 = 0.87$; $h_3 = 4$mm; $E_3 = 36$GPa; $\rho_3 = 1900$kg/m^3; $\nu_3 = 0.28$; $\eta_3 = 0.004$; $b(width) = 6$mm; $L = 600$mm. In this example, we considered the elastic layers to have complex Young's modulus. The core layer is considered viscoelastic with complex shear modulus in which the loss factor η does not change with frequency.

We investigated the first five frequencies and the corresponding loss factor for both simply supported and cantilever beams using PVW and the FEM elasticity case. Frequency results are shown in Table 2.6 and loss factor results are shown in Table 2.7. We compared our results with Barkanov [23]. Barkanov used four finite elements with 61 degrees of freedom for the simply supported beam and ten finite elements with 150 degrees of freedom for the cantilever beam. Barkanov used Lanczos method for solving the complex eigenvalue problem. Frequencies obtained by using the two methods are lower than Barkanov [23].

Table 2.7: Loss factor for Sandwich Beam with Damped Face Layers

	MCE			MSE		
	PVW	4 Node	9 Node	4 Node	9 Node	Barkanov [23]
Simply-Supported	0.394	0.210	0.238	0.254	0.290	0.182
	0.239	0.187	0.226	0.194	0.237	0.188
	0.151	0.120	0.150	0.122	0.152	0.132
	0.100	0.081	0.101	0.082	0.101	0.092
	0.071	0.059	0.072	0.060	0.073	0.067
Cantilever	0.15	0.12	0.14	0.16	0.18	0.147
	0.22	0.19	0.22	0.21	0.24	0.209
	0.18	0.15	0.18	0.16	0.19	0.167
	0.13	0.10	0.13	0.10	0.13	0.111
	0.09	0.07	0.09	0.07	0.09	0.077

The loss factor estimates were higher than that of Barkanov for the simply supported boundary conditions and were close to the results obtained for cantilever boundary conditions. It turns out that if we use higher approximation for the elasticity case we can get higher loss factors. The convergence of the fundamental frequency is shown in Fig. 2.5 for both four and nine noded elements, for a simply supported (S-S) damped sandwich beam. The CPU time for using MCE was 763 seconds as compared to 24 seconds for MSE using 1600 quadrilateral elements.

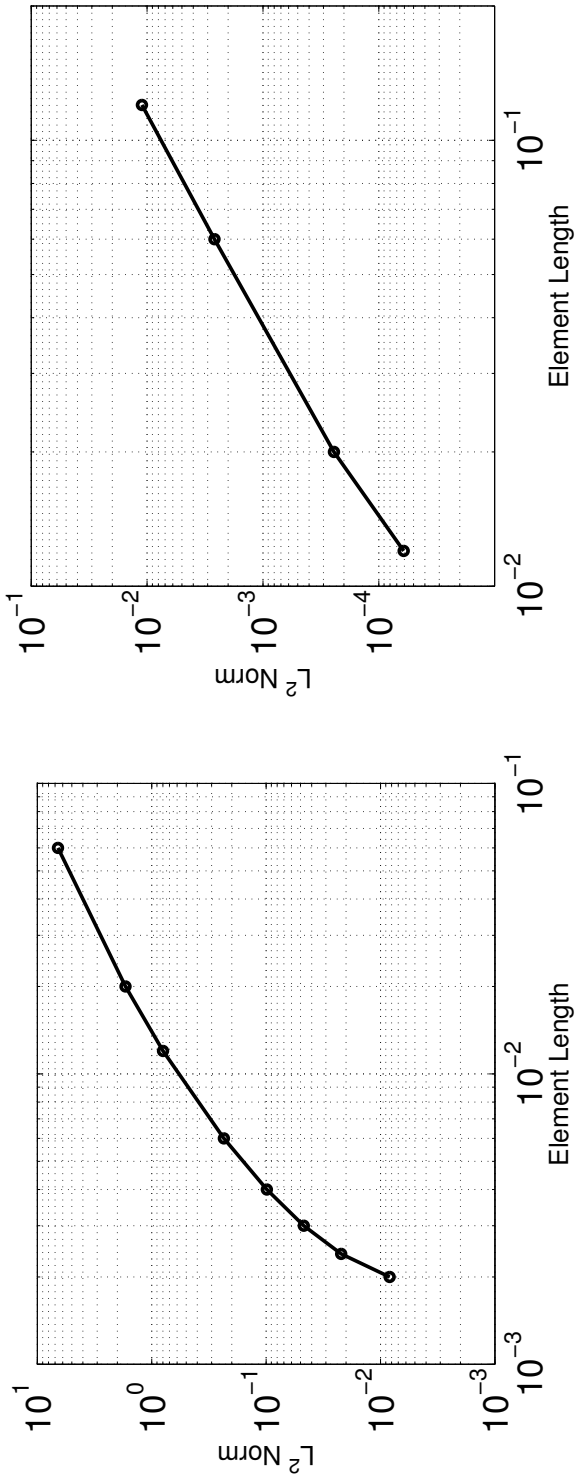

(a) Convergence using 4 Nodes

(b) Convergence using 9 Nodes

Figure 2.5: Convergence Plot for Sandwich Beam with Damped Face Layers

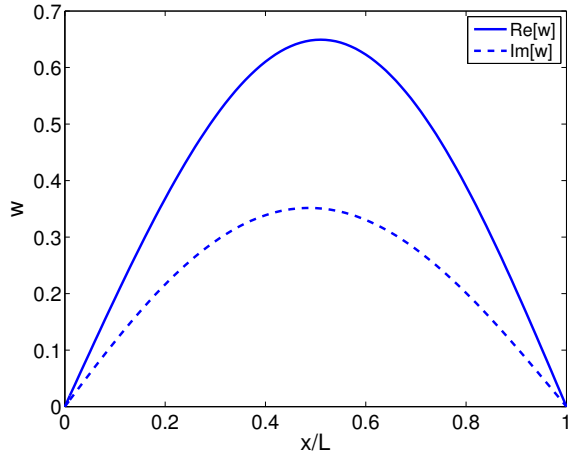

(a) 1^{st} Mode

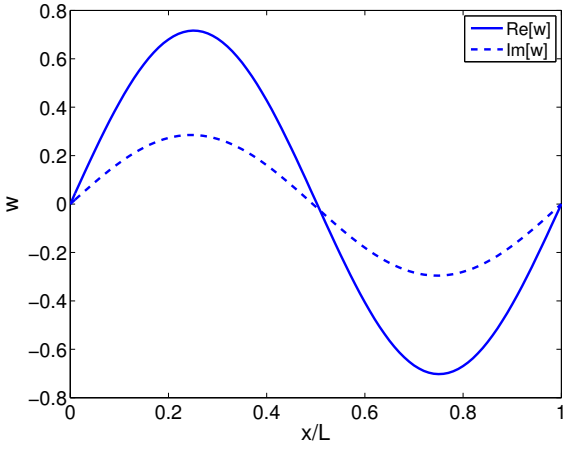

(b) 2^{nd} Mode

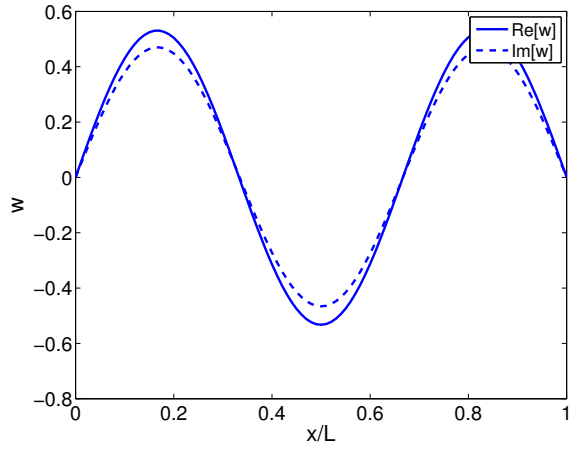

(c) 3^{rd} Mode

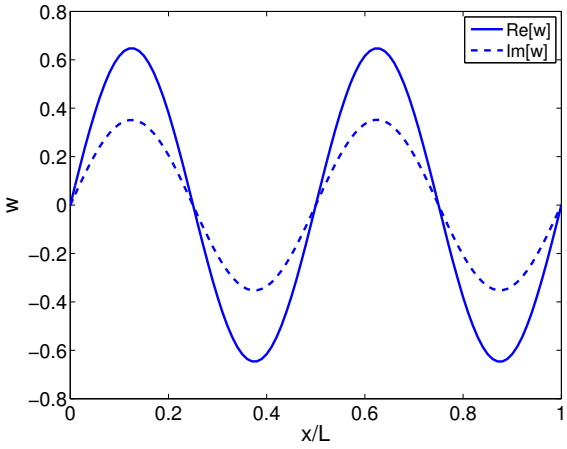

(d) 4^{th} Mode

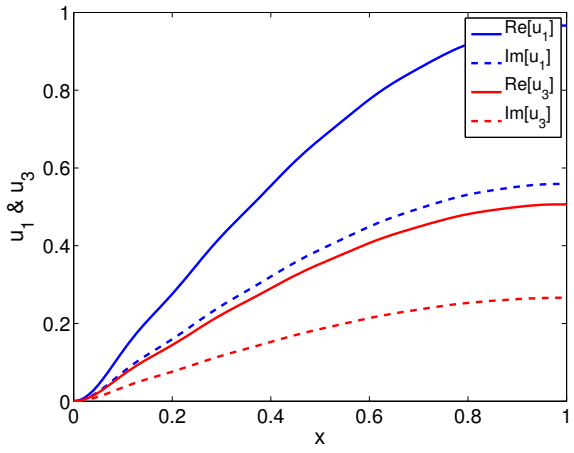

(e) 5^{th} Mode

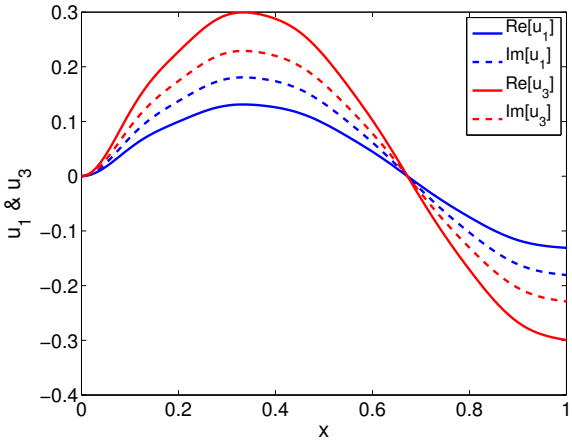

(f) 6^{th} Mode

Figure 2.6: The Real and Imaginary Parts of Mode Shapes for S-S Sandwich Beam with Damped Face Layers

First six mode shapes for the simply-supported beam using PVW are shown in Fig. 2.6 with real and imaginary parts. We note that the real and imaginary parts of the each mode have the same shape but different amplitude as reported by Krenk [63], and Bilasse, Daya and Azrar [60]. Moreover, mode shapes for u_1 and u_3 were different because of the different material and thickness used.

2.5 Complex Modes

Role of non-proportional damping on the complex mode shapes in structures has been reported in the literature. Koruk and Sanliturk [64] developed a new complexity factor for general structures based on conservation of energy principle, for quantification of complex modes. They reported that the mode shape complexity in non-proportionally damped structures is generally higher than proportionally damped structures. Therefore, the notion of normal modes cannot be used in the modal analysis for highly non-proportionally damped structures. Koruk and Sanliturk [55] reported that the accuracy of the MSE method decreases as the mode shape complexity increases in general damped structures. Lampoh, Charpentier, and Mostafa [65] used homotopy-based asymptotic numerical method, to determine the sensitivity of complex eigenvalue solution in damped sandwich structures to various perturbations. Adhikari [66] developed a normalization procedure for complex modes, using a least-square error minimisation approach.

2.5.1 Investigation of Complex Mode Shapes of a Viscoelastically Damped Sandwich Beam with End Viscous Damper

We investigated the complex mode shapes in detail for the numerical examples studied above and the numerical problem considered by Barkanov [67]. We found out that although the eigenvalues and eigenvectors are complex in the case of constrained viscoelastic layer damping, we still get stationary nodes unlike non-proportional viscously damped structures. Zarek and Gibbs [68], and Prater and Singh [69], reported that the presence of lumped viscous dampers in the structure move nodes during the cyclic oscillations, and we do not get a single point on the structure where all the displacements goes to zero at every time. This lead us to study

a cantilever viscoelastic beam with a viscous damper at the free end as shown in Fig. 2.7, to see how a lumped damper at the boundary can alter the nodal displacements during cyclic oscillations in a damped sandwich beam.

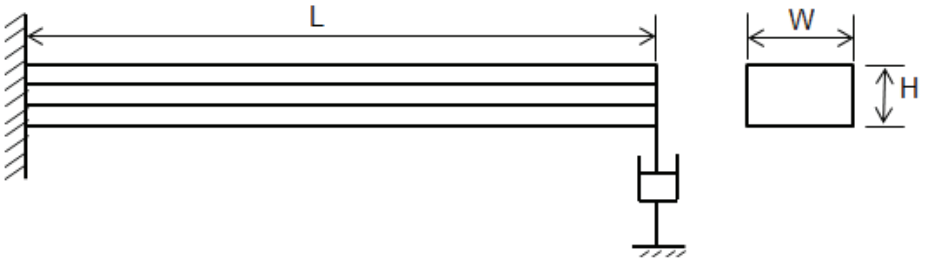

Figure 2.7: Schematic of a Viscoelastic Sandwich Beam with End Viscous Damper

Barkanov [67] used a value of $C = 5.00E{-}04$ N.s/mm, but we noticed that as we increase the value above $5.00E{-}05$ N.s/mm, the first damped frequency start decreasing and eventually goes to zero at $C = 5.00E{-}04$ N.s/mm. This lead us to study a homogeneous beam with an end viscous damper and its equivalent single degree of freedom (SDOF) model included in Appendix A. It can be concluded that as we increase C above critical damping value, the imaginary part of the complex eigenvalue goes to zero. This implies that the damped natural frequency vanishes at the critical value of C.

The viscoelastic beam considered by Barkanov [67] has the following geometric and material properties: $h_1 = 1.45$mm; $E_1 = 127$GPa; $\rho_1 = 1900$ kg/m^3; ; $\eta_1 = 0.0029$; $h_2 = 0.127$mm; $E_2 = 0.00176$GPa; $\rho_1 = 980$kg/m^3; $\nu_2 = 0.49$; $\eta_2 = 0.87$; $h_3 = 0.254$mm; $E_3 = 69$GPa; $\rho_3 = 2760$kg/m^3; $\nu_3 = 0.32$; $\eta_3 = 0.033$; $W = 19.05$mm; $L = 203.2$mm.

We first considered a viscoelastic sandwich beam without a lumped viscous damper. We noticed that we get nodes for each mode, along the length of the beam, for which displacement goes to zero during cyclic oscillations. Figure 2.8 shows displacements for 2^{nd} mode during the one half cycle. Next, we neglected the loss factors in each layer of the cantilever beam and applied a viscous damper at the right end as shown in Fig. 2.7. we noticed that in this case, we do not get a single point along the beam where all the displacements go to zero during one half cycle as shown in Fig. 2.9. Moreover, it was noticed that the dispersion of zero displacement points, for higher modes, is wider near the right end of the beam, where

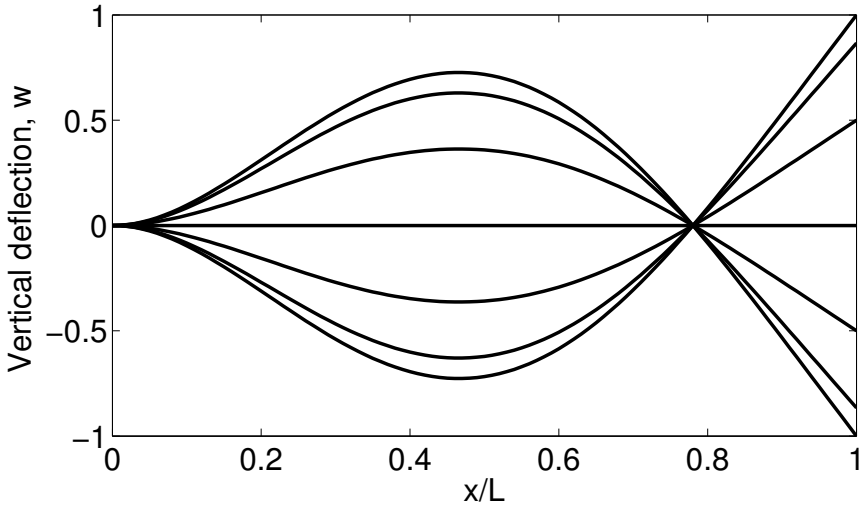

Figure 2.8: Displacement of Viscoelastic Sandwich Cantilever Beam at Different Times of Cyclic Oscillations

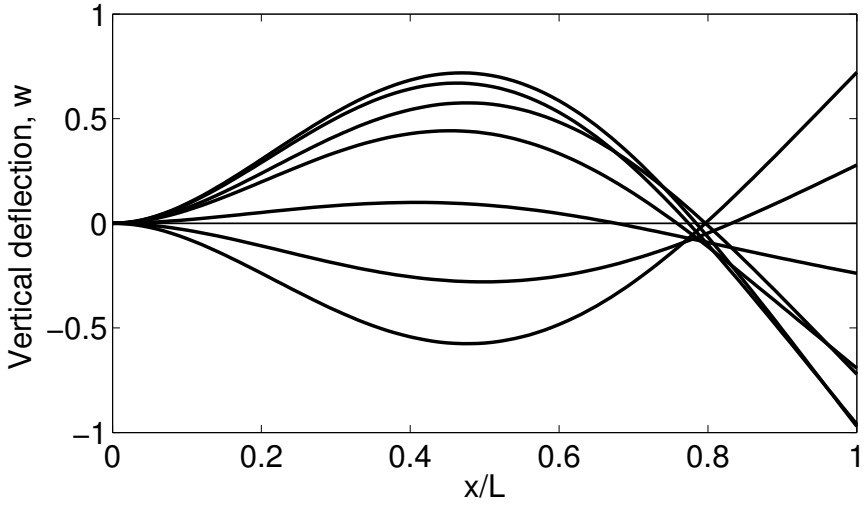

Figure 2.9: Displacement of Sandwich Cantilever Beam with End Viscous Damper at Different Times of Cyclic Oscillations, $\eta = 0$

viscous damper is mounted. Viscous damping value was considered to be $5.00E{-}05$ N.s/mm.

As a last case, we considered viscoelastic damped sandwich beam using both loss factor in each layer and right end viscous damper. As can be seen from Fig. 2.10, we again do

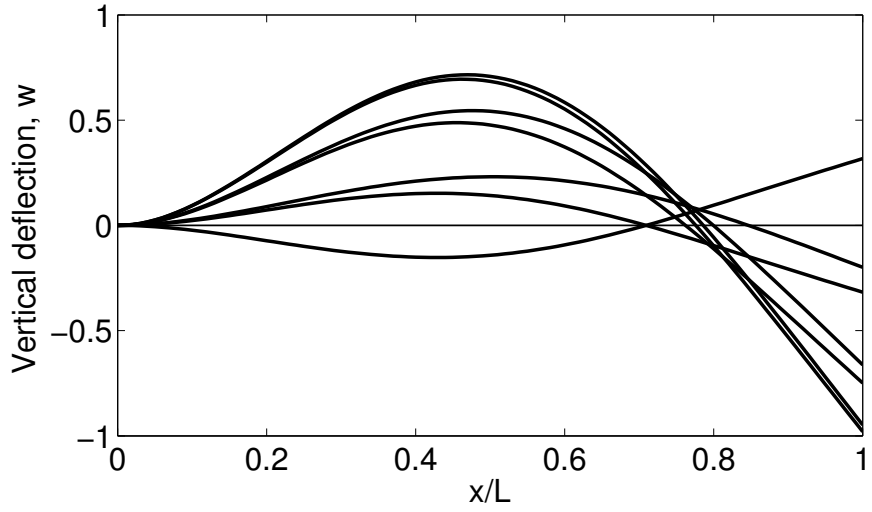

Figure 2.10: Displacement of Viscoelastic Sandwich Cantilever Beam with End Viscous Damper at Different Times of Cyclic Oscillations

not get stationary points along the beam and the dispersion of zero displacement points was wider than when only a viscous damper considered. It was also found that for higher modes this dispersion becomes smaller and we again start seeing stationary nodes along the length of the beam.

2.6 Conclusions

The investigation of sandwich beams with different boundary conditions helped us obtain good estimates of natural frequencies and loss factors by using trigonometric functions as compared to using simple polynomials, by using less number of terms in PVW. We found that higher degree elements used in the FE elasticity analysis, gives us better estimates of the loss factor and the natural frequency unlike using the beam elements, especially in the problem in which we consider complex stiffness in the elastic layers. Moreover, MCE method gives accurate results but with higher computational cost, especially when a fine mesh in considered. MSE is a cost-effective method but for damping treatments with high loss factors, it overestimates the overall damping of the system.

Furthermore, we observed that although the eigenvalues and eigenvectors are complex in

the case of constrained viscoelastic layer damping, we still get stationary nodes unlike non-proportional viscously damped structures. Despite the fact that constrained layer treatment can be quite damped, mode shapes are close to normal modes, and it can be concluded that viscoelastic damping is very close to being proportional. On the other hand, in the case of a viscoelastic damped sandwich beam with end viscous damper, it was noticed that we do not get a single point along the length of the beam where the displacement goes to zero at different times during cyclic oscillations, i.e. the concept of having a node at a point at all times does not exist. Moreover, the mode shapes of the lower modes of a beam with a viscous damper at the free end are more sensitive to the viscous damping coefficient. The complexity of a mode shape is smaller for higher modes of the beam with a viscous damper at the end.

Chapter 3

Free Vibration Analysis of An Integrally Stiffened Plate

3.1 Introduction

Stiffened structures have been extensively studied in the published literature to avoid critical frequencies and provide local stiffness to the structure. In these structures, no consideration is given to the damping in the material. These stiffened panels as well as the stepped plates are widely used in the aerospace, ship and automobile industries; and investigation of damping can greatly help in controlling vibration and noise, general safety and consumer experience. Although, rib-type stiffeners can alter the response of a structure to external excitations by providing appropriate stiffness, but it is difficult to incorporate enough quantity of viscoelastic material to achieve high damping due to the small cross-sectional area of the rib stiffeners. In view of this, we wanted to investigate the response of a plate structure with adhesively bonded plate-type stiffeners. In this way, we will be able to add more damping to the system utilizing viscoelastic material.

As a first step, we wanted to investigate the response of an integrally stiffened plate with plate-strip stiffeners and/or stepped plate, without considering viscoelastic damping. Stepped plates can be used in the aerospace industry where weight, material saving, structural frequency and local stiffness are of great importance [70, 71]. A considerable amount of

research has been conducted in the past decade on the vibration and buckling response of stepped plates. Moreover, these structural elements have been effectively used in certain parts of the vehicles in the automotive industry because of their light weight and high-strength structural properties [72].

In this chapter, we investigated the natural frequencies and mode shapes of a freely vibrating, integrally stiffened and/or stepped plate. We used the layerwise first-order shear deformation theory (FSDT), for both plate and stiffeners, which employs the transverse shear deformation and rotary inertias. The deflections and rotations were assumed to be a tensor product of static Timoshenko beam functions, chosen appropriately according to the given boundary conditions. The governing differential equations were solved using the Rayleigh-Ritz method. Unlike Navier and Levy's solution techniques, the approach used in this chapter can also be applied to fully clamped, free and cantilever supported stiffened plates.

Development of stiffness and mass matrix consumes huge amount of CPU time due to integration of beam functions, which are sets of trigonometric functions, especially when solving for clamped-clamped and clamped-free boundary conditions. A technique is suggested to significantly decrease the amount of CPU time, by avoiding the recursive integration in a loop structure in the computer program. The integrand was symbolically integrated using MATLAB® once, and the solution was obtained in terms of the iteration symbols used in the loop structure. The details of this technique can be found in Section 3.5.

The numerical results were compared with the exact solutions available in the literature and the commercially available finite element software ABAQUS®, and the results were found to be highly satisfactory. Some parametric studies were carried out to show the influence of certain important parameters on the overall natural frequencies of the stiffened plate.This work was presented in 56th AIAA Structural Dynamics and Materials (SDM) Conference [73] and was subsequently published in the AIAA Journal [74].

Chopra [75] provided an exact solution for the vibration of thin isotropic rectangular stepped plates using the classical plate theory (CPT). This study was amongst the first few investigations of a stepped plate; however, only simply-supported boundary conditions were considered. The procedure involved dividing the non-uniform stepped plate into uniform plates of different thicknesses, and then applying the continuity conditions at the interface

between two plates. This method is commonly referred to as the classical method in the published literature.

Guo, Keane and Mosherefi-Torbati [76] pointed out that the continuity conditions used by Chopra [75] must be changed before being used for stepped plates having different materials. They also noted the complications in solving the eigenvalue problem for higher modes using the classical method. Guo, Keane and Mosherefi-Torbati [76] made use of the improved classical finite strip method (FSM), that proved to be more accurate and efficient, particularly for the case of higher modes. The improvements in FSM were introduced by using dynamic shape functions instead of normally used static functions. Again, only simply-supported boundary conditions were considered in the analysis.

Boscolo and Banerjee [77] developed dynamic stiffness elements, for plates with uniform/non-uniform thicknesses, that can be used to provide exact analytical solutions. They reported results using both CPT as well as first order shear deformation theory (FSDT). The dynamic stiffness method (DSM) makes use of the exact closed form solution of the structure's differential equations, to obtain a dynamic frequency dependent stiffness matrix, that contains both mass and stiffness properties. This approach can only solve for plates, which have two opposite edges as simply-supported. The complications in developing the dynamic stiffness elements for non-uniform plates, as well as the method leading to non-linear eigenvalue problem presents some disadvantages of DSM.

Hull and Buchanan [70] used FSDT and finite element analysis to study the vibration of thick orthotropic stepped plates. Duan and Wang [71] used a discrete singular convolution (DSC) algorithm for the vibration analysis of thin rectangular stepped plates using interpolation polynomials on each step. Two jump and continuity conditions at the interface were used to connect the two steps in the plate. Demasi and Yu [78] used invariant axiomatic scheme called as generalized unified formulation, to assess the variational asymptotic plate and shell analysis (VAPAS). They considered sandwich structures with high face to core stiffness ratios, and found out that VAPAS with one equivalent single-layer theory, attains comparable accuracy to various fourth order zig-zag and layerwise theories.

Kapania and Liu [79] developed an equivalent plate model for handling discontinuities in general built-up wing structures. Specific example such as free vibration analysis of a clamped

trapezoidal plate with nonuniform thickness was considered in the study. The problem was formulated using FSDT and analyzed by Ritz method utilizing Legendre polynomials. Kapania and Lovejoy [80] employed FSDT and Chebychev polynomials in the Rayleigh-Ritz method for the free vibrational analysis of thick laminated discontinuous quadrilateral plates with cantilever boundary conditions.

Yuceoglu, Javanshir, and Güvendik [72, 81] investigated the free vibration response of an integrally stiffened rectangular plate with central and non-central plate-strip stiffeners. The procedure was built on Levy's solution and FSDT was used to obtain the governing equations of motion. Both orthotropic and isotropic materials were considered for the stiffened plate. The governing equations were reduced to first order ordinary differential equations and then solved by using modified transfer matrix method utilizing interpolation polynomials. Yuceoglu, Germalmayan, and Sunar [82] used the same procedure to study the free vibration response of an integrally stiffened rectangular plate with non-central plate stiffener. Moreover, Javanshir, Farsadi, and Yuceoglu [83] and Yuceoglu and Özerciyes [84], utilized this procedure to study the free vibration of a bonded stiffened plate with plate-strip stiffeners.

3.2 Mathematical Formulation for the Stiffened Plate

Consider an isotropic thick rectangular plate with stiffeners on both top and bottom surfaces of the plate as shown in Figure 3.1. The material properties of the stiffened plate are given by Young's modulus E, the shear modulus of rigidity $G = E/[2(1+\nu)]$ and the Poisson's ratio ν. The thickness of the stiffened plate in the y-direction does not change. We will use the principle of virtual work for plate and stiffeners separately, to independently evaluate the mass and stiffness matrix for the stiffener. This will help us in formulating problems with different materials for the plate and stiffeners. Based on the first order shear deformation layerwise theory, the displacements and rotations in the plate are assumed in the following form, as shown in Figure 3.2:

$$u^{(2)}(x,y,z,t) = u_0^{(2)}(x,y,t) + z^{(2)}\phi_x^{(2)}(x,y,t) \tag{3.1}$$

$$v^{(2)}(x,y,z,t) = v_0^{(2)}(x,y,t) + z^{(2)}\phi_y^{(2)}(x,y,t) \tag{3.2}$$

$$w^{(2)}(x,y,z,t) = w_0(x,y,t) \tag{3.3}$$

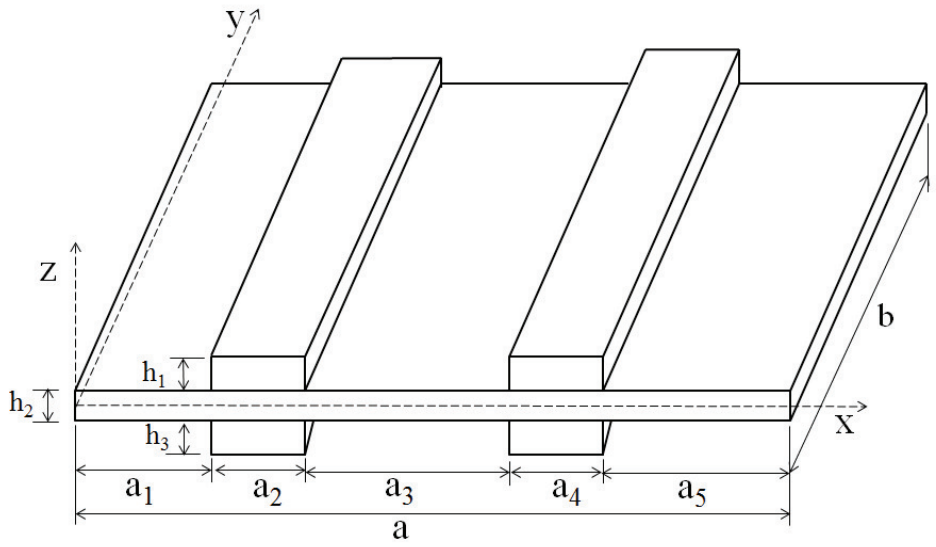

Figure 3.1: Schematic of a Stiffened Rectangular Plate

where u, v, w are displacements in the x, y, and z-direction, respectively, the subscript 0 refers to the displacement of the middle surface of the plate and ϕ_x and ϕ_y are the rotations about the y and x axis, respectively. The deformation in the thickness direction is assumed to be zero, therefore w is independent of the z-direction. It should be noted that same transverse deflection will be used for both plate and stiffener.

Similarly, the displacements and rotations in the stiffeners are assumed in the following form:

$$u^s(x,y,z,t) = u_0^s(x,y,t) + z^s\phi_x^s(x,y,t) \tag{3.4}$$

$$v^s(x,y,z,t) = v_0^s(x,y,t) + z^s\phi_y^s(x,y,t) \tag{3.5}$$

$$w^s(x,y,z,t) = w_0(x,y,t) \tag{3.6}$$

Superscripts p and s will be used for the plate and the stiffener, respectively, throughout this chapter. At the interface between the plate and the stiffener, we exploit the continuity of displacements for the stiffener on the top surface of the plate as shown in Figure 3.2:

$$u_0^{(2)} + \frac{h_2}{2}\phi_x^{(2)} = u_0^{(1)} - \frac{h_1}{2}\phi_x^{(1)} \tag{3.7}$$

$$v_0^{(2)} + \frac{h_2}{2}\phi_y^{(2)} = v_0^{(1)} - \frac{h_1}{2}\phi_y^{(1)} \tag{3.8}$$

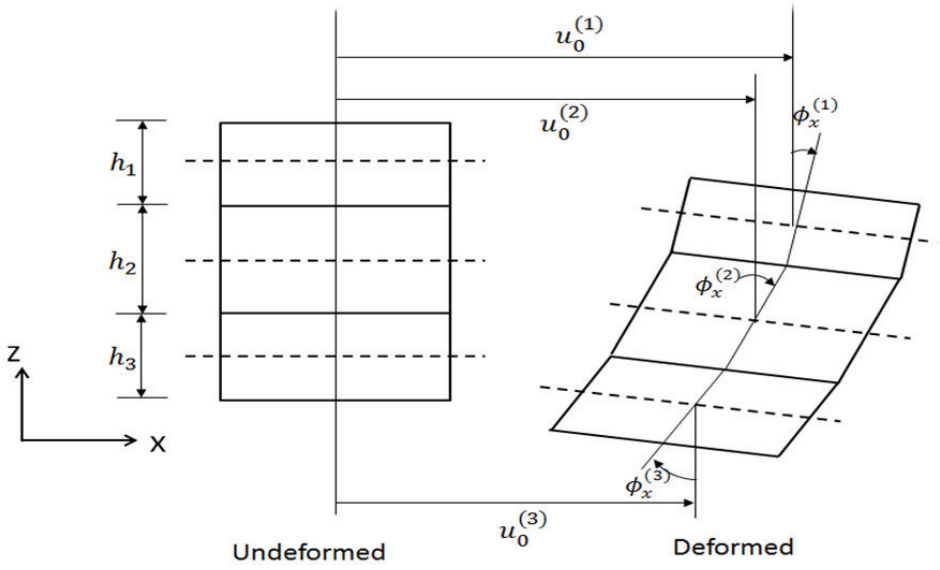

Figure 3.2: Undeformed and Deformed Sections of the Stiffened Plate

So, we can say that,

$$u_0^{(1)} = u_0^{(2)} + \frac{h_2}{2}\phi_x^{(2)} + \frac{h_1}{2}\phi_x^{(1)} \tag{3.9}$$

$$v_0^{(1)} = v_0^{(2)} + \frac{h_2}{2}\phi_y^{(2)} + \frac{h_1}{2}\phi_y^{(1)} \tag{3.10}$$

Equations (3.9) and (3.10) shows that we can equate the in-plane displacements of the middle layer of the stiffener, in terms of the in-plane displacements of the middle layer and rotation of the plate. Thus, we can write the displacement field for the stiffener on the top surface of the plate as:

$$u^{(1)} = u_0^{(2)} + \frac{h_1}{2}\phi_x^{(1)} + \frac{h_2}{2}\phi_x^{(2)} + z^{(1)}\phi_x^{(1)} \tag{3.11}$$

$$v^{(1)} = v_0^{(2)} + \frac{h_1}{2}\phi_y^{(1)} + \frac{h_2}{2}\phi_y^{(2)} + z^{(1)}\phi_y^{(1)} \tag{3.12}$$

$$w^{(1)} = w_0 \tag{3.13}$$

Similarly, for the stiffener on the bottom surface of the plate, the displacement field can be given as:

$$u^{(3)} = u_0^{(2)} - \frac{h_3}{2}\phi_x^{(3)} - \frac{h_2}{2}\phi_x^{(2)} + z^{(3)}\phi_x^{(3)} \tag{3.14}$$

$$v^{(3)} = v_0^{(2)} - \frac{h_3}{2}\phi_y^{(3)} - \frac{h_2}{2}\phi_y^{(2)} + z^{(3)}\phi_y^{(3)} \tag{3.15}$$

$$w^{(3)} = w_0 \tag{3.16}$$

3.2.1 The Principle of Virtual Work for the Plate

Components of strain at a point in the plate according to the Green-Lagrange definition of infinitesimal strain, can be given as:

$$\varepsilon_{xx} = \frac{\partial u_0}{\partial x} + z\frac{\partial \phi_x}{\partial x} \tag{3.17}$$

$$\varepsilon_{yy} = \frac{\partial v_0}{\partial y} + z\frac{\partial \phi_y}{\partial y} \tag{3.18}$$

$$\gamma_{xy} = \frac{\partial u_0}{\partial y} + \frac{\partial v_0}{\partial x} + z\frac{\partial \phi_x}{\partial y} + z\frac{\partial \phi_y}{\partial x} \tag{3.19}$$

$$\gamma_{xz} = \phi_x + \frac{\partial w_0}{\partial x} \tag{3.20}$$

$$\gamma_{yz} = \phi_y + \frac{\partial w_0}{\partial y} \tag{3.21}$$

Stresses and strains in the plate are related by the material property matrix as:

$$\begin{Bmatrix} \sigma_{xx} \\ \sigma_{yy} \\ \tau_{xy} \\ \tau_{xz} \\ \tau_{yz} \end{Bmatrix} = \begin{bmatrix} \frac{E}{(1-\nu^2)} & \frac{\nu E}{(1-\nu^2)} & 0 & 0 & 0 \\ \frac{\nu E}{(1-\nu^2)} & \frac{E}{(1-\nu^2)} & 0 & 0 & 0 \\ 0 & 0 & G & 0 & 0 \\ 0 & 0 & 0 & \kappa G & 0 \\ 0 & 0 & 0 & 0 & \kappa G \end{bmatrix} \begin{Bmatrix} \varepsilon_{xx} \\ \varepsilon_{yy} \\ \gamma_{xy} \\ \gamma_{xz} \\ \gamma_{yz} \end{Bmatrix} \tag{3.22}$$

where κ is the shear correction factor normally used along with the first order shear deformation theory (FSDT).

The virtual work done by the internal stresses in the plate can be expressed as:

$$\delta W_i = \int_V [\sigma_{xx}\delta\varepsilon_{xx} + \sigma_{yy}\delta\varepsilon_{yy} + \tau_{xy}\delta\gamma_{xy} + \tau_{xz}\delta\gamma_{xz} + \tau_{yz}\delta\gamma_{yz}]dV \tag{3.23}$$

By using the d'Alembert's principle, the virtual work due to the inertial forces can be written as:

$$\delta W_{inertial} = \rho \int_V [(\ddot{u}_0 + z\ddot{\phi}_x)\delta(u_0 + z\phi_x) + (\ddot{v}_0 + z\ddot{\phi}_y)\delta(v_0 + z\phi_y) + \ddot{w}_0\delta w_0]dV \tag{3.24}$$

It should be noted here that we used rotational as well as the in-plane inertia, in determining the virtual work due to inertial forces.

3.2.2 The Principle of Virtual Work for the Stiffener

Components of strain in the stiffener, on the top surface of the plate, according to the Green-Lagrange definition of infinitesimal strain, can be given as:

$$\varepsilon_{xx}^{(1)} = \frac{\partial u_0^{(2)}}{\partial x} + \frac{h_1}{2}\frac{\partial \phi_x^{(1)}}{\partial x} + \frac{h_2}{2}\frac{\partial \phi_x^{(2)}}{\partial x} + z^{(1)}\frac{\partial \phi_x^{(1)}}{\partial x} \tag{3.25}$$

$$\varepsilon_{yy}^{(1)} = \frac{\partial v_0^{(2)}}{\partial y} + \frac{h_1}{2}\frac{\partial \phi_y^{(1)}}{\partial y} + \frac{h_2}{2}\frac{\partial \phi_y^{(2)}}{\partial y} + z^{(1)}\frac{\partial \phi_y^{(1)}}{\partial y} \tag{3.26}$$

$$\begin{aligned}\gamma_{xy}^{(1)} = {} & \frac{\partial u_0^{(2)}}{\partial y} + \frac{h_1}{2}\frac{\partial \phi_x^{(1)}}{\partial y} + \frac{h_2}{2}\frac{\partial \phi_x^{(2)}}{\partial y} + z^{(1)}\frac{\partial \phi_x^{(1)}}{\partial y} \\ & + \frac{\partial v_0^{(2)}}{\partial x} + \frac{h_1}{2}\frac{\partial \phi_y^{(1)}}{\partial x} + \frac{h_2}{2}\frac{\partial \phi_y^{(2)}}{\partial x} + z^{(1)}\frac{\partial \phi_y^{(1)}}{\partial x}\end{aligned} \tag{3.27}$$

$$\gamma_{xz}^{(1)} = \phi_x^{(1)} + \frac{\partial w_0}{\partial x} \tag{3.28}$$

$$\gamma_{yz}^{(1)} = \phi_y^{(1)} + \frac{\partial w_0}{\partial y} \tag{3.29}$$

The virtual work done by the internal stresses in the stiffener can be expressed as:

$$\delta W_i = \int_V \left[\sigma_{xx}\delta\varepsilon_{xx} + \sigma_{yy}\delta\varepsilon_{yy} + \tau_{xy}\delta\gamma_{xy} + \tau_{xz}\delta\gamma_{xz} + \tau_{yz}\delta\gamma_{yz}\right] dV \tag{3.30}$$

By using the d'Alembert's principle, the virtual work due to the inertial forces can be written as:

$$\begin{aligned}\delta W_{inertial} = \int_V \rho \Bigg[& \left(\ddot{u}_0^{(2)} + \frac{h_1}{2}\ddot{\phi}_x^{(1)} + \frac{h_2}{2}\ddot{\phi}_x^{(2)} + z^{(1)}\ddot{\phi}_x^{(1)}\right)\delta\left(u_0^{(2)} + \frac{h_1}{2}\phi_x^{(1)} + \frac{h_2}{2}\phi_x^{(2)}\right. \\ & \left. + z^{(1)}\phi_x^{(1)}\right) + \left(\ddot{v}_0^{(2)} + \frac{h_1}{2}\ddot{\phi}_y^{(1)} + \frac{h_2}{2}\ddot{\phi}_y^{(2)} + z^{(1)}\ddot{\phi}_y^{(1)}\right)\delta\left(v_0^{(2)} + \frac{h_1}{2}\phi_y^{(1)}\right. \\ & \left. + \frac{h_2}{2}\phi_y^{(2)} + z^{(1)}\phi_y^{(1)}\right) + \ddot{w}_0\delta w_0\Bigg] dV\end{aligned} \tag{3.31}$$

Similarly, the principle of virtual work can be used for stiffeners on the bottom surface of the plate. In the absence of external forces, the principle of virtual work for the entire structure can be obtained by using Eqs. (3.23),(3.24),(3.30) and (3.31) as:

$$\left(\delta W_i^p + \sum_{m=1}^{B}\left(\delta W_i^s\right)_m\right) + \left(\delta W_{inertial}^p + \sum_{m=1}^{B}\left(\delta W_{inertial}^s\right)_m\right) = 0 \tag{3.32}$$

where B is the number of stiffeners used in the analysis.

3.3 Timoshenko Beam Functions

Huang [85] provided vibrating Timoshenko beam functions by solving the coupled equations of a Timoshenko beam for various boundary conditions and harmonic loads. The coefficients involved in these beam functions were dependent on the plate geometric and material properties as well as boundary conditions. Dawe and Roufaeil [86] used Rayleigh-Ritz method to analyze Mindlin plates by using a series of products of these vibrating Timoshenko beam functions for various boundary conditions. The results obtained by using these beam functions were found to be accurate with a small number of terms in the Ritz method.

The major disadvantage of using these vibrating Timoshenko beam functions is to solve a transcendental equation for determining the coefficients involved in these functions. With a change in the geometric properties and/or boundary conditions, one has to solve for coefficients in these beam functions and this makes the whole process cumbersome. Cheung and Zhou [87] came up with a solution to this issue by developing static Timoshenko beam functions. The advantage of utilizing these static Timoshenko beam functions is two-fold; we do not have to solve a transcendental equation for obtaining coefficients in the beam functions for every changing boundary condition and a single program can be written for plates with arbitrary boundary conditions and thicknesses. Cheung and Zhou [87] called these functions to be static Timoshenko beam functions, because they were obtained by solving a static Timoshenko beam problem, with static loads. We will use these static Timoshenko beam functions in our analysis. A quick overview of these functions is given below, details can be found in the paper by Cheung and Zhou. [87]

Consider a uniform beam of length L, area of cross-section A, Young's modulus E, shear modulus G, Poisson's ratio ν and shear correction factor κ. For a Timoshenko beam, the vertical deflection w, and the rotation of the cross-section ϕ, can be written in the non-dimensional form as follows:

$$w(\xi) = \sum_{i=1}^{\infty} a_i W_i(\xi), \qquad \phi(\xi) = \sum_{i=1}^{\infty} b_i \Phi_i(\xi) \tag{3.33}$$

where $\xi = x/L$, and W and Φ are the spatial variations of w and ϕ, respectively. According to Cheung and Zhou [87], these spatial variations can be obtained as follows, by solving the differential equation of motion of Timoshenko beam under a series of sinusoidal distributed

loads.

$$W_i(\xi) = C_0^i + C_1^i\xi + C_2^i\xi^2/2 + C_3^i(\xi^3/6 - R\xi) + [R(i\pi)^2 + 1]\sin(i\pi\xi) \tag{3.34}$$

$$\Phi_i(\xi) = C_1^i + C_2^i\xi + C_3^i\xi^2/2 + (i\pi)\cos(i\pi\xi) \tag{3.35}$$

where $R = (EI)/(GA\kappa L^2)$, and constants C_j depend on the boundary conditions and can be obtained from Table 3.1, reported by Cheung and Zhou [87]. Clamped (C), simply-supported (S), and free (F), boundary conditions are considered here. It should be noted that for beams with S-S, S-C, C-S, C-C, C-F and F-C boundary conditions, Eqs. (3.34) and (3.35) can be used as admissible functions in the Ritz method. [87] But when solving for S-F and F-S boundary conditions, Eqs. (3.34) and (3.35) can be used as the second and higher admissible functions because of the presence of rigid body modes. To account for rigid body modes Eqs. (3.34) and (3.35) should be augmented with first admissible functions, such as for S-F boundary conditions:

$$w_1 = \xi, \qquad \Phi_1 = 1 \tag{3.36}$$

and for F-S boundary condition:

$$w_1 = \xi - 1, \qquad \Phi_1 = 1 \tag{3.37}$$

For free-free boundary conditions, Eqs. (3.34) and (3.35) can be used as the third and higher admissible functions because of the presence of two rigid body modes. The first and second admissible functions can be given as follows, [87]

$$\begin{aligned} w_1 &= 1, & \Phi_1 &= 0 \\ w_2 &= \xi - 0.5, & \Phi_2 &= 1 \end{aligned} \tag{3.38}$$

3.4 Ritz Analysis of the Stiffened Plate

On the assumption of harmonic vibration, we can write the displacements and rotations for the plate in the form:

$$u_0(x, y, t) = U(x, y)e^{i\omega t} \tag{3.39}$$

$$v_0(x, y, t) = V(x, y)e^{i\omega t} \tag{3.40}$$

Table 3.1: Coefficients of the Static Timoshenko Beam Functions

Boundary Conditions	C_0^m	C_1^m	C_2^m	C_3^m
C-C	0	$-m\pi$	$2m\pi[1+\{1+(-1)^m\}$ $\times(1-6R)/(1+12R)]$	$-6m\pi\{1+(-1)^m\}/(1+12R)$
C-S	0	$-m\pi$	$3m\pi/(1+3R)]$	$-3m\pi/(1+3R)$
S-C	0	$(-1)^m m\pi(1-6R)/(2+6R)]$	0	$-3(-1)^m m\pi/(1+3R)$
C-F	0	$-m\pi$	$-(-1)^m(m\pi)^3$	$(-1)^m(m\pi)^3$
F-C	$m\pi[(-1)^m+$ $(m\pi)^2(1/3+R)]$	$-m\pi\{(-1)^m+(m\pi)^2/2\}$	0	$(m\pi)^3$
S-S	0	0	0	0

$$w_0(x,y,t) = W(x,y)e^{i\omega t} \tag{3.41}$$

$$\phi_x(x,y,t) = \Phi_x(x,y)e^{i\omega t} \tag{3.42}$$

$$\phi_y(x,y,t) = \Phi_y(x,y)e^{i\omega t} \tag{3.43}$$

where $U(x,y)$, $V(x,y)$, $W(x,y)$, $\Phi_x(x,y)$, $\Phi_y(x,y)$ are the spatial variations of $u(x,y,t)$, $v(x,y,t)$, $w(x,y,t)$, $\phi_x(x,y,t)$, and $\phi_y(x,y,t)$, respectively. Dawe and Roufaeil [86] reported that for any type of boundary condition, the spatial variation of $\Phi_x(x,y)$ in the y-direction is equivalent to the spatial variation of $W(x,y)$ in the y-direction and in the same manner the variation of $\Phi_y(x,y)$ in the x-direction is equal to the variation of $W(x,y)$ in the x-direction. These spatial variations can be written as a product of unidirectional functions by using separation of variables:

$$U(x,y) = \sum_{m=1}^{M}\sum_{n=1}^{N} a_{mn}U_m(x)U_n(y) \tag{3.44}$$

$$V(x,y) = \sum_{m=1}^{M}\sum_{n=1}^{N} b_{mn}V_m(x)V_n(y) \tag{3.45}$$

$$W(x,y) = \sum_{m=1}^{M}\sum_{n=1}^{N} c_{mn}W_m(x)W_n(y) \tag{3.46}$$

$$\Phi_x(x,y) = \sum_{m=1}^{M}\sum_{n=1}^{N} d_{mn}\Phi_m(x)W_n(y) \tag{3.47}$$

$$\Phi_y(x,y) = \sum_{m=1}^{M}\sum_{n=1}^{N} e_{mn}W_m(x)\Phi_n(y) \tag{3.48}$$

where M and N are the total number of terms considered in the x and y-direction, respectively. It should be noted that the five coefficients, the so-called generalized co-ordinates, **a**,**b**,**c**,**d**, and **e** are arbitrary as well as independent from each other. By using these displacement functions in Eqs. (3.23) and (3.24), we can obtain the stiffness and the mass matrices for the plate. The size of both of these matrices will be 5×M×N.

The static Timoshenko beam functions from Section 3.3 can be used as admissible functions in Eqs. (3.46-3.48) for $W_m(x)$, $W_n(y)$, $\Phi_m(x)$and $\Phi_n(y)$. As far as $U_m(x)$, $U_n(y)$, $V_m(x)$, and $V_n(y)$ are concerned, a combination of trigonometric functions such as cosine and

sine, can be used to satisfy the specified boundary conditions in Eqs. (3.44) and (3.45). For example,

For simply-supported plate (SS-SS-SS-SS):

$$U_m(x) = \cos(i\pi x) \tag{3.49}$$

$$U_n(y) = \sin(i\pi y) \tag{3.50}$$

$$V_m(x) = \sin(i\pi x) \tag{3.51}$$

$$V_n(y) = \cos(i\pi y) \tag{3.52}$$

For a fully clamped plate (C-C-C-C):

$$U_m(x) = \sin(i\pi x) \tag{3.53}$$

$$U_n(y) = \sin(i\pi y) \tag{3.54}$$

$$V_m(x) = \sin(i\pi x) \tag{3.55}$$

$$V_n(y) = \sin(i\pi y) \tag{3.56}$$

For a plate with simply-supported and fixed edges (SS-C-SS-C):

$$U_m(x) = \cos(i\pi x) \tag{3.57}$$

$$U_n(y) = \sin(i\pi y) \tag{3.58}$$

$$V_m(x) = \sin(i\pi x) \tag{3.59}$$

$$V_n(y) = \sin(i\pi y) \tag{3.60}$$

For a cantilever supported plate (C-F-F-F):

$$U_m(x) = V_m(x) = 1 - \cos\left(\frac{(2i-1)\pi x}{2}\right) \tag{3.61}$$

$$U_n(y) = V_n(y) = \cos(i\pi y) \tag{3.62}$$

For a free plate (F-F-F-F):

$$U_m(x) = \cos(i\pi x) \tag{3.63}$$

$$U_n(y) = \cos(i\pi y) \tag{3.64}$$

$$V_m(x) = \cos(i\pi x) \tag{3.65}$$

$$V_n(y) = \cos(i\pi y) \tag{3.66}$$

It should be noted from Section 3.2, that the in-plane displacements, u and v, of the stiffeners were written interms of the in-plane displacements of the plate. Moreover, we assumed that the plate and stiffeners have the same vertical deflection. So the only independent degree of freedom for the stiffeners are the rotations, Φ_x^s and Φ_y^s. We considered two different cases: first, we assumed that the rotations of the plate and the stiffeners are the same i.e., $\Phi_x^s = \Phi_x^p$ and $\Phi_y^s = \Phi_y^p$. The rotational terms of the stiffeners were added to the rotational terms of the plate, as they are no more independent degrees of freedom. By using this assumption, the overall size of the assembly matrices was 5×M×N.

Next, we considered different rotations for the plate and the stiffeners i.e., $\Phi_x^s \neq \Phi_x^p$ and $\Phi_y^s \neq \Phi_y^p$. In this case, we will have 5×M×N size for the plate's mass and stiffness matrices and 2×M×N for each stiffener, so the total size of the mass as well as the stiffness matrix for the entire structure with four stiffeners will be 13×M×N.

3.5 CPU Time Reduction Technique

Ritz method is widely used in the field of structural dynamics to analyze vibration and stresses in the system. The procedure implemented in this work and generally in the analysis of sandwich structures, Ritz method, specifically the generation of stiffness and mass matrices in it, can consume a large amount of CPU time especially when higher order and trigonometric functions are employed as admissible functions. The time taken during the analyses of a simply-supported uniform thickness square plate using FSDT and static Timoshenko beam functions is about 28.3 minutes, in order to calculate the stiffness and the mass matrices, for merely 5×5 terms used in the Ritz method. Table 3.1 clearly shows that to analyze structures with boundary conditions different than the simply-supported ones, the admissible functions become complicated, and hence require more computational time. For a fully clamped square plate with 5×5 terms used in the Ritz approximation, it takes 39.43 minutes to develop stiffness and mass matrices. Moreover, it is noticed that for a simply-supported square plate, we obtain converged results for lower modes using merely 4×4 terms as opposed to 15×15 terms used for fully clamped plate. This is because of the availability and use of exact solution

of the mode shape functions in developing the admissible functions for simply-supported plates. [87]

Most of the CPU time, utilized in calculating the mass and the stiffness matrices, is due to the accurate integration of trigonometric functions recurring in the loop. If we can avoid this integration, we can save a lot of CPU time. As discussed in Section 3.4, the admissible functions used in the Ritz approximation can be written as a product of unidirectional functions. For example, consider one of the integrals used in calculating the mass matrix. As the unidirectional functions are independent of each other, we can integrate them separately as:

$$I = \int_{\Omega} W_m(x,y) W_n(x,y) dA = \int_{\Omega} X_i(x) Y_j(y) X_p(x) Y_q(y) dA$$
$$I = \int_{a_1}^{a_2} X_i(x) X_p(x) dx \int_{b_1}^{b_2} Y_j(y) Y_q(y) dy \tag{3.67}$$

Instead of integrating the product of unidirectional functions over and over again, we can symbolically integrate it once using MATLAB or Mathematica and the resulting solution will be obtained in terms of the iteration symbols used in the loop.

$$I = \int_{0.3}^{0.4} \sin(i\pi x) \sin(j\pi x) dx \tag{3.68}$$

$$I = \begin{cases} 1/20 + [\sin(3i\pi/5) - \sin(4i\pi/5)]/(4i\pi) & \text{if } i = j, \\ [\sin(2\pi(j-i)/5) - \sin(3\pi(j-i)/10)]/[2\pi(j-i)] & \text{otherwise} \\ -[\sin(2\pi(j+i)/5) - \sin(3\pi(j+i)/10)]/[2\pi(j+i)] & \end{cases} \tag{3.69}$$

For example, Eq. 3.69 is obtained by symbolically integrating Eq. 3.68 using MATLAB. In this way, we can avoid unnecessary recursive integration and save a huge amount of CPU time. By implementing this procedure in our MATLAB code, it took only 0.13 seconds instead of 28.3 minutes for simply-supported square uniform thickness plate and 0.55 seconds as opposed to 39.4 minutes for fully clamped plate.

The above given CPU times were purely for a uniform thickness plate, if we consider a plate with four stiffeners it will take substantially large amount of CPU time to obtain converged results for the entire stiffened structure. By using the above time reduction tech-

nique, it took only 0.85 seconds to calculate the stiffness and the mass matrices for a simply-supported stiffened plate using 10×10 terms and 7.64 seconds for a clamped stiffened plate.

3.6 Results

To demonstrate the application of the above mentioned procedure utilizing static Timoshenko beam functions, a square plate with four stiffeners are considered in the study, as shown in Fig. 3.1. Natural Frequencies and mode shapes were obtained by implementing the above procedure in a MATLAB® program on a dual-core Macintosh 2.4 GHz Intel core i5 computer with 8GB RAM. The results obtained were compared to those available in the literature and the commercially available finite element software ABAQUS®. Convergence and some parametric studies for different boundary conditions are also reported in this section.

3.6.1 Free Vibration Analysis of a Square Stiffened Plate

Consider a square isotropic stiffened plate with four plate type stiffeners as shown in Fig. 3.1. Aluminum is considered as a material for both the stiffeners and the plate with the following material properties: Young's Modulus $E = 71.2$ GPa, Poisson's ratio $\nu = 0.3$, density $\rho = 2700$ kg/m^3. The dimensions of the stiffened plate are: $b = 1$m, $a/b = 1$, $a_1 = a_5 = 0.3a$, $a_2 = a_4 = 0.1a$, $a_3 = 0.2a$. For direct comparison with the results obtained by Boscolo and Banerjee [77], the natural frequencies (ω) are not non-dimensionalised and thickness dimensions are considered as: $t_1 = h_2$, $t_2 = h_1 + h_2 + h_3$. Two different ratios of stiffener to plate thickness $t_2/t_1 = 1.2$, and 1.5, and two different aspect ratios, $a/t_1 = 10$, and 1000, are used in this example. Shear correction factor $\kappa = 5/6$, was used in the analysis. SS-SS-SS-SS, SS-C-SS-C,C-C-C-C, F-F-F-F and C-F-F-F boundary conditions were considered in this study.

The natural frequencies obtained by following the procedure of this chapter are compared with those reported by Boscolo and Banerjee [77], who used dynamic stiffness matrix (DSM) approach to obtain the solution for stepped plates. DSM approach can only be used for stiffened plates with two opposite edges simply-supported and therefore no comparison is provided for C-C-C-C, F-F-F-F and C-F-F-F stiffened plate using this method. Results for

each boundary condition were also validated with 2D-shell and 3D finite element models using ABAQUS. Four noded S4R shell elements and a fine mesh of 100×100 elements was used for 2D-shell model in ABAQUS. A 20 noded quadratic brick, reduced integration, solid element (C3D20R) was used in the 3D model in ABAQUS. Each edge of the plate was divided into 67 equal parts, whereas 4 solid elements were used in the thickness direction of the plate. Similarly, 67 elements were used along the long edge, 7 along the width, and 1 element through the thickness of the stiffener. It should be noted that in the 3D solid model, the whole edge of the plate should be constrained, instead of only applying the boundary conditions to the middle line of the edge.

Ritz approximation, with 30×30 terms, using FSDT was used to get the converged frequencies for the case when $\phi^s = \phi^p$. Figure 3.3 shows the convergence of first and second natural frequency with respect to the number of terms used in the Ritz method for the stiffened plate, $a/t_1 = 10$, $t_2/t_1 = 1.5$ and $\phi^s = \phi^p$, with SS-SS-SS-SS and C-C-C-C boundary conditions, respectively. Moreover, for the case when the rotations of the plate and stiffener are different ($\phi^s \neq \phi^p$), 15×15 terms were used to get the converged natural frequencies. Figure 3.4 shows the convergence of first and second natural frequency for stiffened plate, $\phi^s \neq \phi^p$, with SS-SS-SS-SS and C-C-C-C boundary conditions, respectively.

Results for the aspect ratio $a/t_1 = 1000$ in Table 3.2, are shown here, just to compare with the results reported using classical method (CM) and DSM. The high aspect ratio of the plate suggest that CPT will suffice to obtain natural frequencies of the stiffened structure. Tables 3.3, 3.4, 3.5, 3.6, 3.7 and 3.8 present the results for first ten flexural natural frequencies(rad/s) of the stiffened plate, with two different ratios of stiffener to plate thickness $t_2/t_1 = 1.2$, and 1.5 and different boundary conditions. The CPU time spent for calculating the mass and the stiffness matrices for the stiffened plate was: 38 seconds for SS-SS-SS-SS, 47 seconds for F-F-F-F, 225 seconds for C-F-F-F, 275 for SS-C-SS-C, and 420 seconds for C-C-C-C boundary conditions. It should be noted that for F-F-F-F stiffened plate, we obtained five requisite rigid-body modes and the results presented in Table 3.7 are the natural frequencies corresponding to the deformed modes. Moreover, the percentage error is presented between the Ritz method for assuming the plate and stiffeners rotations to be the same rotations and those when assuming the two rotations to be different.

It can be noticed from Tables 3.3, 3.4, 3.5, 3.6, 3.7 and 3.8, that the percentage error between the two cases considered is approximately 2%. The nature of a specific application will determine the significance of this 2% inaccuracy. Moreover, the percentage error is less than 1%, for each boundary condition, compared to the results obtained using ABAQUS. Table 3.3 clearly reveals that the difference between Ritz method with same rotation and Ritz method with different rotations is less than 1%, when $t_2/t_1 = 1.2$. This difference increases to approximately 2%, when the thickness of the stiffeners is increased, as shown in Table 3.4. From this we can conclude that, when the thickness of stiffeners is small, we can use same rotations for the plate and stiffeners to get accurate results.

It can be noticed from the results for the stiffened plate with different boundary conditions, that we considered the two limiting casess i.e., $\phi^s = \phi^p$ and $\phi^s \neq \phi^p$. But it may happen that it is neither of both the cases and the actual results lie in between these two scenarios. To investigate this, we considered a running rotational constant, K_θ, in the formulation used for $\phi^s \neq \phi^p$, which was zero for the unconstrained case ($\phi^s \neq \phi^p$) and a very large number (essentially infinite) for the constrained case ($\phi^s = \phi^p$). The running rotational constant, K_θ, was included in the virtual work as follows,

$$\delta W_i = K_\theta \int [(\phi_x^p - \phi_x^s)\delta(\phi_x^p - \phi_x^s) + (\phi_y^p - \phi_y^s)\delta(\phi_y^p - \phi_y^s)]dxdy \tag{3.70}$$

It can be noticed from Table 3.9 that as we increase the value of K_θ from zero, $\phi^s \neq \phi^p$ case, the natural frequencies of the stiffened system increase towards the limiting case $\phi^s = \phi^p$. It is clear from Table 3.9 that we reach the limiting case $\phi^s = \phi^p$ at $K_\theta \approx 1.70E10$, as for more higher value of K_θ the natural frequencies were much higher than the $\phi^s = \phi^p$ case. Although, the results in Table 3.9 look promising and a specific value of K_θ can be used to get the required results, but the 3D results do not lie in between these two limiting cases. Unfortunately, we cannot come up with a strong reasoning by comparing our results with the 3D results, as we are using Ritz method with some assumptions.

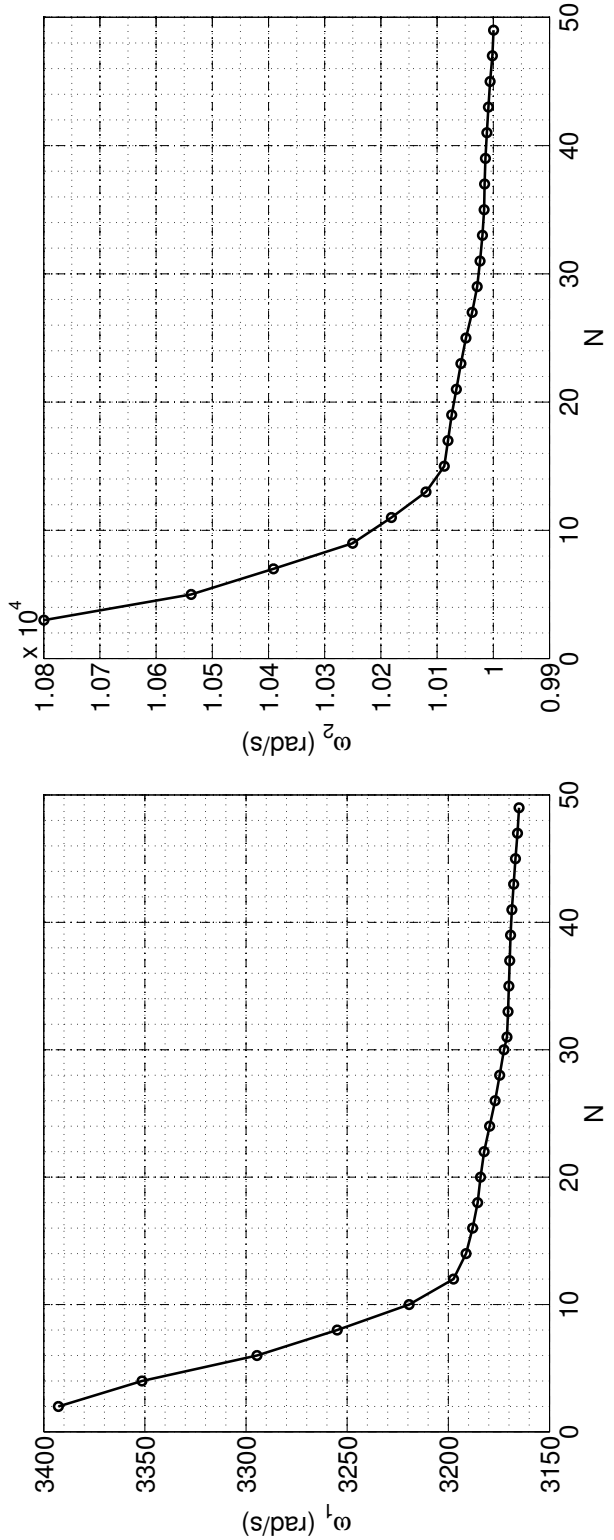

(b) 2^{nd} Natural Frequency; C-C-C-C

(a) Fundamental Frequency; SS-SS-SS-SS

Figure 3.3: Convergence of the Natural Frequencies for the Stiffened Plate, with Aspect Ratio; $a/t_1 = 10$ and Ratio of Stiffener to Plate Thickness; $t_2/t_1 = 1.5$, Against the Number of Terms Used (N) in the Ritz Method, With Same Rotations for Plate and Stiffeners ($\phi^s = \phi^p$).

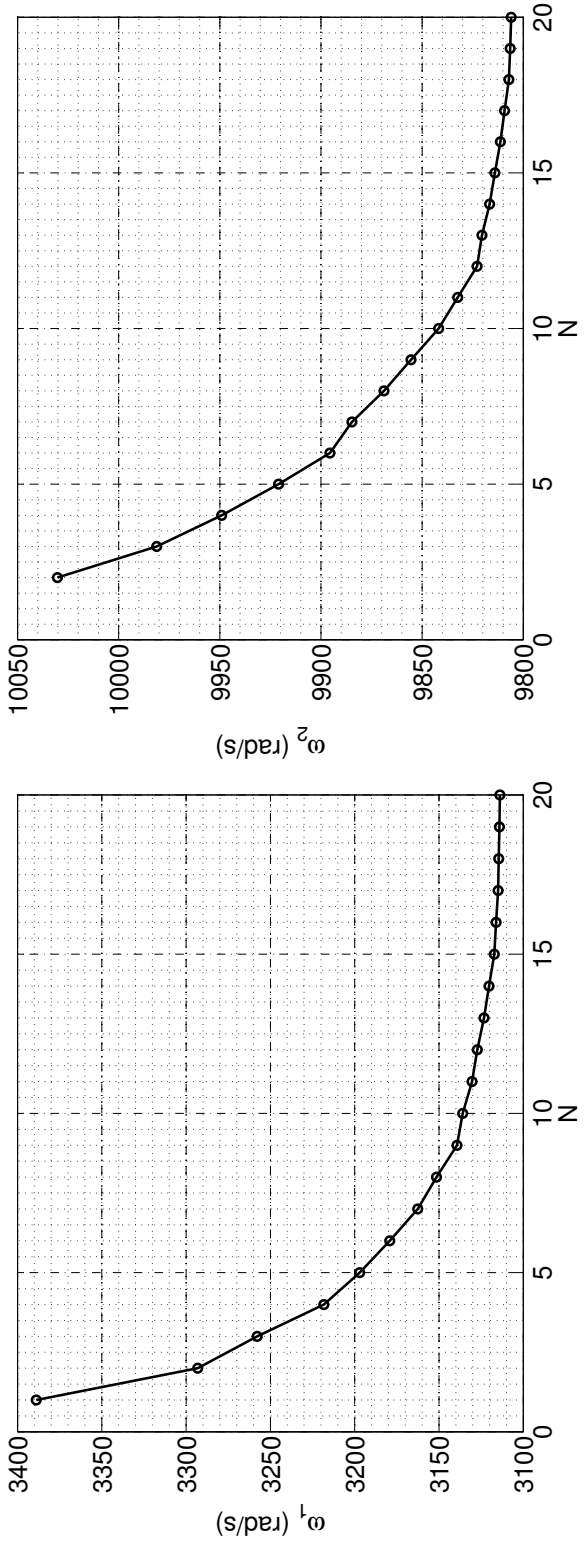

(a) Fundamental Frequency; SS-SS-SS-SS

(b) 2^{nd} Natural Frequency; C-C-C-C

Figure 3.4: Convergence of the Natural Frequencies for the Stiffened Plate, with Aspect Ratio; $a/t_1 = 10$ and Ratio of Stiffener to Plate Thickness; $t_2/t_1 = 1.5$, Against the Number of Terms Used (N) in the Ritz Method, With Different Rotations for Plate and Stiffeners ($\phi^s \neq \phi^p$).

Table 3.2: Comparison of Natural Frequencies(rad/s) for Square Stiffened plate with SS-SS-SS-SS Boundary Conditions, with aspect ratio $a/t_1 = 1000$ and $t_2/t_1 = 1.5$

Mode No.	CM	DSM [77]	ABAQUS 2D-Shell	Ritz Method $\phi^s = \phi^p$	ABAQUS 3D	Ritz Method $\phi^s \neq \phi^p$	Difference (%)
1	33.17	33.17	33.17	33.31	33.18	33.45	0.83
2	81.69	81.69	81.68	82.18	81.76	82.67	1.20
3	87.64	87.67	87.67	87.82	87.71	87.96	0.33
4	134.20	134.20	134.20	134.69	134.30	135.16	0.71
5	161.50	161.50	161.46	161.81	161.61	162.17	0.44
6	179.00	179.00	179.09	179.25	179.24	179.43	0.19
7	221.10	221.00	221.01	221.26	221.21	221.47	0.21
8	222.0	221.80	221.92	222.36	222.11	222.80	0.39
9	—	—	284.57	287.91	285.41	291.17	2.27
10	—	—	305.73	305.90	306.19	306.12	0.13

Table 3.3: Comparison of Natural Frequencies(rad/s) for Square Stiffened plate with SS-SS-SS-SS Boundary Conditions, with aspect ratio $a/t_1 = 10$ and $t_2/t_1 = 1.2$

Mode No.	ABAQUS 2D-Shell	Ritz Method $\phi^s = \phi^p$	ABAQUS 3D	Ritz Method $\phi^s \neq \phi^p$	Difference (%)
1	3052.1	3056.0	3033.3	3039.9	0.53
2	7252.8	7262.1	7206.2	7218.8	0.60
3	7363.9	7365.8	7363.7	7335.1	0.42
4	11129.0	11138.7	11117.0	11081.8	0.51
5	13396.0	13399.0	13350.0	13302.4	0.73
6	13787.0	13780.8	13834.0	13708.2	0.53
7	17004.0	17015.5	16999.0	16944.3	0.42
8	17031.0	17033.9	17084.0	16905.2	0.76
9	21339.0	21415.8	21365.0	21253.7	0.76
10	21592.0	21578.4	21726.0	21423.9	0.72

Table 3.4: Comparison of Natural Frequencies(rad/s) for Square Stiffened plate with SS-SS-SS-SS Boundary Conditions, with aspect ratio $a/t_1 = 10$ and $t_2/t_1 = 1.5$

Mode No.	DSM [77]	ABAQUS 2D-Shell	Ritz Method $\phi^s = \phi^p$	ABAQUS 3D	Ritz Method $\phi^s \neq \phi^p$	Difference (%)
1	3154.6	3154.9	3171.4	3090.5	3115.6	1.79
2	7339.7	7342.0	7390.0	7143.3	7235.6	2.13
3	7854.5	7857.2	7871.4	7824.4	7792.1	1.02
4	11433.5	11437.0	11489.3	11293.0	11314.7	1.54
5	13481.9	13491.0	13542.5	13292.0	13295.0	1.86
6	14698.5	14710.0	14724.6	14742.0	14568.6	1.07
7	17404.8	17413.0	17526.1	17241.0	17219.3	1.78
8	17630.0	17640.0	17709.4	17598.0	17467.7	1.38
9	21566.8	21596.0	21790.7	21092.0	21351.6	2.06
10	22797.0	22827.0	22822.4	22883.0	22789.9	0.14

Table 3.5: Comparison of Natural Frequencies(rad/s) for Square Stiffened plate with SS-C-SS-C Boundary Conditions, with aspect ratio $a/t_1 = 10$ and $t_2/t_1 = 1.5$

Mode No.	DSM [77]	ABAQUS 2D-Shell	Ritz Method $\phi^s = \phi^p$	ABAQUS 3D	Ritz Method $\phi^s \neq \phi^p$	Difference (%)
1	4247.3	4248.0	4269.4	4187.4	4199.3	1.67
2	8395.5	8398.2	8418.7	8363.7	8322.7	1.15
3	9416.9	9421.8	9482.3	9203.3	9290.3	2.07
4	12775.7	12780.0	12843.1	12628.0	12636.7	1.63
5	15004.0	15015.0	15028.3	15049.0	14863.5	1.11
6	15939.6	15954.0	16009.9	15780.0	15708.8	1.92
7	18475.4	18486.0	18502.1	18450.0	18292.8	1.14
8	19298.8	19311.0	19409.4	19171.0	19084.4	1.70
9	22995.4	23025.0	23023.9	23171.0	22752.3	1.19
10	24131.0	24168.0	24316.4	23769.0	23895.1	1.76

Table 3.6: Comparison of Natural Frequencies(rad/s) for Square Stiffened plate with C-C-C-C Boundary Conditions, with aspect ratio $a/t_1 = 10$ and $t_2/t_1 = 1.5$

Mode No.	ABAQUS 2D-Shell	Ritz Method $\phi^s = \phi^p$	ABAQUS 3D	Ritz Method $\phi^s \neq \phi^p$	Difference (%)
1	5404.5	5422.2	5380.9	5371.1	0.95
2	9961.7	10018.0	9777.5	9860.5	1.59
3	10611.0	10650.9	10665.0	10562.8	0.83
4	14194.0	14261.8	14131.0	14093.6	1.19
5	16153.0	16206.6	15999.0	15973.4	1.45
6	17500.0	17508.2	17670.0	17322.2	1.07
7	19961.0	20052.2	19877.0	19884.9	0.84
8	20346.0	20388.2	20442.0	20155.9	1.15
9	24331.0	24478.1	23942.0	24180.9	1.22
10	25333.0	25364.5	25426.0	25113.7	0.99

Table 3.7: Comparison of Natural Frequencies(rad/s) for Square Stiffened plate with F-F-F-F Boundary Conditions, with aspect ratio $a/t_1 = 10$ and $t_2/t_1 = 1.5$

Mode No.	ABAQUS 2D-Shell	Ritz Method $\phi^s = \phi^p$	ABAQUS 3D	Ritz Method $\phi^s \neq \phi^p$	Difference (%)
1	2231.5	2256.8	2190.6	2225.3	1.41
2	3323.8	3343.2	3227.4	3285.5	1.76
3	4029.2	4056.2	3930.0	3976.7	2.00
4	5312.1	5365.0	5162.0	5261.7	1.96
5	5425.5	5465.2	5368.6	5424.4	0.75
6	9173.5	9244.8	8806.1	9064.6	1.99
7	9230.2	9335.0	9038.8	9140.7	2.12
8	9463.8	9474.0	9466.8	9444.9	0.31
9	9893.8	9966.6	9667.8	9851.4	1.17
10	11106.0	11179.8	10919.0	11046.5	1.21

Table 3.8: Comparison of Natural Frequencies(rad/s) for Square Stiffened plate with C-F-F-F Boundary Conditions, with aspect ratio $a/t_1 = 10$ and $t_2/t_1 = 1.5$

Mode No.	ABAQUS 2D-Shell	Ritz Method $\phi^s = \phi^p$	ABAQUS 3D	Ritz Method $\phi^s \neq \phi^p$	Difference (%)
1	541.3	543.2	532.8	537.0	1.16
2	1350.0	1361.9	1331.6	1345.0	1.26
3	3269.8	3292.3	3160.0	3211.3	2.52
4	4366.1	4386.6	4337.2	4364.1	0.52
5	4570.2	4612.8	4470.1	4542.8	1.54
6	7800.2	7859.9	7704.5	7792.9	0.86
7	8819.2	8887.2	8498.9	8671.5	2.49
8	9418.0	9482.6	9233.8	9389.5	0.99
9	10138.0	10192.4	10025.0	10098.6	0.93
10	12750.0	12855.7	12518.0	12732.1	0.97

Table 3.9: Comparison of Natural Frequencies(rad/s) for different values of rotational stiffness constant, K_θ, for Square Stiffened plate with SS-SS-SS-SS Boundary Conditions, with aspect ratio $a/t_1 = 10$ and $t_2/t_1 = 1.5$

Mode No.	$K_\theta = 0$ ($\phi^s \neq \phi^p$)	$K_\theta = 1.00E10$	$K_\theta = 1.50E10$	$K_\theta = 1.70E10$	$K_\theta = 1.00E11$	$\phi^s = \phi^p$
1	3115.6	3163.5	3167.0	3168.1	3178.6	3171.4
2	7235.6	7376.5	7386.3	7389.1	7418.1	7390.0
3	7792.1	7863.7	7867.4	7868.4	7878.9	7871.4
4	11314.7	11476.1	11486.3	11489.4	11519.2	11489.3
5	13295.0	13533.7	13544.8	13547.8	13577.4	13542.5

3.6.2 Mode Shapes

Normalized modes for square stiffened plate with SS-SS-SS-SS, C-C-C-C, F-F-F-F and C-F-F-F boundary conditions are shown in Figs. 3.5, 3.6, 3.7, 3.8, respectively. Figures 3.5 and 3.6 show the pronounced effect of the four plate-strip stiffeners on the mode shapes of the plate with boundary conditions SS-SS-SS-SS and C-C-C-C, respectively. A less significant effect of the stiffeners on the mode shapes is noticed, in the case of a stiffened plate with F-F-F-F and C-F-F-F boundary conditions, as compared to a plate without stiffeners, as shown in Figs. 3.7 and 3.8.

3.6.3 Parametric Studies

Some parametric studies are carried out to exhibit the influence of certain important parameters on the natural frequencies of the stiffened plate. Figure 3.9 shows the effect of the change in the ratio of the stiffener thickness to the plate thickness, t_2/t_1, on the natural frequencies of a square stiffened plate (SS-SS-SS-SS) with four plate stiffeners. It should be noted that when the ratio is equal to 1, there is no stiffener present in the analysis. It can be concluded from this study that the natural frequencies of the overall system increase linearly as the ratio t_2/t_1 is increased.

Figure 3.10 displays the effect of change in the ratio of plate width to plate length, b/a, on the natural frequencies of a stiffened plate (C-C-C-C-) with four plate stiffeners, with ratio $= 0.5$ for a rectangular plate to ratio $= 1$ for a square plate. It can be seen that as the ratio is increased from 0.5 to 1, there is a significant decrease in the overall natural frequencies of the stiffened system.

Figure 3.11 shows the effect of change in the ratio of stiffeners width ($a_2 = a_4$)to plate length (a), on the natural frequencies of a square stiffened plate (C-C-C-C) with four plate stiffeners. It can be concluded from this parametric study, that the change in the width of the stiffener does not have a substantial effect on the natural frequencies of the entire system.

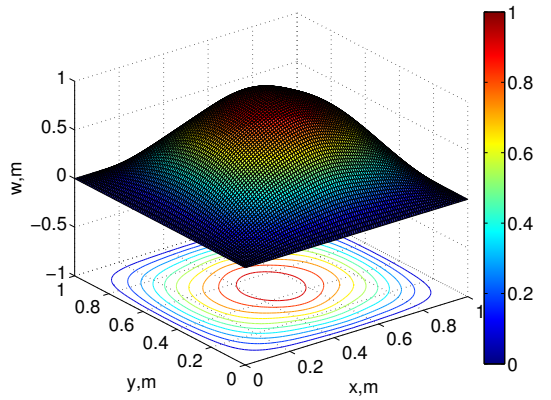

(a) 1^{st} Mode

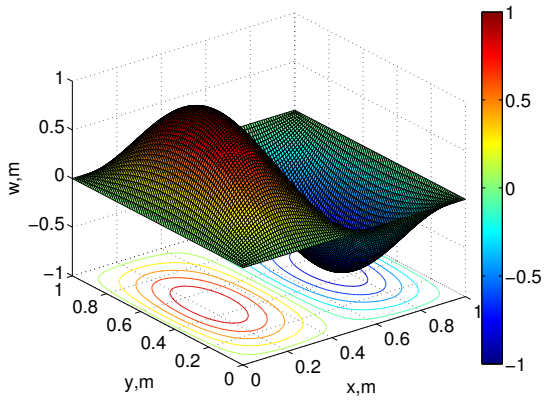

(b) 2^{nd} Mode

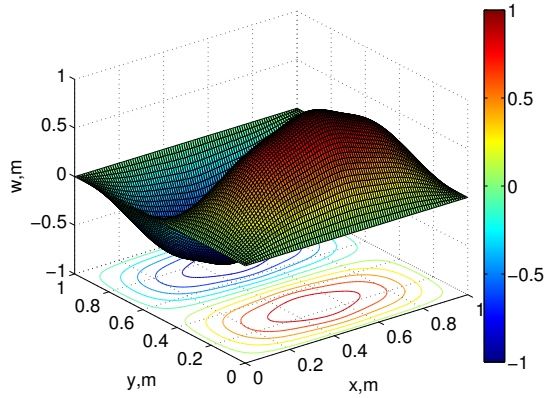

(c) 3^{rd} Mode

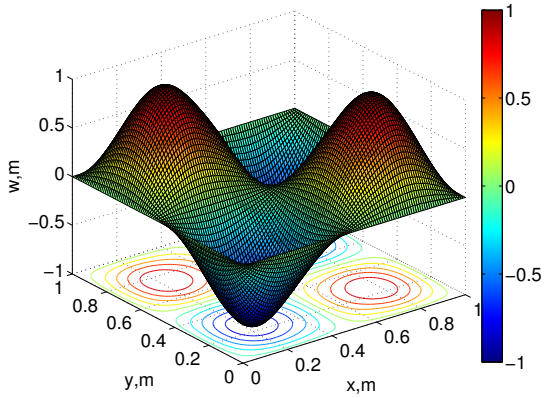

(d) 4^{th} Mode

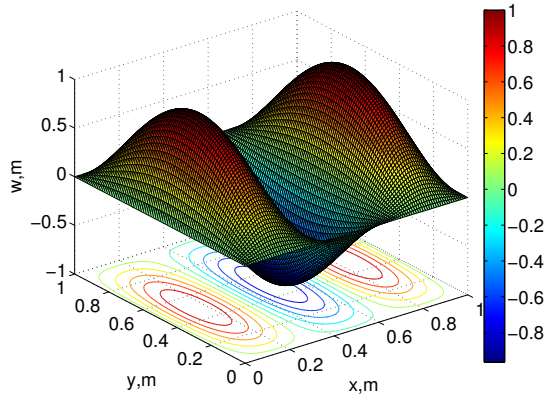

(e) 5^{th} Mode

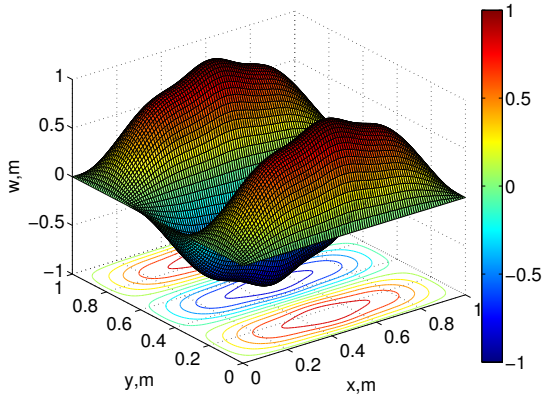

(f) 6^{th} Mode

Figure 3.5: Normalized Natural Modes for the Stiffened Plate, SS-SS-SS-SS

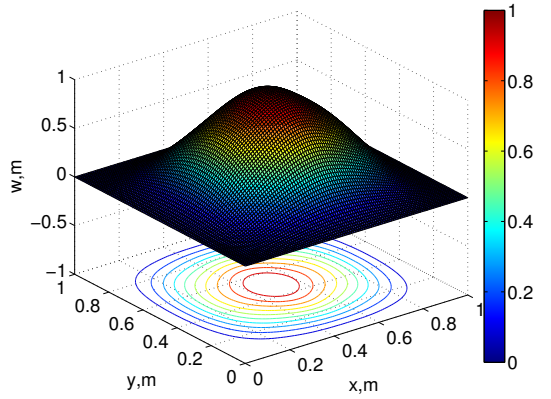

(a) 1^{st} Mode

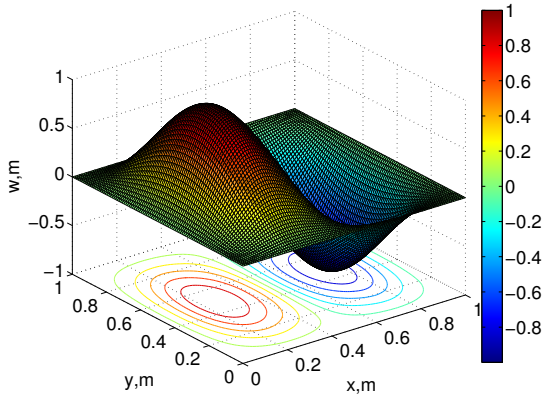

(b) 2^{nd} Mode

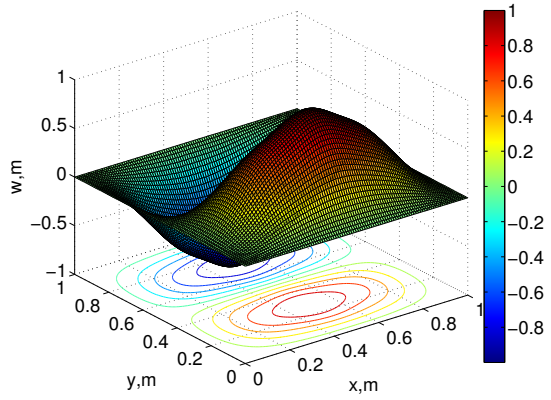

(c) 3^{rd} Mode

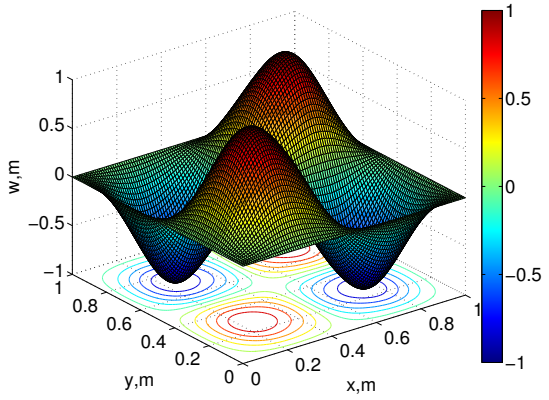

(d) 4^{th} Mode

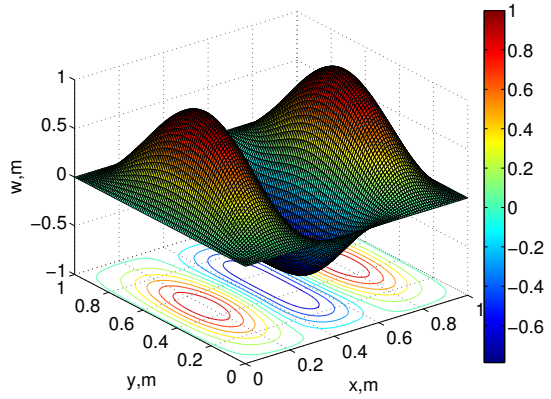

(e) 5^{th} Mode

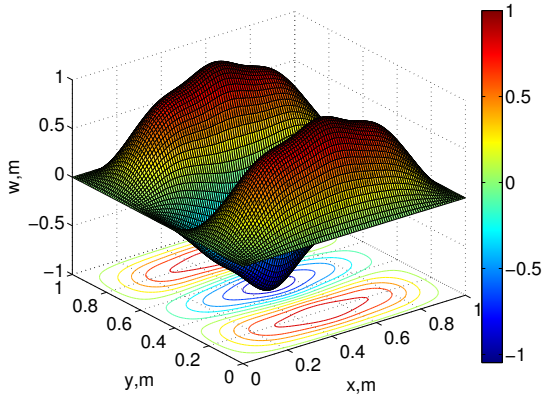

(f) 6^{th} Mode

Figure 3.6: Normalized Natural Modes for the Stiffened Plate, C-C-C-C

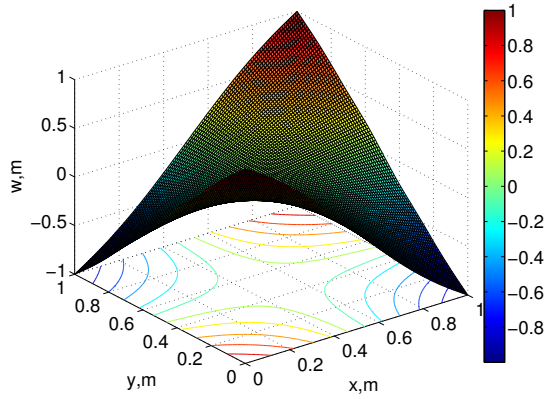

(a) 1^{st} Mode

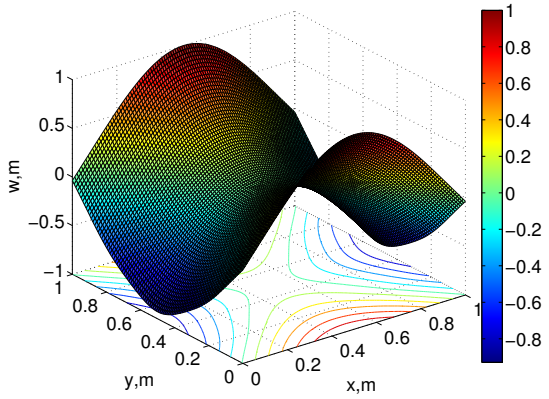

(b) 2^{nd} Mode

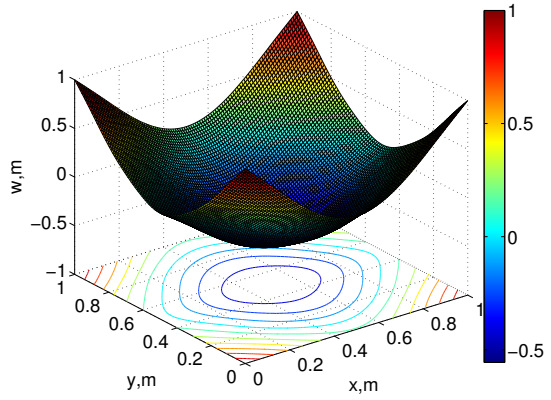

(c) 3^{rd} Mode

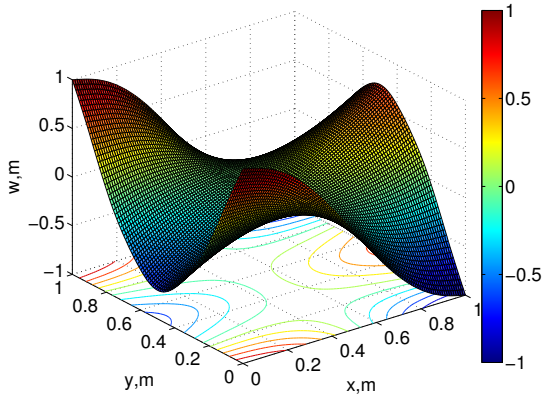

(d) 4^{th} Mode

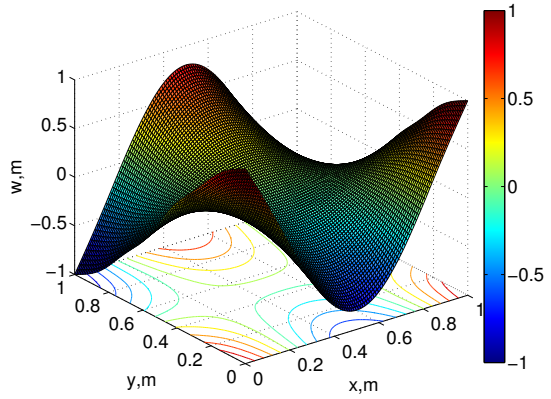

(e) 5^{th} Mode

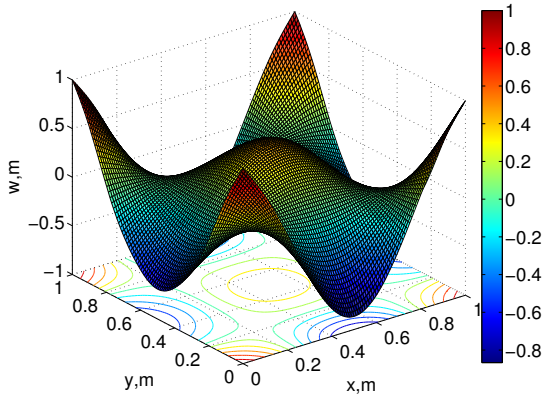

(f) 6^{th} Mode

Figure 3.7: Normalized Natural Modes for the Stiffened Plate, F-F-F-F

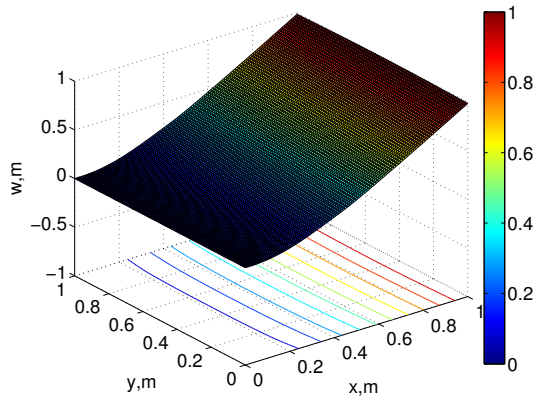

(a) 1^{st} Mode

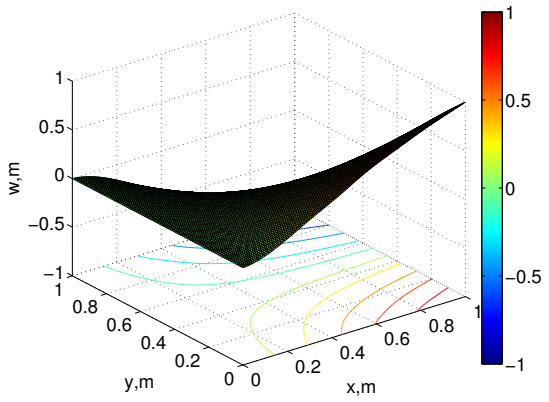

(b) 2^{nd} Mode

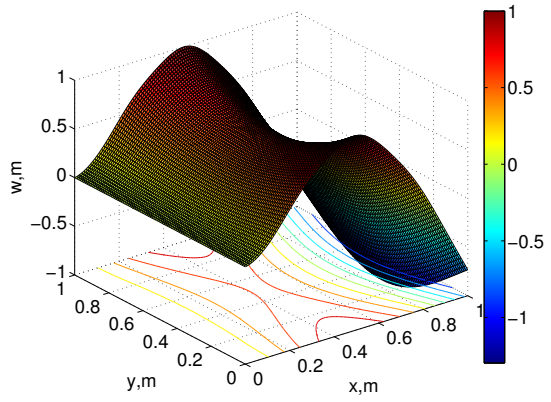

(c) 3^{rd} Mode

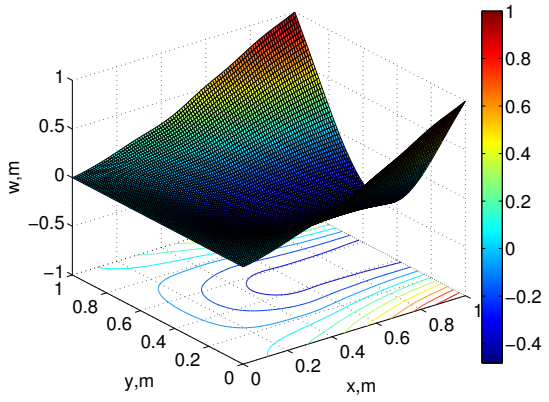

(d) 4^{th} Mode

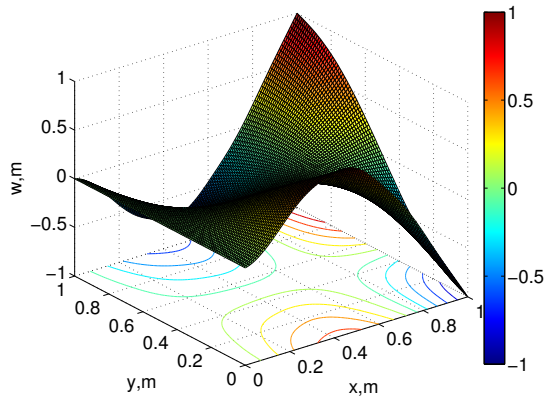

(e) 5^{th} Mode

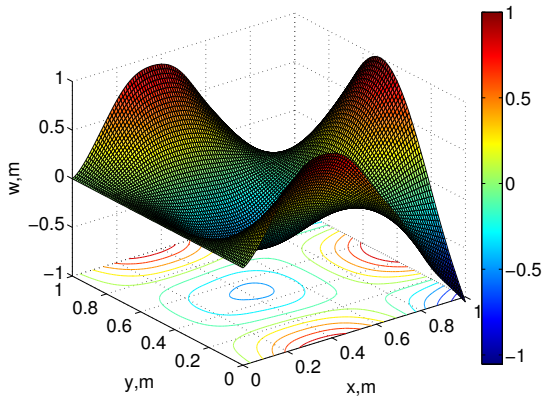

(f) 6^{th} Mode

Figure 3.8: Normalized Natural Modes for the Stiffened Plate, C-F-F-F

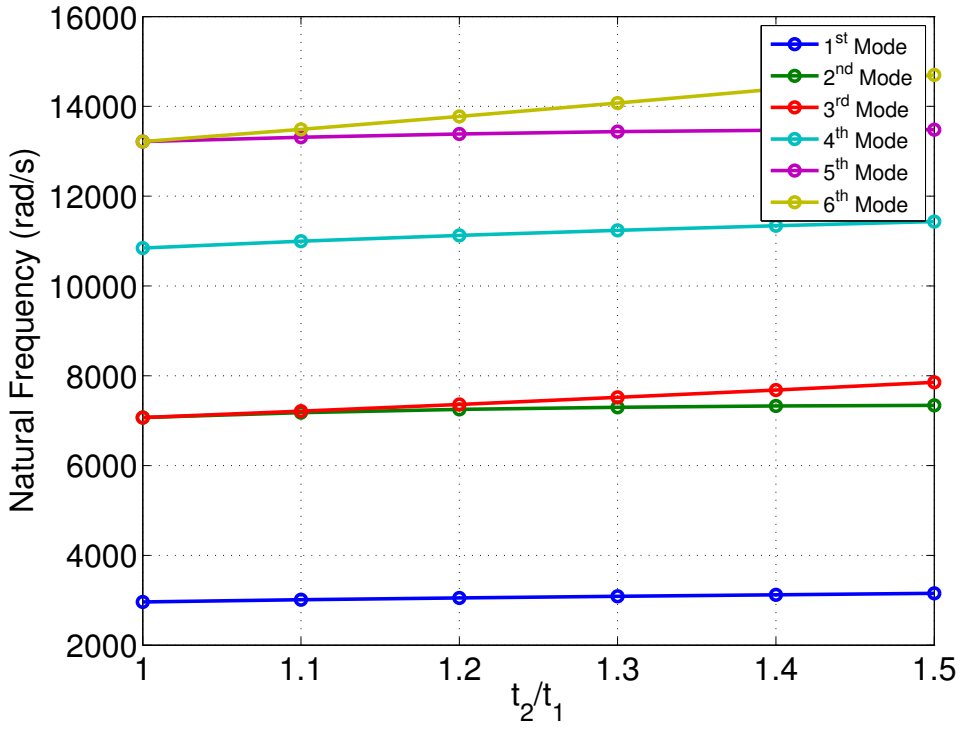

Figure 3.9: Effect of Change in the Ratio of the Stiffener Thickness to the Plate Thickness, t_2/t_1, on the Natural Frequencies of a Square Stiffened Plate (SS-SS-SS-SS) with Four Plate Stiffeners, $t_1 = 0.1m$, $t_2 = h_1 + h_2 + h_3$, $b = 1$m, $a/b = 1$, $a_1 = a_5 = 0.3a$, $a_2 = a_4 = 0.1a$, $a_3 = 0.2a$

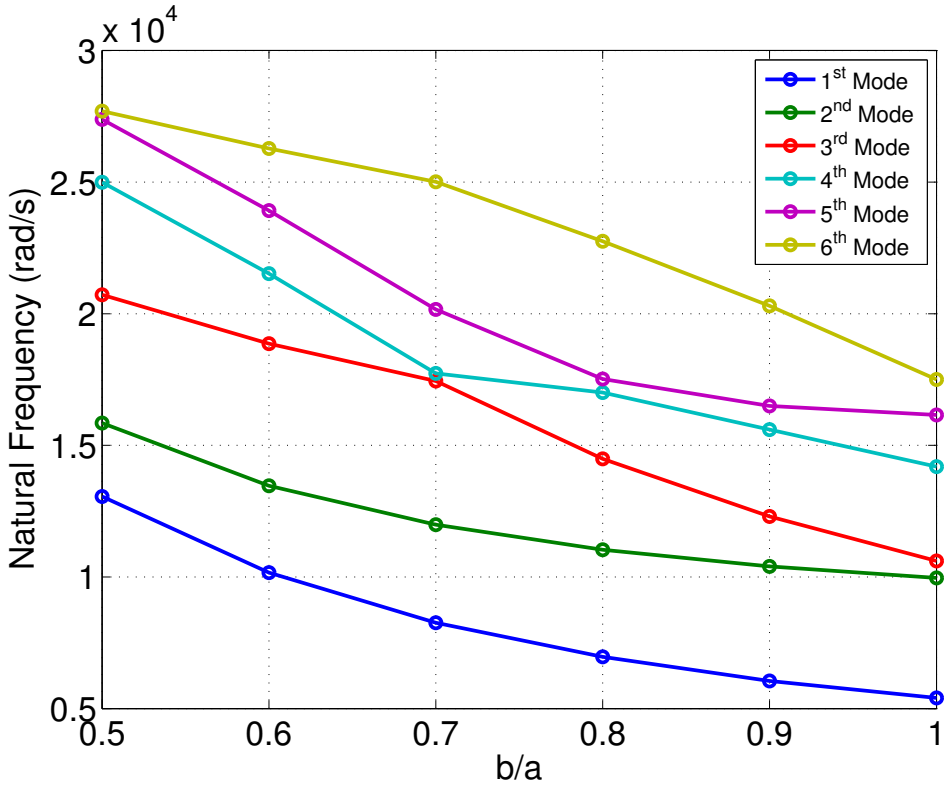

Figure 3.10: Effect of Change in the Ratio of Plate Width to Plate Length, b/a, on the Natural Frequencies of a Stiffened Plate (C-C-C-C) with Four Plate Stiffeners, $t_2/t_1 = 1.5$, $a = 1\text{m}$, $a_1 = a_5 = 0.3a$, $a_2 = a_4 = 0.1a$, $a_3 = 0.2a$

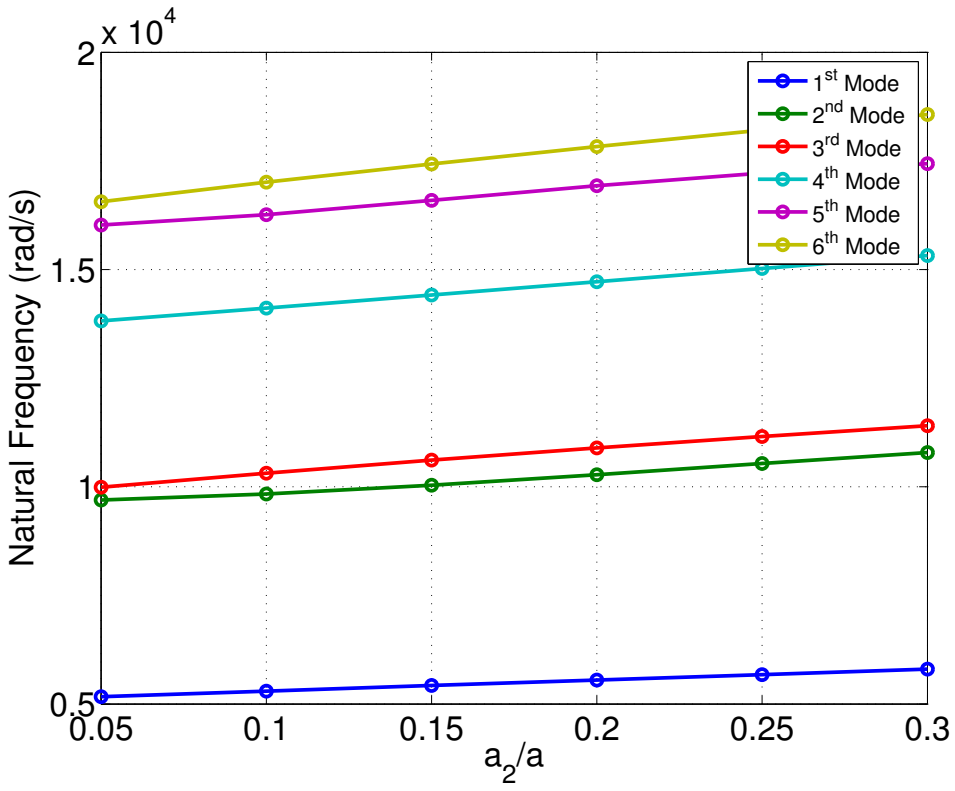

Figure 3.11: Effect of Change in the Ratio of Stiffeners Width ($a_2 = a_4$)to Plate Length (a), on the Natural Frequencies of a Square Stiffened Plate (C-C-C-C) with Four Plate Stiffeners, $t_2/t_1 = 1.5$, $b = 1$m, $a/b = 1$

3.6.4 Cantilever Plate with Viscous Dampers at the Corners

Next, we investigated the role of non-proportional damping on the mode shapes of a structures, by including lumped viscous dampers on the corners of a C-F-F-F plate. Zarek and Gibbs [68], and Prater and Singh [69], reported that the presence of lumped viscous dampers at the end of a beam move nodes during the cyclic oscillations, and we do not get a single point on the structure where all the displacements go to zero at any time. However, in the case of a plate, we obtain nodal lines instead of nodal points. To illustrate this, we first considered a thick plate with C-F-F-F boundary condition, and noticed that we get nodal lines at the same location at different times during cyclic oscillations. Figure 3.12 displays the fifth and six modes of a C-F-F-F plate, during one half cycle of cyclic oscillation.

As a next step, we placed two viscous dampers at the corners of a C-F-F-F plate, at locations (x,y)=(a,0) and (a,b), with damping coefficient value C=1.00E05N.s/m. Figure 3.13 shows the fifth and sixth modes of a C-F-F-F plate with two viscous dampers, during one half cycle of a cyclic oscillation. It can be observed from this figure that the nodal lines change their location from time to time, and we do not get a single location on the plate where all the displacements go to zero. It was noticed that the dispersion of zero displacement points, for higher modes, is wider near the right end of the plate, where viscous damper is mounted. Moreover, it was also seen that the increase in damping coefficient value C, increases the dispersion of the nodal lines from a specific location.

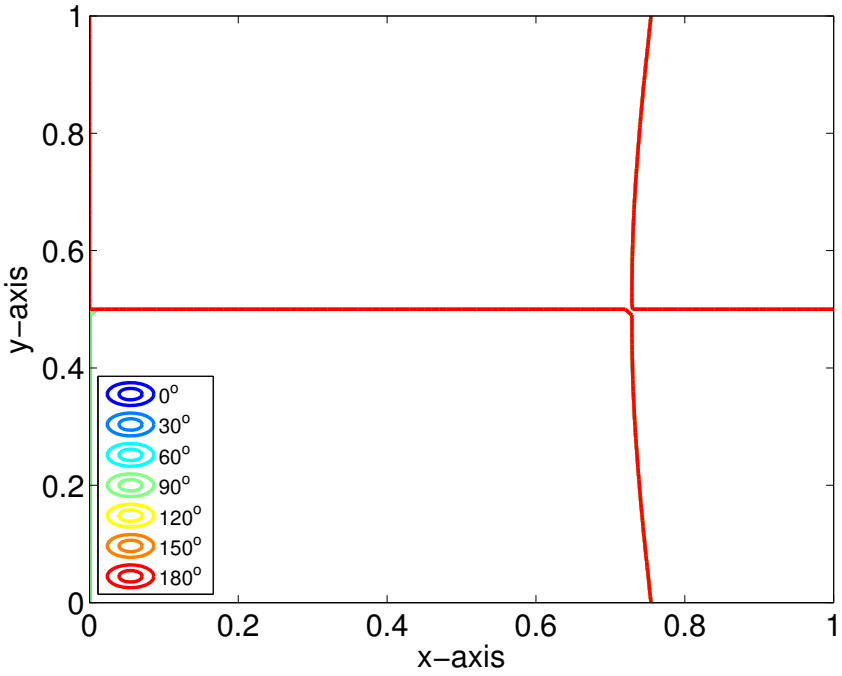

(a) 5^{th} Mode

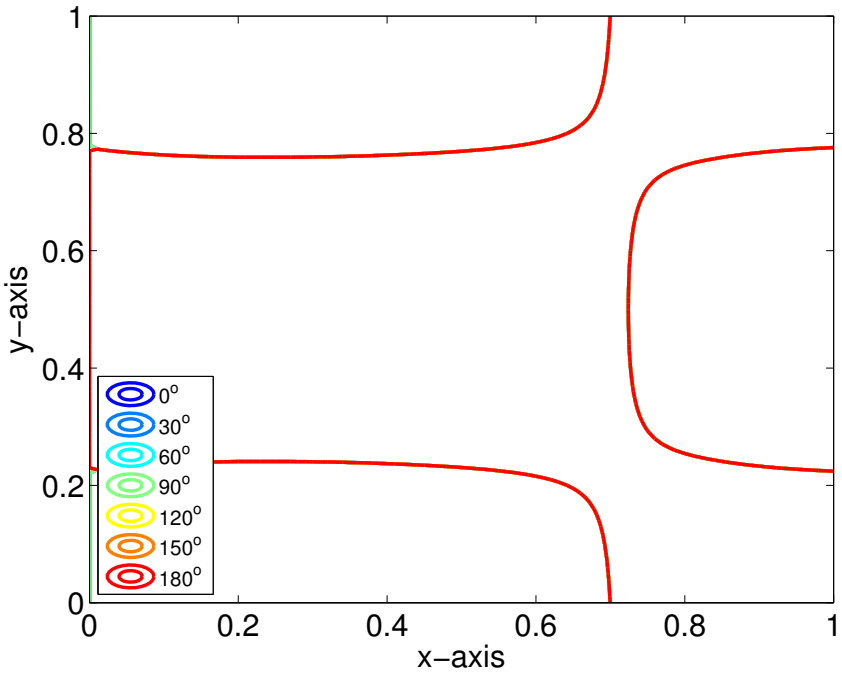

(b) 6^{th} Mode

Figure 3.12: Zero Deflection (Nodal) Lines of a Cantilever Plate (C-F-F-F), at Different Times of Cyclic Oscillations

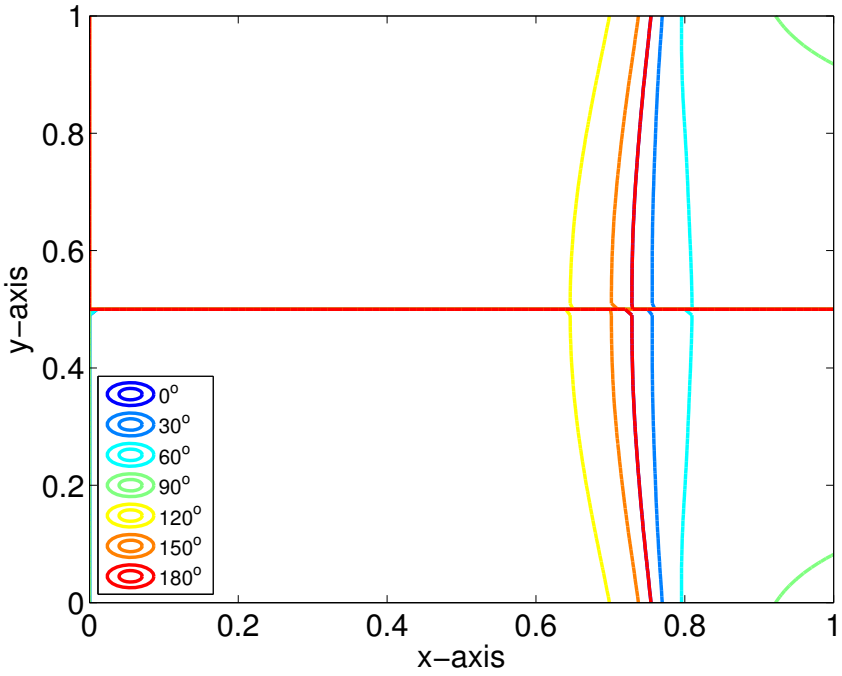

(a) 5^{th} Mode

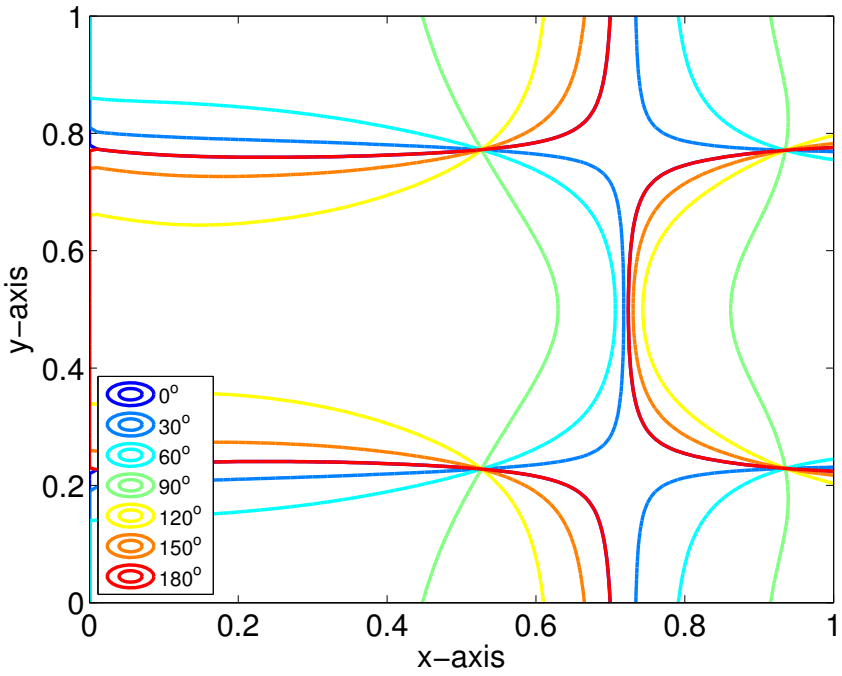

(b) 6^{th} Mode

Figure 3.13: Zero Deflection Lines of a Cantilever Plate (C-F-F-F) with Two Viscous Dampers at Free ends, $(x, y) = (a, 0)$ and (a, b), at Different Times of Cyclic Oscillations

3.7 Conclusions

We successfully utilized static Timoshenko beam functions, to analyse the free vibration response of a stiffened plates with plate-strip stiffeners using FSDT and Ritz method. Development of stiffness and mass matrix consumes huge amount of CPU time due to integration of trigonometric beam functions. A CPU time reduction technique was proposed to greatly decrease, in some cases by two orders of magnitude, the amount of CPU time. The numerical results were compared with the exact solutions available in the literature and finite element software ABAQUS, and the results were found to be highly satisfactory.

Unlike Navier and Levy solution techniques, the approach used in this chapter can also solve for fully clamped, free and cantilever supported stiffened plates. Moreover, the layerwise First order shear deformation theory can be extended to account for orthotropic and composite materials. The procedure adopted here can be used to analyze square and rectangular plates, as well as eccentrically and concentrically stiffened plates.

It was deduced that when the thickness of the stiffeners is small as compared to the plate thickness, stiffener and plate rotations can be assumed to be the same. Moreover, it was concluded that by increasing the ratio of stiffener to plate thickness, we obtain a linear increase in the overall natural frequencies of the system. A substantial decrease in the overall natural frequencies is attained, when the plate dimensions are changed from rectangular to square geometry.

Chapter 4

Damped Response of a Bonded Stiffened Plate

4.1 Introduction

In this chapter, damped vibration response of a thick stiffened plate with adhesively bonded plate-strip stiffeners will be investigated. Both the plate and the stiffeners will be analyzed using the first-order shear deformation theory (FSDT). On the assumption of no slip condition at the interface between the adhesive and the adherend layers, the adhesive will be deformed in shear during cyclic oscillations. The deflections and rotations will be assumed as a tensor product of static Timoshenko beam functions, chosen appropriately according to the given boundary conditions. The problem will be analyzed using the principle of virtual work (PVW).

At first, we will not consider damping in the adhesive in order to validate our code, by comparing our results with those available in the literature as well as with the results obtained using ABAQUS® 3D modelling. We will also consider the effect of changing the stiffness of the adhesive layer on the vibration of the bonded system. As a second step, we will examine damping in the stiffened structure using complex modulus approach, a widely used technique to represent the rheology of the viscoelastic materials. The damping characteristics of the stiffened structure will be tested for different kinds of viscoelastic material and variation of

the adhesive thickness. This work was presented in AIAA SciTech 2016 Conference in San Diego, CA [88].

The structures with plate-strip stiffeners fall under the category of plates with varying thickness, a good example of which is a stepped plate. Stepped plates are widely used in the aerospace industry where weight, local stiffness, natural frequencies and the corresponding mode shapes are of great importance. A more specific application of stepped plates is in the wings of high-speed and high performance aircraft [89]. Plates with varying thickness have also been effectively used in vehicles in the automotive industry, because of their lightweight and high stiffness structural properties [72].

The main difference between the stepped plates and the bonded stiffened plate with plate-strip stiffeners is the existence of an adhesive layer. Adhesively bonded joints are lightweight and provide excellent load transfer capabilities, and are therefore, widely used in the aerospace and ship industries [90, 91]. Moreover, viscoelastic adhesive bonding contributes towards noise and vibration mitigation, and can easily join together two structural components with different material properties [92, 93]. Adams [94] reported that structures including adhesive joints provide 10 times more damping than structures without joints. Therefore, the main objective of this work is to investigate the damped response of an adhesively bonded plate with plate-strip stiffeners.

Ko, Lin and Chu [90] studied the response of an adhesively bonded lap joint using finite element method (FEM). They proposed a 16 noded isoparametric adhesive interface element by including the effects of adherend layers on the adhesive layer. For the adherend layers, they used 8-noded isoparametric plate elements using FSDT. Different vertical deflections were considered for the upper and lower adherends. Lin and Ko [91] used the same procedure to analyze the response of a bonded plate with a patch in the center. In both the analysis, damping was not considered in the adhesive layer.

Yuceoglu, Javanshir, and Güvendik [95], Javanshir [96], and Javanshir, Farsadi, and Yuceoglu [83] investigated the free flexural vibration response of an adhesively bonded stiffened rectangular plate with two and three plate-strip stiffeners. The procedure was built on Levy's solution and FSDT was used to obtain the governing equations of motion. Both orthotropic and isotropic materials were considered for the stiffened plate. The governing

equations were reduced to first order ordinary differential equations and then solved by using modified transfer matrix method utilizing interpolation polynomials. The solution was built on Levy's technique, two opposite boundary conditions were supposed to be simply supported, and as a result the formulation used cannot be applied to problems with fully clamped, free and clamped boundary conditions. In the analysis, they also did not consider any damping in the adhesive layer.

Bilasse, Azrar and Daya [97] reported the damped vibration response of viscoelastic sandwich beams and plates based on FEM. They used Kirchhoff-Love plate theory to model the elastic face layers and von Karman nonlinear strain-displacement relation to model the nonlinearities caused by high amplitude vibration. Linear model with constant viscoelastic complex modulus was also considered in the study. Kung and Singh [98] predicted the damped natural frequencies and loss factor of a rectangular plate with multiple viscoelastic patches using the Rayleigh-Ritz method.

4.2 Mathematical Formulation for the Stiffened Plate

Consider an isotropic thick rectangular plate with plate-strip stiffeners on the top surface of the plate, bonded by adhesive layers as shown in Figure 4.1. The material properties of the plate and the stiffeners are given by Young's modulus (E), the shear modulus of rigidity (G), the Poisson's ratio (ν) and density (ρ), whereas the material properties of the adhesive are given by complex Young's modulus (E_a^*), the complex shear modulus (G_a^*), the Poisson's ratio (ν_a) and density (ρ_a). We will use the principle of virtual work for plate and stiffeners separately, to independently evaluate the mass and stiffness matrix for the stiffener. This will help us in formulating problems with different materials for the plate and stiffeners.

Based on the first order shear deformation layerwise theory, the displacements and rotations in the plate are assumed in the following form:

$$u^p(x,y,z,t) = u_0^p(x,y,t) + z^p\phi_x^p(x,y,t) \tag{4.1}$$

$$v^p(x,y,z,t) = v_0^p(x,y,t) + z^p\phi_y^p(x,y,t) \tag{4.2}$$

$$w^p(x,y,z,t) = w_0(x,y,t) \tag{4.3}$$

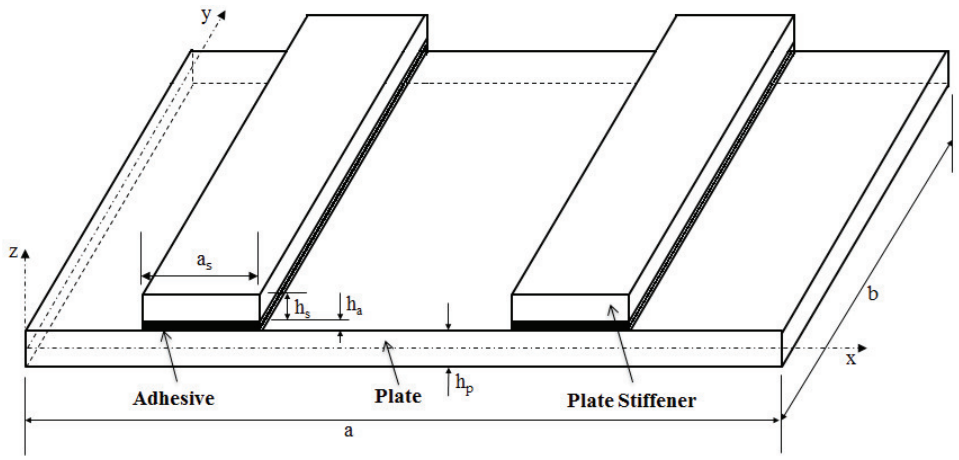

Figure 4.1: Schematic of the Bonded Stiffened Rectangular Plate

where u, v, w are the displacements in the x, y, and z-direction, respectively, the subscript 0 refers to the displacement of the the middle surface of the plate and ϕ_x and ϕ_y are the rotations about the y and x axis, respectively. The deformation in the thickness direction is assumed to be zero, therefore w is independent of the z-direction. It should be noted that same transverse deflection will be used for both the plate and stiffeners. The superscripts p, s and a will represent plate, stiffener and adhesive, respectivley.

Similarly, the displacements and rotations in the stiffener are assumed in the following form:

$$u^s(x,y,z,t) = u_0^s(x,y,t) + z^s\phi_x^s(x,y,t) \tag{4.4}$$

$$v^s(x,y,z,t) = v_0^s(x,y,t) + z^s\phi_y^s(x,y,t) \tag{4.5}$$

$$w^s(x,y,z,t) = w_0(x,y,t) \tag{4.6}$$

4.2.1 The Principle of Virtual Work for the Plate And Stiffeners

Components of strain at a point in the plate assuming infinitesimal strain, can be given as:

$$\varepsilon_{xx} = \frac{\partial u_0}{\partial x} + z\frac{\partial \phi_x}{\partial x} \tag{4.7}$$

$$\varepsilon_{yy} = \frac{\partial v_0}{\partial y} + z\frac{\partial \phi_y}{\partial y} \tag{4.8}$$

$$\gamma_{xy} = \frac{\partial u_0}{\partial y} + \frac{\partial v_0}{\partial x} + z\frac{\partial \phi_x}{\partial y} + z\frac{\partial \phi_y}{\partial x} \tag{4.9}$$

$$\gamma_{xz} = \phi_x + \frac{\partial w_0}{\partial x} \tag{4.10}$$

$$\gamma_{yz} = \phi_y + \frac{\partial w_0}{\partial y} \tag{4.11}$$

Stresses and strains in the plate are related by the material property matrix as:

$$\begin{Bmatrix} \sigma_{xx} \\ \sigma_{yy} \\ \tau_{xy} \\ \tau_{xz} \\ \tau_{yz} \end{Bmatrix} = \begin{bmatrix} \frac{E}{(1-\nu^2)} & \frac{\nu E}{(1-\nu^2)} & 0 & 0 & 0 \\ \frac{\nu E}{(1-\nu^2)} & \frac{E}{(1-\nu^2)} & 0 & 0 & 0 \\ 0 & 0 & G & 0 & 0 \\ 0 & 0 & 0 & \kappa G & 0 \\ 0 & 0 & 0 & 0 & \kappa G \end{bmatrix} \begin{Bmatrix} \varepsilon_{xx} \\ \varepsilon_{yy} \\ \gamma_{xy} \\ \gamma_{xz} \\ \gamma_{yz} \end{Bmatrix} \tag{4.12}$$

where κ is the shear correction factor normally used along with the first order shear deformation theory (FSDT). The virtual work done by the internal stresses in the plate can be expressed as:

$$\delta W_i = \int_V \left[\sigma_{xx}\delta\varepsilon_{xx} + \sigma_{yy}\delta\varepsilon_{yy} + \tau_{xy}\delta\gamma_{xy} + \tau_{xz}\delta\gamma_{xz} + \tau_{yz}\delta\gamma_{yz}\right] dV \tag{4.13}$$

By using the d'Alembert's principle, the virtual work due to the inertial forces in the plate can be written as:

$$\delta W_{inertial} = \rho \int_V [(\ddot{u}_0 + z\ddot{\phi}_x)\delta(u_0 + z\phi_x) + (\ddot{v}_0 + z\ddot{\phi}_y)\delta(v_0 + z\phi_y) + \ddot{w}_0\delta w_0]dV \tag{4.14}$$

It should be noted here that we used rotational as well as the in-plane inertia, in determining the virtual work due to inertial forces. Similarly, we can use the procedure above to get the virtual work done by each stiffener.

4.2.2 The Principle of Virtual Work for the Adhesive Section

Transverse shear strain in the adhesive core layer, as shown in Fig. 4.2, can be written as:

$$\gamma_{axz} = \alpha + \beta = \frac{\partial u}{\partial z} + \frac{\partial w}{\partial x} \tag{4.15}$$

where

$$\frac{\partial u}{\partial z} = \beta_1 = \beta_2 = \frac{1}{h_a}\left[\left(u^s - \frac{h_s}{2}\phi_x^s\right) - \left(u^p + \frac{h_p}{2}\phi_x^p\right)\right] \tag{4.16}$$

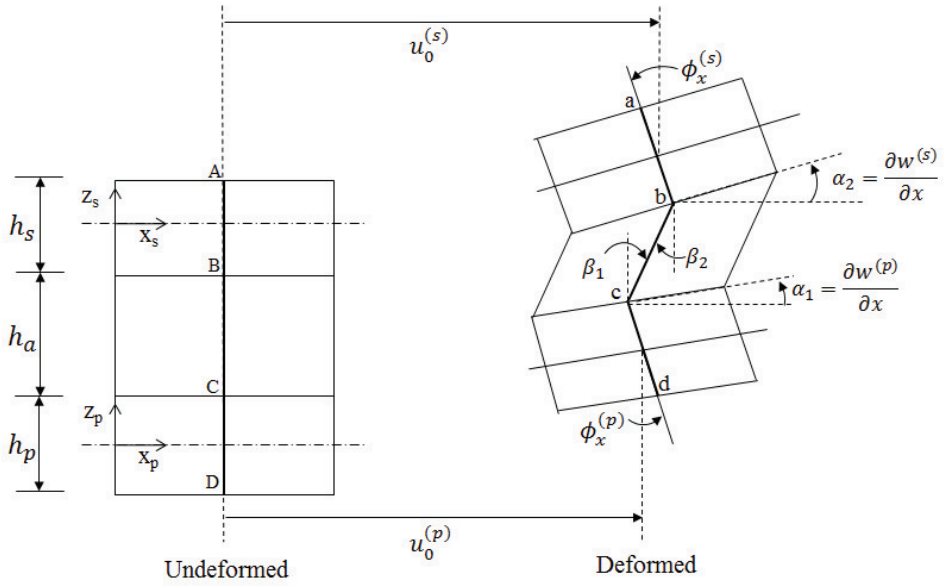

Figure 4.2: Undeformed and Deformed Segments of the Bonded Stiffened Rectangular Plate

As the vertical deflection w is considered same for the plate and stiffener so we can say that $\alpha_1 = \alpha_2$. It should be noted here that we also considered different vertical deflections for the plate and the stiffeners, but it did not had a considerable effect on the vibration response of the structure, mainly because of the very small thickness of the adhesive layer as compared to the adherends thickness. Now, we can write the shear deformation γ_{xz} in the adhesive layer as:

$$\gamma_{axz} = \frac{1}{h_a}\left(u^s - u^p - \frac{h_s}{2}\phi_x^s - \frac{h_p}{2}\phi_x^p\right) + \frac{\partial w}{\partial x} \tag{4.17}$$

Similarly, the shear deformation γ_{yz} in the adhesive layer can be given as:

$$\gamma_{ayz} = \frac{1}{h_a}\left(v^s - v^p - \frac{h_s}{2}\phi_y^s - \frac{h_p}{2}\phi_y^p\right) + \frac{\partial w}{\partial y} \tag{4.18}$$

Only transverse shear deformation are considered in the adhesive sections, so we can write the virtual work done by the internal stresses in the adhesive layer as:

$$\delta W_i = \int_V [\tau_{axz}\delta\gamma_{axz} + \tau_{ayz}\delta\gamma_{ayz}]dV \tag{4.19}$$

where

$$\tau_{axz} = G_a^*\gamma_{axz} \tag{4.20}$$

$$\tau_{ayz} = G_a^* \gamma_{ayz} \tag{4.21}$$

An asterisk in the supercript denotes a complex quantity throughout this chapter; for example $G_a^* = G_a(1 + i\eta_a)$ is the complex shear modulus with η_a as the loss factor of the viscoelastic adhesive layer. As a result of including the complex shear modulus, we will end up have a complex stiffness matrix for the core layer. Although, for the first case of vibration response without damping this modulus will be a real number and hense the stiffness matrix will be real.

By using the d'Alembert's principle, the virtual work due to the inertial forces in the adhesive section can be written as:

$$\delta W_{inertial} = \rho_a \int_V \ddot{w_0} \delta w_0 dV \tag{4.22}$$

Similarly, the principle of virtual work can be used for the other stiffener and adhesive section. In the absence of external forces, the principle of virtual work for the entire structure can be obtained by using Eqs. (4.13),(4.14),(4.19) and (4.22) as:

$$\left\{ \delta W_i^p + \sum_{m=1}^{B} \Big[(\delta W_i^s)_m + (\delta W_i^a)_m \Big] \right\} + \left\{ \delta W_{inertial}^p + \sum_{m=1}^{B} \Big[(\delta W_{inertial}^s)_m + (\delta W_{inertial}^a)_m \Big] \right\} = 0 \tag{4.23}$$

where B is the number of stiffeners used in the analysis.

4.3 Free Vibration Analysis of the Stiffened Plate

We can write the displacements and rotations for the plate in the form:

$$u_0(x, y, t) = U(x, y) e^{i\omega^* t} \tag{4.24}$$

$$v_0(x, y, t) = V(x, y) e^{i\omega^* t} \tag{4.25}$$

$$w_0(x, y, t) = W(x, y) e^{i\omega^* t} \tag{4.26}$$

$$\phi_x(x, y, t) = \Phi_x(x, y) e^{i\omega^* t} \tag{4.27}$$

$$\phi_y(x, y, t) = \Phi_y(x, y) e^{i\omega^* t} \tag{4.28}$$

where $U(x,y)$, $V(x,y)$, $W(x,y)$, $\Phi_x(x,y)$, $\Phi_y(x,y)$ are the spatial variations of $u_0(x,y,t)$, $v_0(x,y,t)$, $w_0(x,y,t)$, $\phi_x(x,y,t)$, and $\phi_y(x,y,t)$, respectively, and ω^* represent the complex eigen frequency. These spatial variations can be written as a product of unidirectional functions by using separation of variables:

$$U(x,y) = \sum_{m=1}^{M}\sum_{n=1}^{N} a_{mn}U_m(x)U_n(y) \tag{4.29}$$

$$V(x,y) = \sum_{m=1}^{M}\sum_{n=1}^{N} b_{mn}V_m(x)V_n(y) \tag{4.30}$$

$$W(x,y) = \sum_{m=1}^{M}\sum_{n=1}^{N} c_{mn}W_m(x)W_n(y) \tag{4.31}$$

$$\Phi_x(x,y) = \sum_{m=1}^{M}\sum_{n=1}^{N} d_{mn}\Phi_m(x)W_n(y) \tag{4.32}$$

$$\Phi_y(x,y) = \sum_{m=1}^{M}\sum_{n=1}^{N} e_{mn}W_m(x)\Phi_n(y) \tag{4.33}$$

where M and N are the total number of terms considered in the x and y-direction, respectively. It should be noted that the five coefficient vectors, the vectors of so-called generalized co-ordinates, **a**,**b**,**c**,**d**, and **e** are arbitrary as well as independent from each other. By using these displacement functions in Eq. (4.23), we can obtain the stiffness and the mass matrices for the plate. The size of both of these matrices will be 5×M×N.

A combination of trigonometric functions such as cosine and sine, can be used in Eqs. (4.29) and (4.30) for $U_m(x)$, $U_n(y)$, $V_m(x)$, and $V_n(y)$ and the static Timoshenko beam functions can be used as admissible functions in Eqs. (4.31)-(4.33) for $W_m(x)$, $W_n(y)$, $\Phi_m(x)$and $\Phi_n(y)$, as given in Chapter 3, Section 3.5.

It should be noted from Section 4.2, that the vertical deflection of the plate and stiffeners is the same, so the independent degree of freedom for the stiffeners are; u^s, v^s, Φ_x^s and Φ_y^s. The size of the assembled stiffness and the mass matrices will be 13×M×N, 5×M×N for the plate and 4×M×N for each stiffener.

4.3.1 Frequency and Loss Factor Calculation

Following the above procedure, we can come up with a system of equations, which can be written in the matrix form as:

$$\mathbf{M}\ddot{\mathbf{x}} + \mathbf{K}^*\mathbf{x} = 0 \tag{4.34}$$

By looking at Eq. (4.34), we see that the stiffness matrix $\mathbf{K}^*$ is complex, because of the inclusion of complex shear modulus of the adhesive layer. We can solve this equation by the usual way in which we generally solve a real eigenvalue problem, but in this case we will get complex eigenvalues and eigenvectors. Johnson and Kienholz [34] reported that the complex modes we get are orthogonal in nature and we can get uncoupled equations of motion. This method assumes displacements to be harmonic in nature [22] and to be of the form:

$$x^* = x_0^* e^{i\omega^* t} \tag{4.35}$$

where ω^* is the complex frequency and x_0^* is the complex eigenvector. For free vibration, we can write Eq. (4.34) as:

$$\left(-\lambda^* M + K^*\right) x_0^* = 0 \tag{4.36}$$

where $\lambda^* = (\omega^*)^2$ is the complex eigenvalue. By solving the above system of equations, we get complex eigenvalues and complex frequencies for the damped structure:

$$\lambda^* = \lambda + i\lambda' \tag{4.37}$$

$$\omega^* = \omega + i\omega' \tag{4.38}$$

The loss factor η_n corresponding to each frequency can be obtained by the following ratio [22]:

$$\eta_n = \frac{\lambda_n'}{\lambda_n} \tag{4.39}$$

where λ_n and λ_n' are the real and the imaginary parts of the complex eigenvalue, λ_n^*, respectively. It is also possible to calculate the loss factor from the complex frequencies ω^* [22], as follows:

$$\eta = 2 \arctan \frac{\omega'}{\omega}$$

where ω and ω' are the real and the imaginary parts of the complex frequency, ω^*, respectively.

4.4 Numerical Results

To demonstrate the application of the above mentioned procedure utilizing static Timoshenko beam functions, a rectangular plate with two stiffeners bonded by two adhesive layers are considered in the study, as shown in Fig. 4.1. Natural Frequencies and mode shapes were obtained by implementing the above procedure in a MATLAB® program on a dual-core Macintosh 2.4 GHz Intel core i5 computer with 8GB RAM. The results obtained were compared to those available in the literature and the commercially available finite element software ABAQUS®. Convergence and the influence of adhesive Young's modulus is also studied in this section. Moreover, the effect of change in the thickness and the damping properties of the adhesive layer is thoroughly investigated in this section.

4.4.1 Free Vibration Analysis of the Stiffened Plate Without Damping

In order to validate our code, we first consider a fully clamped square plate with a patch of the same thickness at the center of the plate to compare our results with Lin and Ko [91] and ABAQUS FEM Software. The material properties of the patch and plate are as follows: Young's modulus $E = 68.95$ GPa, Poisson's ratio $\nu = 0.3$, density $\rho = 2770$ kg/m^{3}and material properties of the adhesive are given as: Young's modulus $E_a = 3.068$ GPa, Poisson's ratio $\nu_a = 0.3485$, density $\rho_a = 332.4$ kg/m^3. The geometric properties of the thick plate with bonded patch are: $a \times a \times 5.08$mm, $b \times b \times 5.08$mm, where $a = 508$mm, $b = 3a/7$. It should be noted that damping is not included in this problem, so the shear modulus of the adhesive is a real number.

Results for this example were validated with a 3D finite element model using ABAQUS. For the plate and Patch, 20-noded quadratic brick, reduced integration, solid elements (C3D20R) were used, whereas, 20-noded quadratic brick solid elements (C3D20) with full integration were used in the adhesive layer. It is necessary to use full integration in the adhesive layer, because reduced integration will give singularities in the adhesive layer due to high aspect ratio of the elements used in the adhesive layer. As the thickness of the adhesive layer is very small, reducing the aspect ratio will significantly increase the number of elements in the adhesive layer, which in turn will increase the computational cost and time. For the

Table 4.1: Natural Frequency (rad/s) Results for a Fully Clamped Square Plate with a Central Patch

Modulus of Adhesive(A)		Mode			
		1	2	3	4
1	ABAQUS 3D	1187.9	2310.7	2310.8	3877.0
	Present Method	1206.2	2348.5	2348.5	3888.5
	FEM [91]	1216.4	2399.8	2399.8	4146.5
0.1	ABAQUS 3D	1170.0	2270.0	2270.0	3830.0
	Present Method	1183.6	2301.1	2301.1	3835.7
	FEM [91]	1200.7	2367.2	2367.2	4093.0
0.01	ABAQUS 3D	1110.1	2172.4	2172.4	3651.3
	Present Method	1124.4	2204.0	2204.0	3658.2
	FEM [91]	1129.6	2247.2	2247.2	3867.5
0.001	ABAQUS 3D	986.7	2031.9	2031.9	3296.8
	Present Method	1001.9	2081.2	2081.2	3323.8
	FEM [91]	998.2	2086.2	2086.2	3484.4

E'_a=A$\times E_a$, E_a=3.068GPa

plate and patch, 2 layer of C3D20R elements were used in thickness direction; a total of 6106 elements were used in the plate, 968 elements in the patch and 484 elements were used in the adhesive layer.

The natural frequencies obtained by following the procedure of this paper using the PVW, as shown in Table 4.1, are compared with those reported by Lin and Ko [91], who used FEM with a 16-node interface element for the adhesive and 8-node isoparametric plate element for the plate and patch. For this problem, 20×20 terms were used in the PVW analysis to get the converged results, and it took 63.6 seconds to compute the mass and stiffness matrix. The natural frequencies obtained were about 2% lower than those obtained by Lin and Ko [91], and closer to the 3D results obtained by using ABAQUS.

Figure 4.3 shows the convergence of fundamental natural frequency for the fully clamped square plate with a patch in the center, against the number of terms (N) used in the PVW.

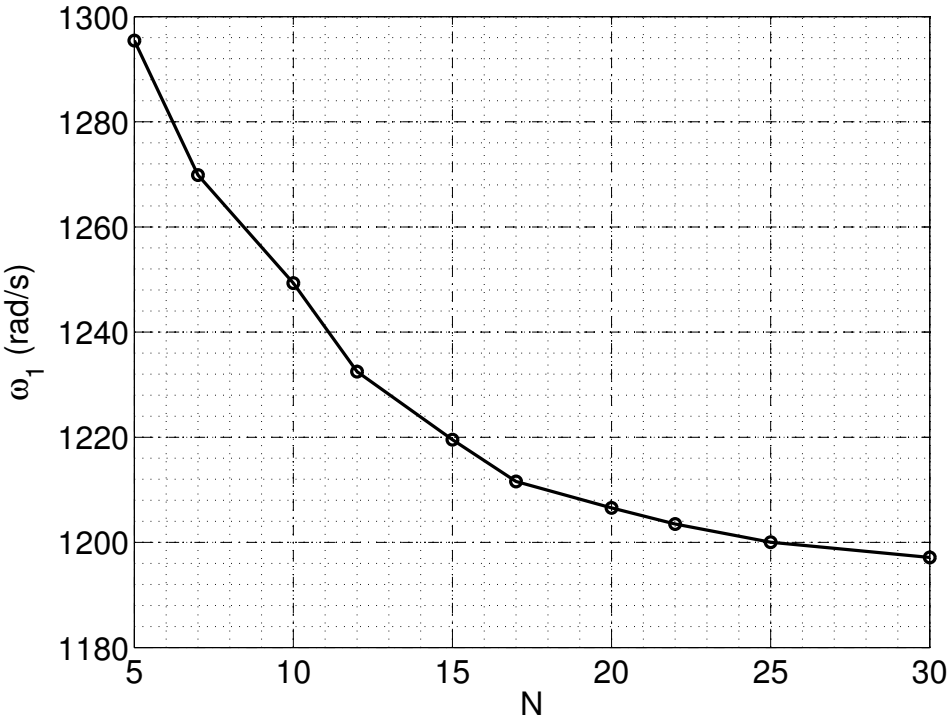

Figure 4.3: Convergence of the Fundamental frequency for the bonded Stiffened Plate with CCCC boundary conditions, Against the Number of Terms (N) Used in the PVW

It should be noted that same number of terms were used in the x and y-direction, so a total of N×N terms were used in the analysis. Figure 4.3 clearly illustrates that we start getting converged results as we reach N= 20, a difference of less than 1% was obtained using N= 20 and N= 30 terms. Figure 4.4 depicts that the overall natural frequencies of the bonded structure increases almost linearly with the increase in the modulus of the adhesive layer.

Now, we turn to the rectangular bonded plate of Fig. 4.1, the material properties of the plate and stiffeners are given as: Young's modulus $E = 72.69$ GPa, Poisson's ratio $\nu = 0.313$, density $\rho = 2796$ kg/m^3. Two types of adhesive were used in this analysis, the one with high Young's and Shear moduli is called "hard adhesive" and the one with low moduli is called "soft adhesive". The material properties of the hard adhesive are given as: Young's modulus $E_a = 4$ GPa, Shear modulus $G_a = 1.4$ GPa, whearas for the soft adhesive: Young's modulus $E_a = 1.771$ MPa, Shear modulus $G_a = 0.453$ MPa. Density for both the adhesives were considered to be $\rho_a = 332.4$ kg/m^3. The geometric properties of the the bonded plate are given as: 1m×0.5m×0.005m for the plate, 0.2m×0.5m×0.005m for the stiffener, and 0.2m×0.5m×0.00015m for the adhesive layer.

The above material and geometrical properties were used to compare our results with Yuceoglu, Javanshir, and Güvendik [84], and Javanshir [82]. They investigated the free flexural vibration response of an adhesively bonded stiffened rectangular plate with two plate-strip stiffeners. The procedure was built on Levy's solution and FSDT was used to obtain the governing equations of motion. The governing equations were reduced to first order ordinary differential equations and then solved by using modified transfer matrix method utilizing interpolation polynomials. The solution was built on Levy's technique, two opposite boundary conditions were supposed to be simply supported, and as a result the formulation used cannot be applied to problems with fully clamped, free and cantilever boundary conditions.

We also used 3D FEM model in ABAQUS, to solve this problem. For the plate and the stiffeners, 20-noded quadratic brick, reduced integration, solid elements (C3D20R) were used, whereas, 20-noded quadratic brick solid elements (C3D20) with full integration were used in the adhesive layer. For the plate and the stiffeners, 2 layer of C3D20R elements were used in the thickness direction: a total of 2500 elements were used to model the plate, 500 elements to model each stiffener and 1000 elements were used to model each adhesive layer.

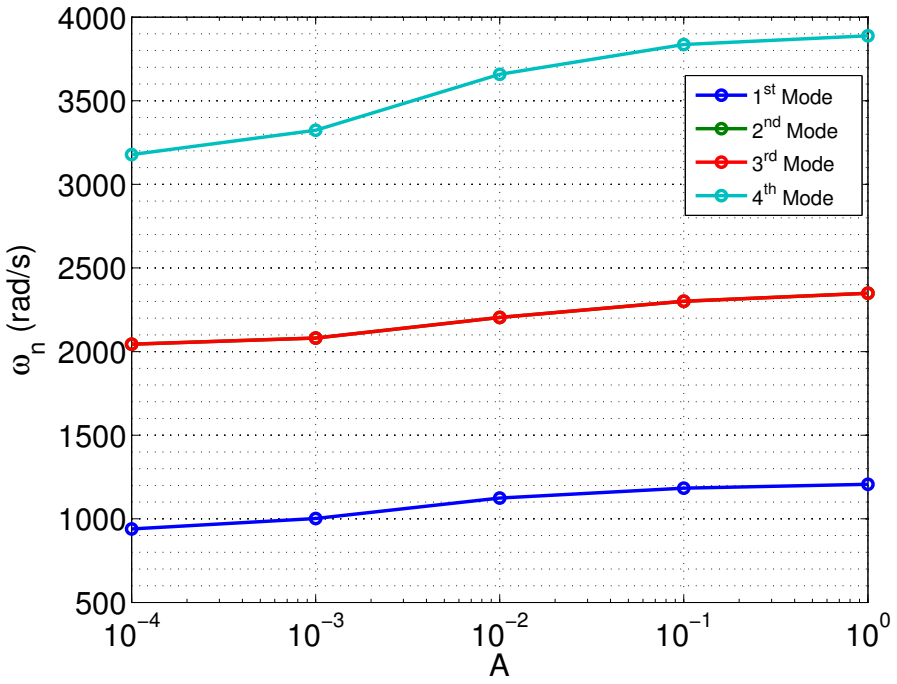

Figure 4.4: Effect of Change in the Young's Modulus of Adhesive Layer on the Overall Natural Frequencies, E_a'=A$\times E_a$, E_a=3.068GPa

Table 4.2 clearly illustrate that the natural frequency results for the rectangular bonded plate obtained using the PVW, with 25×25 terms, are closer to the 3D ABAQUS results. For the soft adhesive, the natural frequencies and mode shapes reported by Yuceoglu, Javanshir, and Güvendik [84], and Javanshir [82]. are closer to the results obtained using the proposed method in this paper as well as the 3D ABAQUS results. On the other hand, the results for the hard adhesive, obtained using the PVW and ABAQUS, are very different than those reported by Yuceoglu, Javanshir, and Güvendik [84], and Javanshir [82]. By looking at the mode shapes and natural frequency results provided by Javanshir [82], it seems that they missed the first seven modes. The first mode natural frequency is closer to the eighth natural frequency obtained using ABAQUS and the PVW. The mode shapes match as well, with the exception that there is a small deflection in the stiffener region with ABAQUS and the PVW than no deflection at all using Javanshir [82]. Yuceoglu, Javanshir, and Güvendik [84], and Javanshir [82] reported that the region of the plate where the stiffeners are attached are completely stationary while using the hard adhesive. This phenomena was not noticed both when using the 3D ABAQUS modeling as well as the PVW proposed here.

Table 4.3 presents the results obtained using PVW and ABAQUS for a rectangular stiffened plate with two plate-strip stiffeners with two opposite side simply-supported and other two clamped (CSCS). Similar to the SSSS boundary condition, for the soft adhesive, the natural frequencies and mode shapes reported by Yuceoglu, Javanshir, and Güvendik [84], and Javanshir [82], are closer to the results obtained using the proposed method in this paper as well as the 3D ABAQUS results. But the same discrepancy is observed for the case of hard adhesive, and it seems that they have missed the first eight modes. The first mode natural frequency is closer to the ninth natural frequency obtained using ABAQUS and the PVW. Table 4.4 illustrates the results obtained for a fully clamped (CCCC) rectangular stiffened plate with two plate-strip stiffeners using PVW and ABAQUS. No comparison is shown with Yuceoglu, Javanshir, and Güvendik [84], and Javanshir [82], as their methodology can only solve problems with one pair of opposite edges as simply-supported.

Table 4.2: Natural Frequency(rad/s) Results for a SSSS Rectangular Plate With Two Adhesively Bonded Plate Strip-Stiffeners

Mode	Hard Adhesive			Soft Adhesive		
No.	ABAQUS	Present Method	Javanshir [82]	ABAQUS	Present Method	Javanshir [82]
1	626.84	629.62	3026.38	459.60	461.21	460.33
2	842.59	860.94	3030.62	637.44	646.33	630.95
3	1442.60	1451.95	3769.35	1086.90	1095.10	1113.25
4	2005.20	2093.45	3772.72	1415.50	1418.50	1384.22
5	2170.50	2177.41	3995.48	1567.00	1598.30	1553.94
6	2378.20	2401.33	4605.38	1593.80	1603.78	1571.20
7	2814.90	2838.78	–	2074.30	2079.68	–
8	3171.70	3250.57	–	2360.90	2377.89	–
9	3404.60	3514.87	–	2538.30	2562.90	–
10	3772.10	3939.46	–	2947.80	2952.99	–

Table 4.3: Natural Frequency(rad/s) Results for a CSCS Rectangular Plate With Two Adhesively Bonded Plate Strip-Stiffeners

Mode No.	Hard Adhesive			Soft Adhesive		
	ABAQUS	Present Method	Javanshir [82]	ABAQUS	Present Method	Javanshir [82]
1	681.28	684.79	3959.00	497.19	498.50	499.71
2	967.19	985.43	4213.62	730.17	739.71	717.92
3	1678.70	1695.00	4247.72	1261.80	1274.16	1277.87
4	2216.60	2225.37	4579.71	1436.10	1439.31	1403.73
5	2320.00	2367.19	4807.79	1647.80	1660.28	1604.53
6	2520.90	2534.05	4830.09	1816.90	1857.44	1822.12
7	3077.90	3101.34	–	2199.40	2208.97	–
8	3764.40	3799.83	–	2748.10	2762.10	–
9	3779.20	3863.45	–	2751.70	2781.79	–
10	4367.20	4472.67	–	2961.30	2966.78	–

Table 4.4: Natural Frequency(rad/s) Results for a CCCC Rectangular Plate With Two Adhesively Bonded Plate Strip-Stiffeners

Mode No.	Hard Adhesive		Soft Adhesive	
	ABAQUS	Present Method	ABAQUS	Present Method
1	1308.00	1310.06	830.01	829.46
2	1537.10	1546.94	1002.00	1009.68
3	1988.30	2001.42	1461.70	1472.00
4	2593.80	2633.30	1976.90	2013.23
5	3195.30	3215.81	2078.20	2075.67
6	3574.50	3581.62	2247.10	2252.57
7	3747.70	3767.34	2711.70	2714.69
8	3924.00	4007.62	2861.50	2874.74
9	4472.50	4506.87	3203.50	3225.19
10	4713.30	4845.50	3682.80	3726.72

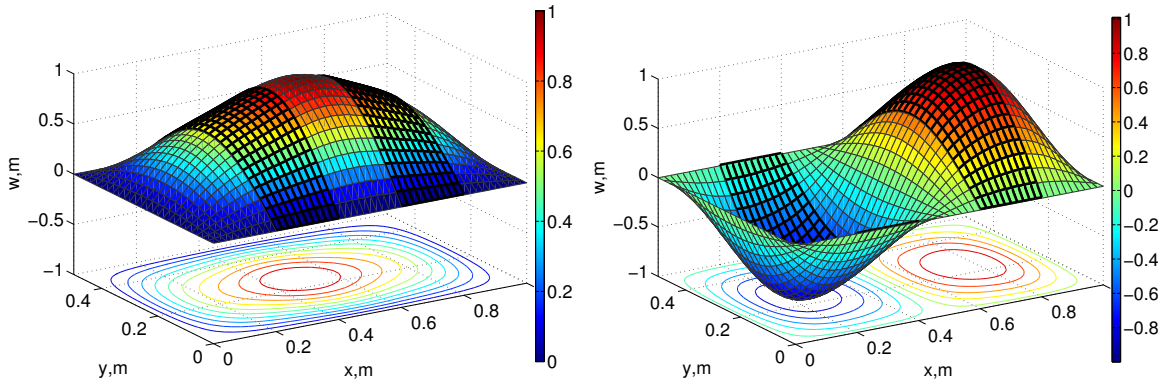

(a) 1^{st} Mode (b) 2^{nd} Mode

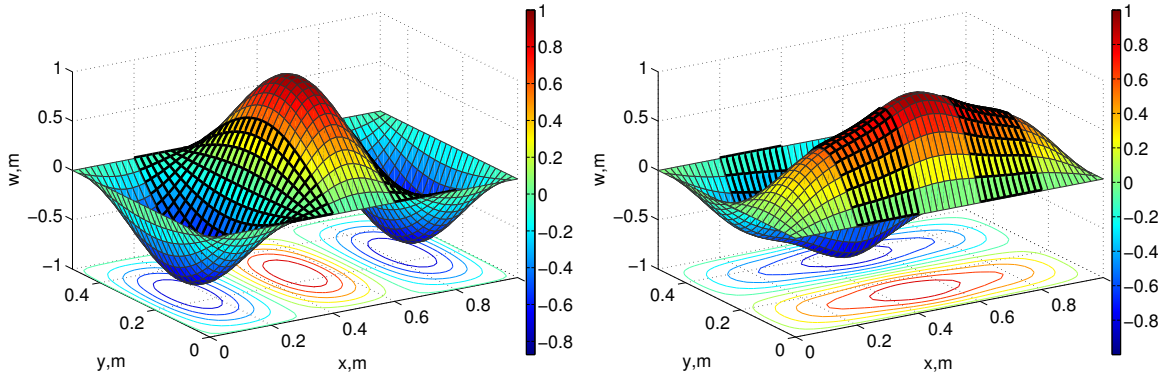

(c) 3^{rd} Mode (d) 4^{th} Mode

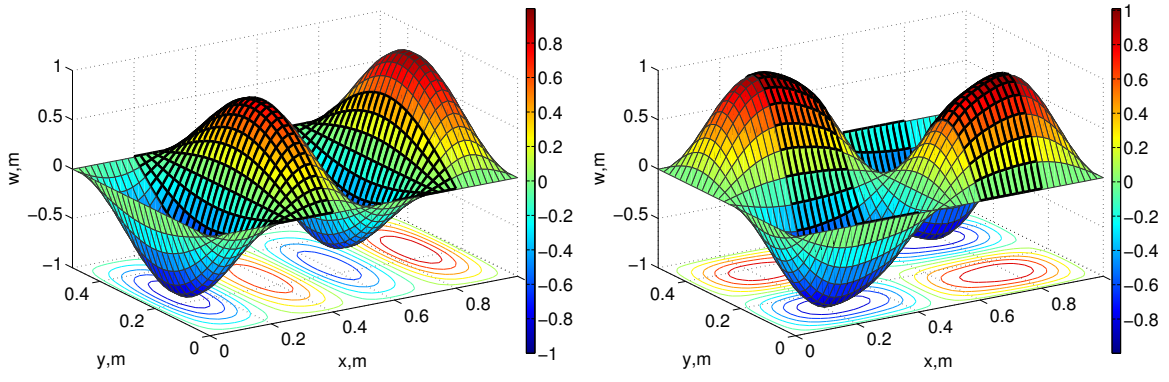

(e) 5^{th} Mode (f) 6^{th} Mode

Figure 4.5: Normalized Natural Bending Modes for the Bonded Stiffened Plate, SS-SS-SS-SS, Stiffeners Bending Shown with Black Color Lines

4.4.2 Free Vibration Analysis of the Stiffened Plate With Damping

In order to validate our code while including damping in the structure, we first considered a three layered sandwich plate with a viscoelastic layer in the middle to compare our results with Bilasse, Azrar and Daya [97], and Cupial and Niziol [99]. The material properties of the elastic layers are as follows: Young's modulus $E = 68.9$ GPa, Poisson's ratio $\nu = 0.3$, density $\rho = 2740$ kg/m^{3}and material properties of the adhesive are given as: Young's modulus $E_a = 2.67$ MPa, Poisson's ratio $\nu_a = 0.49$, density $\rho_a = 999$ kg/m^{3}and loss factor $\eta_a = 0.5$. The length of the plate is $a = 348$mm, width $b = 304.8$mm, elastic layer thickness $h_p = 0.762$mm and core layer thickness $h_a = 0.254$. We considered simply supported (SSSS) and cantilever (CCCC) boundary conditions for this problem. It should be noted that damping is included in this problem, so the Young's and shear moduli of the adhesive layer will be complex numbers, such as $E^* = E(1 + i\eta)$ and $G^* = G(1 + i\eta)$.

A 3D finite element model using ABAQUS was used to get undamped natural frequencies. For the elastic plates, 20-noded quadratic brick, reduced integration, solid elements (C3D20R) were used, whereas, 20-noded quadratic brick hybrid solid elements (C3D20H) with full integration were used in the adhesive layer because of high Poisson's ratio.

The damped natural frequencies and the corresponding loss factor of the entire sandwich plate obtained by following the procedure of this paper using the PVW, as shown in Tables 4.5 and 4.6, are compared with those reported by Bilasse, Azrar and Daya [97], and Cupial and Niziol [99], who used FEM to model this sandwich plate. For this problem, 10×10 terms were used in the PVW to get the converged results. The results for simply supported boundary conditions are also compared with the analytical results provided by Johnson and Kienholz [34]. It can be seen from Tables 4.5 and 4.6, that the results obtained using our code are very close to those reported and loss factor of the overall system is better predicted by PVW than FEM.

Table 4.5: Damped Natural Frequencies and Loss Factors for a Simply-Supported(SSSS) Sandwich Plate

Mode	Frequency (Hz)				Loss Factor (η)		
No.	ABAQUS	Present Method	FEM [99]	Analytical [34]	Present Method	FEM [99]	Analytical [34]
1	59.1	60.5	58.0	60.3	0.190	0.170	0.190
2	114.0	115.8	113.8	115.4	0.203	0.193	0.203
3	129.2	131.1	129.5	130.6	0.199	0.192	0.199
4	177.4	179.2	177.2	178.7	0.181	0.172	0.181
5	194.5	196.1	194.6	195.7	0.174	0.169	0.174
6	232.1	233.4	232.9	–	0.159	0.156	–

Table 4.6: Damped Natural Frequencies and Loss Factors for a Fully Clamped(CCCC) Sandwich Plate

Mode	Frequency (Hz)			Loss Factor (η)	
No.	ABAQUS	Present Method	FEM [97]	Present Method	FEM [97]
1	86.7	87.8	87.4	0.189	0.189
2	148.3	149.4	148.9	0.165	0.164
3	169.3	170.4	170.3	0.154	0.153
4	223.2	224.3	223.9	0.139	0.139
5	240.6	241.4	241.1	0.135	0.134
6	289.8	290.2	291.3	0.119	0.118

Finally, we turn to the rectangular bonded plate of Fig. 4.1, the material properties of the plate and stiffeners are given as: Young's modulus $E = 72.69$ GPa, Poisson's ratio $\nu = 0.313$, density $\rho = 2796$ kg/m^3. We will use the same material properties for the adhesive section as used in the above sandwich plate i.e., $E_a = 2.67$ MPa, Poisson's ratio $\nu_a = 0.49$, density $\rho_a = 999$ kg/m^3. The geometric properties of the the bonded plate are given as: 1m×0.5m×0.005m for the plate, 0.2m×0.5m×0.005m for the stiffener, and 0.2m×0.5m×h_a for the adhesive layer. We will use two values for the loss factor of the viscoelastic adhesive layer $\eta_a = 0.5$, and 1, and two different thickness values $h_a = 0.1016$mm and 0.254mm. These two adhesive thicknesses are usually used for practical purposes in the literature [91].

Table 4.7 present the damped natural frequencies and loss factor for a rectangular adhesively bonded stiffened plate. It can be noticed that both the damped natural frequencies and loss factors decrease as the thickness of the adhesive layer is increased from $h_a = 0.1016$mm to 0.254mm, with the exception of first mode. Intuitively, one will think that as the thickness increases the loss factor should increase, but it's not seen for any of the two cases with $\eta_a = 0.5$ and 1. It is also noticed here that as the loss factor of the core is increased from $\eta_a = 0.5$ to 1, the energy dissipation of the overall structure increases. The same kind of behavior is predicted for the stiffened rectangular plates with CSCS and CCCC boundary conditions, as presented in Tables 4.8 and 4.9, respectively.

Table 4.7: Damped Natural Frequencies and Loss Factors for a SSSS Rectangular Plate with Two Adhesively Bonded Plate Strip-Stiffeners

		h_a=0.1016mm		h_a=0.254mm	
η_c	Mode	Frequency(rad/s)	Loss Factor(η)	Frequency(rad/s)	Loss Factor(η)
0.5	1	510.23	0.106	459.17	0.115
	2	694.33	0.082	643.18	0.076
	3	1143.58	0.060	1091.87	0.042
	4	1532.35	0.107	1407.12	0.073
	5	1654.58	0.050	1590.98	0.068
	6	1722.78	0.100	1592.67	0.032
	7	2164.05	0.057	2071.59	0.037
	8	2472.97	0.059	2368.16	0.035
	9	2657.16	0.055	2552.05	0.033
	10	3091.56	0.071	2934.93	0.041
1	1	526.79	0.172	470.97	0.207
	2	709.98	0.140	652.79	0.142
	3	1156.78	0.111	1097.84	0.079
	4	1564.81	0.197	1418.36	0.144
	5	1669.01	0.095	1598.15	0.062
	6	1756.49	0.186	1602.26	0.132
	7	2185.40	0.108	2079.80	0.072
	8	2496.28	0.112	2374.82	0.069
	9	2678.80	0.105	2559.25	0.064
	10	3122.88	0.137	2943.06	0.081

Table 4.8: Damped Natural Frequencies and Loss Factors for a CSCS Rectangular Plate with Two Adhesively Bonded Plate Strip-Stiffeners

		h_a=0.1016mm		h_a=0.254mm	
η_c	Mode	Frequency(rad/s)	Loss Factor(η)	Frequency(rad/s)	Loss Factor(η)
0.5	1	548.15	0.10	496.27	0.11
	2	791.88	0.08	737.21	0.07
	3	1329.72	0.06	1270.88	0.04
	4	1553.72	0.11	1427.48	0.07
	5	1785.10	0.10	1645.93	0.07
	6	1911.16	0.04	1851.85	0.03
	7	2303.61	0.06	2198.86	0.04
	8	2870.02	0.06	2750.34	0.03
	9	2881.10	0.05	2769.51	0.03
	10	3105.91	0.07	2948.03	0.04
1	1	564.73	0.17	507.45	0.19
	2	808.25	0.14	746.67	0.13
	3	1344.43	0.11	1277.21	0.08
	4	1586.21	0.20	1438.70	0.14
	5	1819.75	0.19	1657.22	0.13
	6	1924.50	0.08	1857.01	0.05
	7	2326.84	0.12	2206.87	0.08
	8	2894.79	0.11	2757.43	0.07
	9	2904.18	0.10	2777.77	0.06
	10	3137.47	0.14	2956.22	0.08

Table 4.9: Damped Natural Frequencies and Loss Factors for a CCCC Rectangular Plate with Two Adhesively Bonded Plate Strip-Stiffeners

		h_a=0.1016mm		h_a=0.254mm	
η_c	Mode	Frequency(rad/s)	Loss Factor(η)	Frequency(rad/s)	Loss Factor(η)
0.5	1	893.47	0.10	823.16	0.07
	2	1081.25	0.10	1002.89	0.06
	3	1528.29	0.05	1469.98	0.04
	4	2072.57	0.04	2013.51	0.03
	5	2175.33	0.07	2063.15	0.04
	6	2368.65	0.08	2238.26	0.04
	7	2801.63	0.05	2707.09	0.03
	8	2983.65	0.06	2865.51	0.03
	9	3323.38	0.04	3218.20	0.03
	10	3830.37	0.04	3721.60	0.02
1	1	910.83	0.19	829.45	0.14
	2	1100.10	0.18	1009.05	0.12
	3	1541.23	0.09	1477.59	0.07
	4	2084.15	0.07	2020.14	0.05
	5	2197.06	0.14	2069.77	0.08
	6	2392.58	0.15	2245.27	0.09
	7	2819.99	0.09	2713.67	0.05
	8	3006.90	0.11	2871.78	0.06
	9	3342.78	0.08	3225.13	0.05
	10	3851.48	0.08	3727.66	0.04

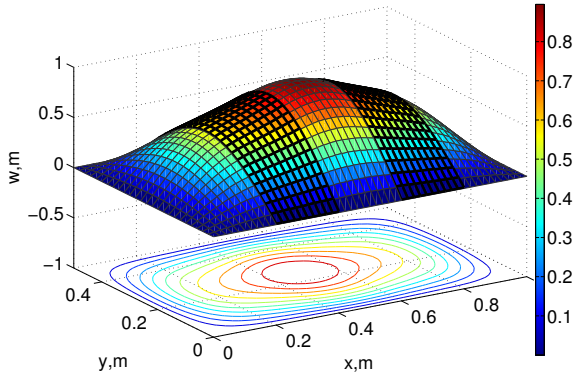

(a) Real Part 1^{st} Mode

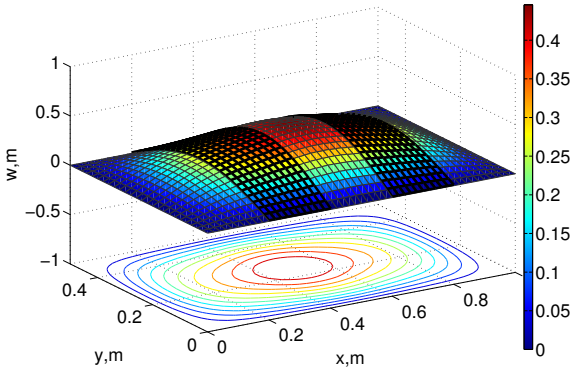

(b) Imaginary Part 1^{st} Mode

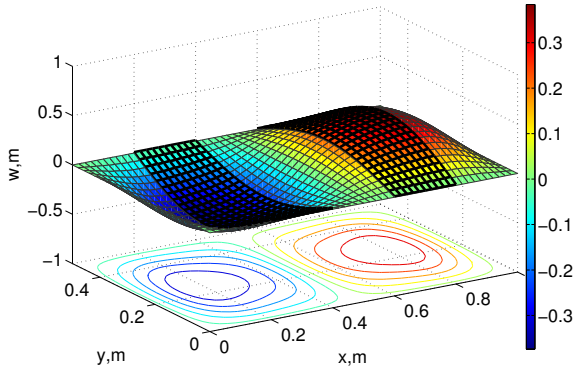

(c) Real Part 2^{nd} Mode

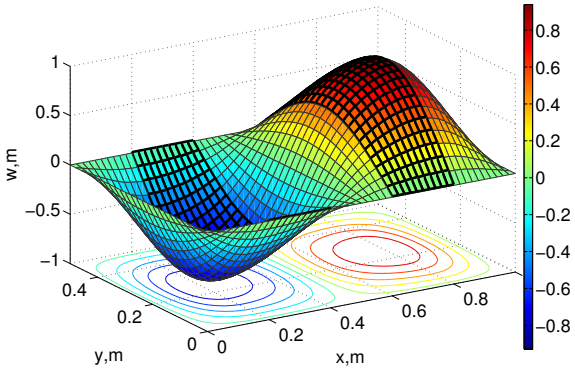

(d) Imaginary Part 2^{nd} Mode

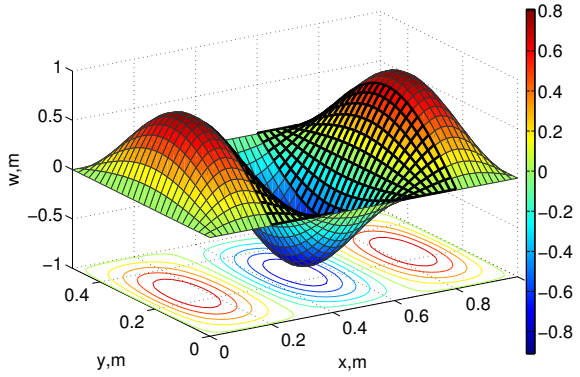

(e) Real Part 3^{rd} Mode

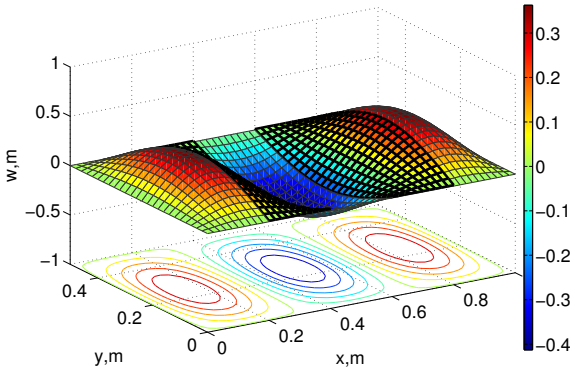

(f) Imaginary Part 3^{rd} Mode

Figure 4.6: First Three Normalized Complex Bending Modes for the Bonded Stiffened Plate, SS-SS-SS-SS, Stiffeners Bending Shown with Black Color Lines

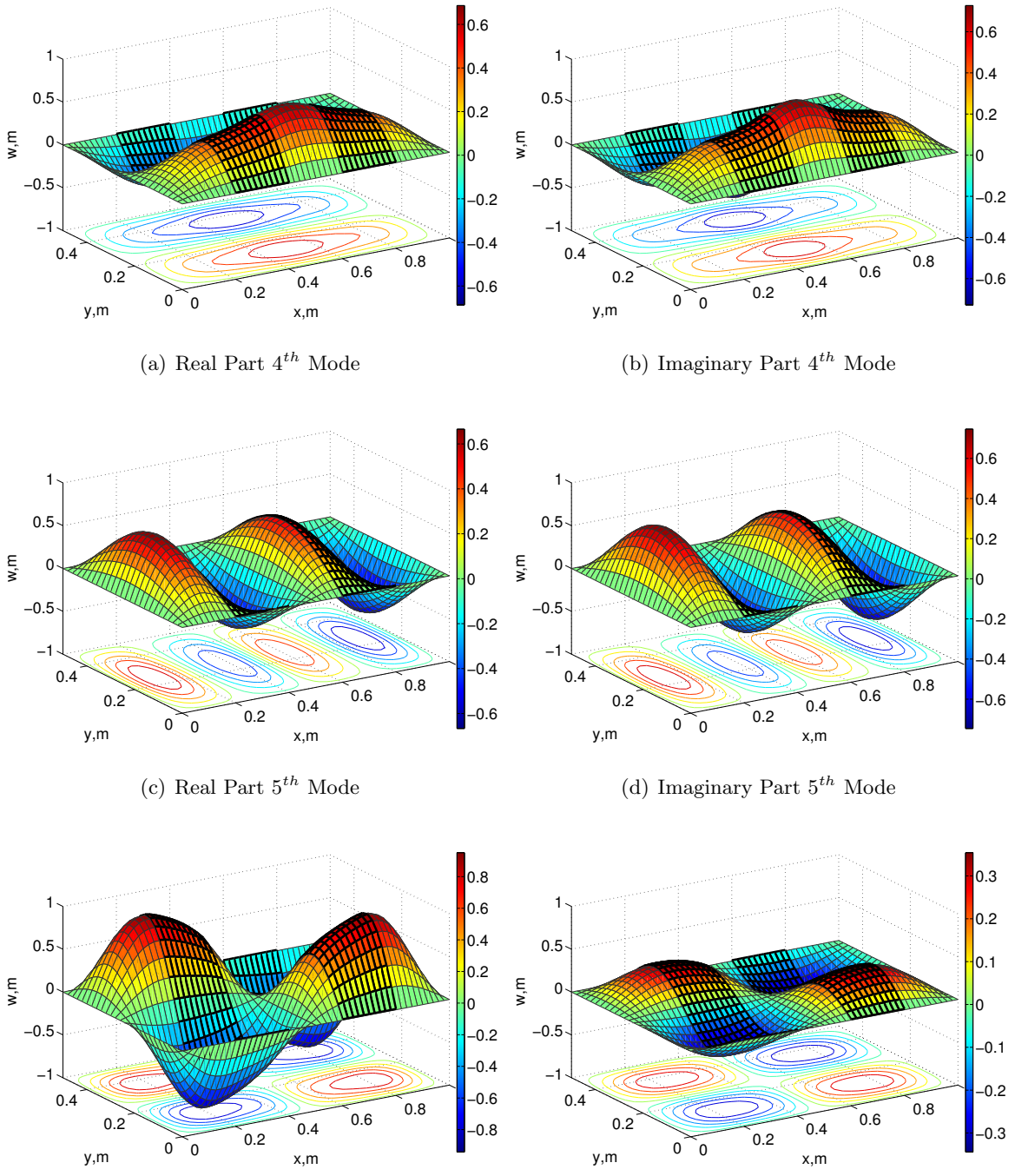

(a) Real Part 4^{th} Mode

(b) Imaginary Part 4^{th} Mode

(c) Real Part 5^{th} Mode

(d) Imaginary Part 5^{th} Mode

(e) Real Part 6^{th} Mode

(f) Imaginary Part 6^{th} Mode

Figure 4.7: Normalized Complex Natural Bending Modes (4-6) for the Bonded Stiffened Plate, SS-SS-SS-SS, Stiffeners Bending Shown with Black Color Lines

4.5 Conclusions

We studied bonded stiffened plate with plate-strip stiffeners using the principle of virtual work and the first order shear deformation theory. The deflections and rotations were assumed as a product of static Timoshenko beam functions, chosen appropriately according to the given boundary conditions. The numerical results were compared with the solutions available in the literature and finite element software ABAQUS, and the results were found to be highly satisfactory. Unlike Navier and Levy solution techniques, the approach used in this paper can also solve for fully clamped, free and cantilever supported stiffened plates. Moreover, the layerwise First order shear deformation theory can be extended to account for orthotropic and composite materials. The procedure adopted here can be used to analyze square and rectangular plates, as well as eccentrically and concentrically stiffened plates. It was concluded that as the Young's modulus of the adhesive is increased, the overall natural frequencies of the system increase almost linearly. Moreover, it was deduced that when the thickness of the adhesive layer is increased, the natural frequencies and loss factor of the stiffened structure decrease. It can be concluded that a viscoelastic material with high damping properties, i.e. high intrinsic loss factor, and small thickness, will be a perfect design variable to obtain overall high damping in the structure.

Chapter 5

Conclusions and Future Recommendations

5.1 Summary

The main goal of this work was to incorporate viscoelastic material in a thick stiffened panel with plate-strip stiffeners, to enhance the damping characteristics of the structure. This was achieved by using constrained layer damping treatment, in which the constraining layer forces the viscoelastic core layer to deform in shear and, hence, provide large damping during cyclic oscillations. The thick stiffeners utilized in this study were plate-strip stiffeners, unlike the rib stiffeners often investigated by researchers. This research effort was divided into three steps; (1) damped response of sandwich beams, (2) free vibration analysis of integrally stiffened plates with plate-strip stiffeners, and (3) damped response of the bonded stiffened plates.

First, we investigated beams in the presence of a viscoelastic layer sandwiched between two elastic layers. The principle of virtual work (PVW) was used along with the Rayleigh beam theory, by including the longitudinal and rotational inertias in the formulation. The damping in the layers was modeled using complex modulus approach. Simple trigonometric functions were used as admissible functions in PVW to obtain the damped response, and the convergence rate of these functions was compared with simple polynomial functions. Moreover, the sandwich beam was formulated and analyzed using plane stress elasticity based

finite-element method, without any assumptions for the transverse shear strains. All the layers were modeled using 2D elements in the normal direction, and transverse shear strains were introduced in both elastic and core layers. Furthermore, an effect on the damped response of the sandwich structure from using 4-noded as well as 9-noded rectangular elements was investigated. The natural frequencies and loss factor were calculated using modal strain energy method and method of complex eigenvalues. The efficiency of the modal strain energy method was tested for different loss factors in the core layer. Complex mode shapes of the beam were studied and a comparison was made between viscoelastically and viscously damped structures.

Secondly, we investigated the natural frequencies and mode shapes of a freely vibrating, integrally stiffened plate. Both plate and stiffeners were analyzed using the layerwise first order shear deformation theory (FSDT), which employs the transverse shear deformation and rotary inertias as well as the longitudinal displacements. The deflections and rotations were assumed to be a tensor product of static Timoshenko beam functions, chosen appropriately according to the given boundary conditions. The governing differential equations were solved using the Rayleigh-Ritz method. Development of stiffness and mass matrix consumes huge amount of CPU time due to integration of beam functions, which are sets of trigonometric functions, especially when solving for clamped-clamped and clamped-free boundary conditions. A technique is suggested to significantly decrease the amount of CPU time, by avoiding the recursive integration in a loop structure in the computer program. The integrand was symbolically integrated using MATLAB® once, and the solution was obtained in terms of the iteration symbols used in the loop structure. The numerical results were compared with the exact solutions available in the literature and the commercially available finite element software ABAQUS®, and the results were found to be highly satisfactory. Some parametric studies were carried out to show the influence of certain important parameters on the overall natural frequencies of the stiffened plate.

Finally, damped vibration response of a thick stiffened plate with adhesively bonded plate-strip stiffeners was investigated using FSDT for both the plate and stiffeners. On the assumption of no slip condition at the interface between the adhesive and the adherend layers, the adhesive was deformed in shear during cyclic oscillations. The deflections and rotations

were assumed as a tensor product of static Timoshenko beam functions, and the problem was analyzed using the principle of virtual work (PVW). At first, we did not consider damping in the adhesive in order to validate our code, by comparing our results with those available in the literature as well as with the results obtained using ABAQUS® 3D modelling. We also considered the effect of changing the stiffness of the adhesive layer on the vibration of the bonded system. As a second step, we examined damping in the stiffened structure using complex modulus approach, a widely used technique to represent the rheology of the viscoelastic materials. The damping characteristics of the stiffened structure was tested for different kinds of viscoelastic material and variation of the adhesive thickness.

5.2 Conclusions

5.2.1 Damped Sandwich Beams

1. We obtained good estimates of natural frequencies and loss factors by using trigonometric functions as compared to using simple polynomials, by using less number of terms in the Ritz method.

2. We found that higher degree elements used in the FE elasticity analysis, gives us better estimates of loss factor and natural frequency unlike using beam elements, especially in the problem in which we consider complex stiffness in the elastic layers.

3. MCE gives accurate results but with higher computational cost, especially when a fine mesh in considered. MSE is a cost-effective method but for damping treatments with high loss factors, it overestimates the overall damping of the system.

4. We observed that although the eigenvalues and eigenvectors are complex in the case of constrained viscoelastic layer damping, we still get stationary nodes unlike non-proportional viscously damped structures. Despite the fact that constrained layer treatment can be quite damped, mode shapes are close to normal modes, and it can be concluded that viscoelastic damping is very close to being proportional.

5. In the case of a viscoelastic damped sandwich beam with end viscous damper, we found

that we do not get a single point along the length of the beam where the displacement goes to zero at different times during cyclic oscillations, i.e. the concept of having a node at a point at all times does not exist.

6. The mode shapes of the lower modes of a beam with a viscous damper at the free end are more sensitive to the viscous damping coefficient. The complexity of a mode shape is smaller for higher modes of the beam with a viscous damper at the end.

5.2.2 Integrally Stiffened Plates

1. Unlike Navier and Levy solution techniques, the approach used for investigating integrally stiffened plates with plate-strip stiffeners using Ritz method, can also be applied to stiffened plate with fully clamped, free and cantilever boundary conditions.

2. Development of stiffness and mass matrix consumes huge amount of CPU time due to integration and use of beam functions. A time reduction technique was proposed to greatly decrease, in some cases by two orders of magnitude, the amount of CPU time.

3. Rectangular and square type plates can be analyzed using this method, as well as eccentrically and concentrically stiffened plates.

4. It was deduced that when the thickness of the stiffeners is small as compared to the plate thickness, stiffener and plate rotations can be assumed to be the same.

5. Moreover, it was concluded that by increasing the ratio of stiffener to plate thickness, we obtain a linear increase in the overall natural frequencies of the system.

6. A substantial decrease in the overall natural frequencies is attained, when the plate dimensions are changed from rectangular to square geometry.

7. It was noticed from the parametric study, that the change in the width of the stiffener does not have a substantial effect on the natural frequencies of the entire system.

8. In the case of beams, we get nodes along the length of the beam during cyclic oscillations, however, in the case of plates we obtain nodal lines. For a plate with cantilever boundary

conditions and viscous dampers at the free end, it was observed that the nodal lines change their location from time to time, and we do not get a single location on the plate where all the displacements go to zero.

9. It was noticed that the dispersion of zero displacement points, for higher modes, is wider near the right end of the plate, where viscous damper is mounted. Moreover, it was also seen that the increase in damping coefficient value C, increases the dispersion of the nodal lines from a specific location.

5.2.3 Damped Adhesively Bonded Stiffened Plates

1. It was noticed that the shear deformation in the core layer is not affected greatly, if we consider different vertical deflections for the plate and stiffeners, due to the very small thickness of the viscoelastic layer as compared to the adherend layers. Therefore, it can be concluded that same vertical deflections for both the plate and stiffeners will give highly accurate vibration results.

2. FSDT was utilized for the plate and stiffeners separately, therefore, different materials can be considered for stiffeners and the plate. Moreover, the layerwise first order shear deformation theory can be extended to account for orthotropic and composite materials.

3. Due to the way the problem is setup, the location of the stiffeners will not affect the accuracy of the results and it can be used to analyze symmetrically or asymmetrically placed stiffeners.

4. It was concluded that as the Young's modulus of the adhesive is increased, the overall natural frequencies of the system increase almost linearly.

5. We observed an overall increase in the natural frequencies of the system, due to the damping provided by the viscoelastic material.

6. Moreover, it was deduced that when the thickness of the adhesive layer is increased, the natural frequencies and loss factor of the stiffened structure decrease.

7. It can be concluded that a viscoelastic material with high damping properties, i.e. high intrinsic loss factor, and small thickness, will be a perfect design variable to obtain overall high damping in the structure.

5.3 Recommendations for Future Work

As nowadays there is a high demand of using composite materials in the aircraft and automobile industries, we would like to extend this work to composite stiffened panels with viscoelastic material. It will also be beneficial if we can include the damping due to laminated composites in the vibration analysis. A piezoelectric ceramic used as a constraining layer, can greatly enhance the damping characteristics of the stiffened panel, especially in the low frequency regime, during which the shear deformation in viscoelastic layer is minimal. On the other hand, if the application needs a thick plate-strip stiffener due to stiffness requirements, a thin PZT patch can be placed on top of the constraining layer to harvest energy during cyclic oscillation for powering small electronic devices. Moreover, as buckling analysis is an important research area specially in aircraft wings, it will be beneficial to study the effects of buckling on adhesively bonded stiffened plates. Furthermore, the location, width, thickness and the number of stiffeners are important parameters for the structural response and, hence, an optimization technique used for this type of stiffened panels with plate-strip stiffeners will highly benefit the implementation of these type of structures in the industry.

Bibliography

[1] Hu, N., Buchholz, H., Herr, M., Spehr, C., and Haxter, S., "Contributions of different aeroacoustic sources to aircraft cabin noise," *Proceedings of the 19th AIAA/CEAS Aeroacoustics Conference*, 2013.

[2] Rao, M. D., "Recent applications of viscoelastic damping for noise control in automobiles and commercial airplanes," *Journal of Sound and Vibration*, Vol. 262, No. 3, 2003, pp. 457–474.

[3] Donaldson, B. K., *Introduction to structural dynamics*, Cambridge University Press, 2006.

[4] Hodges, D. H. and Pierce, G. A., *Introduction to structural dynamics and aeroelasticity*, Vol. 15, Cambridge University Press, 2011.

[5] Mellert, V., Baumann, I., Freese, N., and Weber, R., "Impact of sound and vibration on health, travel comfort and performance of flight attendants and pilots," *Aerospace Science and Technology*, Vol. 12, No. 1, 2008, pp. 18–25.

[6] Jones, D. I., *Handbook of viscoelastic vibration damping*, John Wiley & Sons, 2001.

[7] Hudson, M. and Reynolds, P., "Implementation considerations for active vibration control in the design of floor structures," *Engineering Structures*, Vol. 44, 2012, pp. 334–358.

[8] Nashif, A. D. and Henderson, J. P., *Vibration damping*, John Wiley & Sons, 1985.

[9] Sun, C.-T. and Lu, Y. P., *Vibration damping of structural elements*, Prentice Hall PTR Englewood Cliffs, 1995.

[10] Hu, H., Belouettar, S., Potier-Ferry, M., and Daya, E. M., "Review and assessment of various theories for modeling sandwich composites," *Composite Structures*, Vol. 84, No. 3, 2008, pp. 282–292.

[11] Abdoun, F., Azrar, L., Daya, E. M., and Potier-Ferry, M., "Forced harmonic response of viscoelastic structures by an asymptotic numerical method," *Computers & Structures*, Vol. 87, No. 1, 2009, pp. 91–100.

[12] Baz, A. and Ro, J., "Optimum design and control of active constrained layer damping," *Journal of Mechanical Design*, Vol. 117, No. B, 1995, pp. 135–144.

[13] Zhou, X., Yu, D., Shao, X., Zhang, S., and Wang, S., "Research and applications of viscoelastic vibration damping materials: A review," *Composite Structures*, Vol. 136, 2016, pp. 460–480.

[14] Treviso, A., Van Genechten, B., Mundo, D., and Tournour, M., "Damping in composite materials: Properties and models," *Composites Part B: Engineering*, Vol. 78, 2015, pp. 144–152.

[15] De Espındola, J. J., da Silva Neto, J. M., and Lopes, E. M., "A generalised fractional derivative approach to viscoelastic material properties measurement," *Applied Mathematics and Computation*, Vol. 164, No. 2, 2005, pp. 493–506.

[16] Lee, D. H., "Optimal placement of constrained-layer damping for reduction of interior noise," *AIAA Journal*, Vol. 46, No. 1, 2008, pp. 75–83.

[17] Holman, R. E. and Tanner, J. M., "Finite element modeling techniques for constrained layer damping," *AIAA Journal*, Vol. 21, No. 5, 1983, pp. 792–794.

[18] Nakra, B. C., "Vibration Control with Viscoelastic Materials," *The Shock and Vibration Digest*, Vol. 8, 1975, pp. 114–123.

[19] Kerwin Jr, E. M., "Damping of flexural waves by a constrained viscoelastic layer," *The Journal of the Acoustical Society of America*, Vol. 31, No. 7, 1959, pp. 952–962.

[20] Mead, D. J. and Markus, S., "The forced vibration of a three-layer, damped sandwich beam with arbitrary boundary conditions," *Journal of Sound and Vibration*, Vol. 10, No. 2, 1969, pp. 163–175.

[21] DiTaranto, R. A., "Theory of vibratory bending for elastic and viscoelastic layered finite-length beams," *Journal of Applied Mechanics*, Vol. 32, No. 4, 1965, pp. 881–886.

[22] Rikards, R., "Finite element analysis of vibration and damping of laminated composites," *Composite Structures*, Vol. 24, No. 3, 1993, pp. 193–204.

[23] Barkanov, E. N., "Method of complex eigenvalues for studying the damping properties of sandwich-type structures," *Mechanics of Composite Materials*, Vol. 29, No. 1, 1993, pp. 90–94.

[24] Rikards, R. B. and Barkanov, E. N., "Determination of the dynamic characteristics of vibration-absorbing coatings by the finite-element method," *Mechanics of Composite Materials*, Vol. 27, No. 5, 1992, pp. 529–535.

[25] Rao, Y. V. K. S. and Nakra, B. C., "Vibrations of unsymmetrical sandwich beams and plates with viscoelastic cores," *Journal of Sound and Vibration*, Vol. 34, No. 3, 1974, pp. 309–326.

[26] Rao, D. K., "Frequency and loss factors of sandwich beams under various boundary conditions," *Journal of Mechanical Engineering Science*, Vol. 20, No. 5, 1978, pp. 271–282.

[27] Lall, A. K., Asnani, N. T., and Nakra, B. C., "Damping analysis of partially covered sandwich beams," *Journal of Sound and Vibration*, Vol. 123, No. 2, 1988, pp. 247–259.

[28] Fasana, A. and Marchesiello, S., "Rayleigh-Ritz analysis of sandwich beams," *Journal of Sound and Vibration*, Vol. 241, No. 4, 2001, pp. 643–652.

[29] Singhvi, S. and Kapania, R. K., "Comparison of simple and Chebychev polynomials in Rayleigh-Ritz analysis," *Journal of Engineering Mechanics*, Vol. 120, No. 10, 1994, pp. 2126–2135.

[30] Sainsbury, M. G. and Zhang, Q. J., "The Galerkin element method applied to the vibration of damped sandwich beams," *Computers & Structures*, Vol. 71, No. 3, 1999, pp. 239–256.

[31] Bhimaraddi, A., "Sandwich beam theory and the analysis of constrained layer damping," *Journal of Sound and Vibration*, Vol. 179, No. 4, 1995, pp. 591–602.

[32] Imaino, W. and Harrison, J. C., "A comment on constrained layer damping structures with low viscoelastic modulus," *Journal of Sound and Vibration*, Vol. 149, No. 2, 1991, pp. 354–359.

[33] Sanliturk, K. Y. and Koruk, H., "Development and validation of a composite finite element with damping capability," *Composite Structures*, Vol. 97, 2013, pp. 136–146.

[34] Johnson, C. D. and Kienholz, D. A., "Finite element prediction of damping in structures with constrained viscoelastic layers," *AIAA Journal*, Vol. 20, No. 9, 1982, pp. 1284–1290.

[35] Soni, M. L. and Bogner, F. K., "Finite element vibration analysis of damped structures," *AIAA Journal*, Vol. 20, No. 5, 1982, pp. 700–707.

[36] Kosmatka, J. B. and Liguore, S. L., "Review of methods for analyzing constrained-layer damped structures," *Journal of Aerospace Engineering*, Vol. 6, No. 3, 1993, pp. 268–283.

[37] Haftka, R. T. and Kapania, R. K., "Sensitivity of actively damped structures to imperfections and modeling errors," *AIAA Journal*, Vol. 27, No. 10, 1989, pp. 1434–1440.

[38] Bagley, R. L. and Torvik, P. J., "Fractional calculus in the transient analysis of viscoelastically damped structures," *AIAA Journal*, Vol. 23, No. 6, 1985, pp. 918–925.

[39] Golla, D. F. and Hughes, P. C., "Dynamics of viscoelastic structuresa time-domain, finite element formulation," *Journal of Applied Mechanics*, Vol. 52, No. 4, 1985, pp. 897–906.

[40] McTavish, D. J., Hughes, P. C., Soucy, Y., and Graham, W. B., "Prediction and measurement of modal damping factors for viscoelastic space structures," *AIAA Journal*, Vol. 30, No. 5, 1992, pp. 1392–1399.

[41] Lesieutre, G. A. and Bianchini, E., "Time domain modeling of linear viscoelasticity using anelastic displacement fields," *Journal of Vibration and Acoustics*, Vol. 117, No. 4, 1995, pp. 424–430.

[42] Liu, W. and Ewing, M. S., "Experimental and analytical estimation of loss factors by the power input method," *AIAA Journal*, Vol. 45, No. 2, 2007, pp. 477–484.

[43] De Lima, A., Da Silva, A., Rade, D., and Bouhaddi, N., "Component mode synthesis combining robust enriched Ritz approach for viscoelastically damped structures," *Engineering Structures*, Vol. 32, No. 5, 2010, pp. 1479–1488.

[44] Cao, X., Hua, H., and Zhang, Z., "Acoustic Radiation From Stiffened Cylindrical Shells With Constrained Layer Damping," *Journal of Vibration and Acoustics*, Vol. 135, No. 1, 2013, pp. 011005.

[45] Boucher, M.-A., Smith, C., Scarpa, F., Rajasekaran, R., and Evans, K., "Effective topologies for vibration damping inserts in honeycomb structures," *Composite Structures*, Vol. 106, 2013, pp. 1–14.

[46] Zhou, X., Yu, D., Shao, X., Wang, S., and Zhang, S., "Simplified-super-element-method for analyzing free flexural vibration characteristics of periodically stiffened-thin-plate filled with viscoelastic damping material," *Thin-Walled Structures*, Vol. 94, 2015, pp. 234–252.

[47] Panda, S. and Ray, M., "Active constrained layer damping of geometrically nonlinear vibrations of functionally graded plates using piezoelectric fiber-reinforced composites," *Smart Materials and Structures*, Vol. 17, No. 2, 2008, pp. 025012.

[48] Balamurugan, V. and Narayanan, S., "Finite element modeling of stiffened piezolaminated plates and shells with piezoelectric layers for active vibration control," *Smart Materials and Structures*, Vol. 19, No. 10, 2010, pp. 105003.

[49] Mohammadi, F. and Sedaghati, R., "Vibration analysis and design optimization of sandwich cylindrical panels fully and partially treated with electrorheological fluid materials,"

Journal of Intelligent Material Systems and Structures, Vol. 23, No. 15, 2012, pp. 1679–1697.

[50] Shivakumar, J., Ashok, M., and Ray, M., "Active control of geometrically nonlinear transient vibrations of laminated composite cylindrical panels using piezoelectric fiber reinforced composite," *Acta Mechanica*, Vol. 224, No. 1, 2013, pp. 1–15.

[51] Kattimani, S. and Ray, M., "Active control of large amplitude vibrations of smart magneto–electro–elastic doubly curved shells," *International Journal of Mechanics and Materials in Design*, Vol. 10, No. 4, 2014, pp. 351–378.

[52] Sharma, A., Kumar, R., Vaish, R., and Chauhan, V. S., "Lead-free piezoelectric materials performance in structural active vibration control," *Journal of Intelligent Material Systems and Structures*, Vol. 25, No. 13, 2014, pp. 1596–1604.

[53] Koruk, H. and Sanliturk, K. Y., "Assessment of Modal Strain Energy Method: Advantages and Limitations," *ASME 2012 11th Biennial Conference on Engineering Systems Design and Analysis*, American Society of Mechanical Engineers, 2012, pp. 147–153.

[54] Koruk, H. and Sanliturk, K. Y., "Assesment of the complex eigenvalue and the modal strain energy methods for damping predictions," *Procedings of 18th International Congress on Sound and Vibration, Rio De Janerio, Brazil*, 2011.

[55] Koruk, H. and Sanliturk, K. Y., "Optimisation of damping treatments based on big bang–big crunch and modal strain energy methods," *Journal of Sound and Vibration*, Vol. 333, No. 5, 2014, pp. 1319–1330.

[56] Han, S. M., Benaroya, H., and Wei, T., "Dynamics of transversely vibrating beams using four engineering theories," *Journal of Sound and Vibration*, Vol. 225, No. 5, 1999, pp. 935–988.

[57] Ahmad, N. and Kapania, R. K., "Complex modes in damped sandwich beams using beam and elasticity theories," *54th AIAA/ASCE/AHS/ASC Structures, Structural Dynamics, and Materials Conference*, 2013.

[58] Ahmad, N. and Kapania, R. K., "Complex modes in damped sandwich beams using beam and elasticity theories," *Advances in Aircraft and Spacecraft Science*, Vol. 2, No. 1, 2015, pp. 57–76.

[59] Reddy, J. N., *An introduction to the finite element method*, McGraw-Hill New York, 2nd ed., 1993.

[60] Bilasse, M., Daya, E. M., and Azrar, L., "Linear and nonlinear vibrations analysis of viscoelastic sandwich beams," *Journal of Sound and Vibration*, Vol. 329, No. 23, 2010, pp. 4950–4969.

[61] Daya, E. M. and Potier-Ferry, M., "A numerical method for nonlinear eigenvalue problems application to vibrations of viscoelastic structures," *Computers & Structures*, Vol. 79, No. 5, 2001, pp. 533–541.

[62] Soni, M. L., "Finite element analysis of viscoelastically damped sandwich structures," *The Shock and Vibration Bull*, Vol. 5, No. 1, 1981, pp. 97–109.

[63] Krenk, S., "Complex modes and frequencies in damped structural vibrations," *Journal of Sound and Vibration*, Vol. 270, No. 4, 2004, pp. 981–996.

[64] Koruk, H. and Sanliturk, K. Y., "A novel definition for quantification of mode shape complexity," *Journal of Sound and Vibration*, Vol. 332, No. 14, 2013, pp. 3390–3403.

[65] Lampoh, K., Charpentier, I., and El Mostafa, D., "Eigenmode sensitivity of damped sandwich structures," *Comptes Rendus Mécanique*, 2014.

[66] Adhikari, S., "Optimal complex modes and an index of damping non-proportionality," *Mechanical Systems and Signal Processing*, Vol. 18, No. 1, 2004, pp. 1–27.

[67] Barkanov, E. N., "Natural vibrations of a system with hysteretic and viscous damping," *Mechanics of Composite Materials*, Vol. 29, No. 6, 1994, pp. 613–616.

[68] Zarek, J. H. B. and Gibbs, B. M., "The derivation of eigenvalues and mode shapes for the bending motion of a damped beam with general end conditions," *Journal of Sound and Vibration*, Vol. 78, No. 2, 1981, pp. 185–196.

[69] Prater Jr, G. and Singh, R., "Eigenproblem formulation, solution and interpretation for non-proportionally damped continuous beams," *Journal of Sound and Vibration*, Vol. 143, No. 1, 1990, pp. 125–142.

[70] Hull, P. V. and Buchanan, G. R., "Vibration of moderately thick square orthotropic stepped thickness plates," *Applied Acoustics*, Vol. 64, No. 7, 2003, pp. 753–763.

[71] Duan, G. and Wang, X., "Vibration analysis of stepped rectangular plates by the discrete singular convolution algorithm," *International Journal of Mechanical Sciences*, Vol. 82, 2014, pp. 100–109.

[72] Yuceoglu, U., Germalmayan, N., and Sunar, O., "Free flexural vibrations of integrally-stiffened and/or stepped-thickness rectangular plates or panels with a central plate stiffener," *48th AIAA/ASME/ASCE/AHS/ASC Structures, Structural Dynamics, and Materials Conference*, AIAA, Honolulu, Hawaii, April 2007.

[73] Ahmad, N. and Kapania, R. K., "Free vibration analysis of an integrally stiffened plate with plate-strip stiffeners using a set of static Timoshenko Beam functions," *56th AIAA/ASCE/AHS/ASC Structures, Structural Dynamics, and Materials Conference*, 2015, p. 1167.

[74] Ahmad, N. and Kapania, R. K., "Free vibration analysis of integrally stiffened plates with plate-strip stiffeners," *AIAA Journal*, 2016.

[75] Chopra, I., "Vibration of stepped thickness plates," *International Journal of Mechanical Sciences*, Vol. 16, No. 6, 1974, pp. 337–344.

[76] Guo, S. J., Keane, A. J., and Moshrefi-Torbati, M., "Vibration analysis of stepped thickness plates," *Journal of Sound and vibration*, Vol. 204, No. 4, 1997, pp. 645–657.

[77] Boscolo, M. and Banerjee, J. R., "Dynamic stiffness elements and their applications for plates using first order shear deformation theory," *Computers & Structures*, Vol. 89, No. 3, 2011, pp. 395–410.

[78] Demasi, L. and Yu, W., "Assess the accuracy of the variational asymptotic plate and shell analysis using the generalized unified formulation," *Mechanics of Advanced Materials and Structures*, Vol. 20, No. 3, 2013, pp. 227–241.

[79] Kapania, R. K. and Liu, Y., "Static and vibration analyses of general wing structures using equivalent-plate models," *AIAA Journal*, Vol. 38, No. 7, 2000, pp. 1269–1277.

[80] Kapania, R. K. and Lovejoy, A. E., "Free vibration of thick generally laminated cantilever quadrilateral plates," *AIAA Journal*, Vol. 34, No. 7, 1996, pp. 1474–1486.

[81] Yuceoglu, U., Javanshir, J., and Güvendik, O., "On a general approach to free vibrations response of integrally-stiffened and/or stepped thickness rectangular plates or panels," *2008 ASME International Mechanical Engineering Congress and Exposition, Boston*, ASME, 2008.

[82] Yuceoglu, U., Germalmayan, N., and Sunar, O., "Free bending vibrations of integrally-stiffened and/or stepped-thickness rectangular plates or panels with a non-central plate stiffener," *2007 ASME International Mechanical Engineering Congress and Exposition, Washington*, ASME, 2007.

[83] Javanshir, J., Farsadi, T., and Yuceoglu, U., "Free vibrations of composite base plates stiffened by two adhesively bonded plate strips," *Journal of Aircraft*, Vol. 49, No. 4, 2012, pp. 1135–1152.

[84] Yuceoglu, U. and Özerciyes, V., "Sudden drop phenomena in natural frequencies of partially-stiffened, stepped-thickness, composite plates or panels," *40th AIAA/ASME/ASCE/AHS/ASC Structures, Structural Dynamics, and Materials Conference and Exhibit*, AIAA, St. Louis, MO, 1999.

[85] Huang, T. C., "The effect of rotatory inertia and of shear deformation on the frequency and normal mode equations of uniform beams with simple end conditions," *Journal of Applied Mechanics*, Vol. 28, No. 4, 1961, pp. 579–584.

[86] Dawe, D. J. and Roufaeil, O. L., "Rayleigh-Ritz vibration analysis of Mindlin plates," *Journal of Sound and Vibration*, Vol. 69, No. 3, 1980, pp. 345–359.

[87] Cheung, Y. K. and Zhou, D., "Vibrations of moderately thick rectangular plates in terms of a set of static Timoshenko beam functions," *Computers and Structures*, Vol. 78, No. 6, 2000, pp. 757–768.

[88] Ahmad, N. and Kapania, R. K., "Damped free vibration response of an adhesively bonded stiffened plate with plate-strip stiffeners," *57th AIAA/ASCE/AHS/ASC Structures, Structural Dynamics, and Materials Conference*, 2016, p. 0471.

[89] Xiang, Y. and Wang, C., "Exact Buckling and Vibration Solutions for Stepped Rectangular Plates," *Journal of Sound and Vibration*, Vol. 250, No. 3, 2002, pp. 503 – 517.

[90] Ko, T.-C., Lin, C.-C., and Chu, R.-C., "Vibration of bonded laminated lap-joint plates using adhesive interface elements," *Journal of Sound and Vibration*, Vol. 184, No. 4, 1995, pp. 567 – 583.

[91] Lin, C.-C. and Ko, T.-C., "Free vibration of bonded plates," *Computers and Structures*, Vol. 64, No. 14, 1997, pp. 441 – 452.

[92] Islam, M. M. and Kapania, R. K., "Global–Local Finite Element Analysis of Adhesive Joints and Crack Propagation," *Journal of Aircraft*, Vol. 51, No. 1, 2014, pp. 310–319.

[93] Islam, M. M. and Kapania, R. K., "A Study of the Adhesive Joints and Crack Propagation Using a Global-local Finite Element Method," *54th AIAA/ASME/ASCE/AHS/ASC Structures, Structural Dynamics, and Materials Conference*, AIAA, 2013.

[94] Adams, R., *Adhesive Bonding*, CRC Press LLC, 1st ed., 2005.

[95] Yuceoglu, U., Javanshir, J., and Güvendik, Ö., "Free Flexural (or Bending) Vibrations of Composite Mindlin Base Plates or Panels with Two Bonded Stiffening Plate Strips," *50th AIAA/ASME/ASCE/AHS/ASC Structures, Structural Dynamics, and Materials Conference*, AIAA, 2009.

[96] Javanshir, J., *Free Flexural (or Bending) Vibrations Analysis of Certain Groups of Stiffened Composite Plates or Panels In Flight Vehicle Structures*, Ph. D. Dissertation, Middle East Technical University, Dec. 2009.

[97] Bilasse, M., Azrar, L., and Daya, E., "Complex modes based numerical analysis of viscoelastic sandwich plates vibrations," *Computers and Structures*, Vol. 89, No. 78, 2011, pp. 539 – 555.

[98] Kung, S. W. and Singh, R., "Complex Eigensolutions of Rectangular Plates With Damping Patches," *Journal of Sound and Vibration*, Vol. 216, No. 1, 1998, pp. 1 – 28.

[99] Cupial, P. and Niziol, J., "Vibration and damping analysis of a three-layered composite plate with a viscoelastic mid-layer," *Journal of Sound and Vibration*, Vol. 183, No. 1, 1995, pp. 99 – 114.

Appendix A

First Eigenvalue of a Homogeneous Cantilever Beam with End Viscous Damper

A homogeneous aluminum beam as shown in Fig. A.1 was considered with length= 1m and width=height= 0.01m. The value of C was increased from $1.00E{-}05$ to 7 N.s/m. The real and the imaginary part of the first eigenvalue is shown in Fig. A.2. As the value of C is increased, the imaginary part which is the damped natural frequency gradually goes to zero, and the real part grows. In order to investigate this more, we considered an equivalent SDOF model of the cantilever beam with end viscous damper, as shown in Fig. A.1 on right. The equivalent stiffness and mass considered are given below. It was noticed that the imaginary part goes to zero as soon as the value of C approaches the critical value of 6.735.

$$\begin{aligned} Equivalent\ \ stiffness: &\quad K_{eq} = 3EI/L^3, \\ Equivalent\ \ mass: &\quad m_{eq} = 0.2357m, \\ Critical\ \ damping: &\quad C_c = 2\sqrt{m_{eq}K_{eq}}. \end{aligned}$$

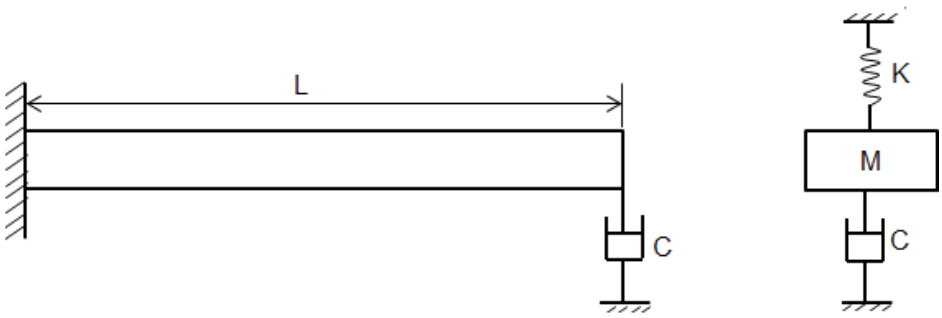

Figure A.1: Schematic of a Homogeneous Cantilever Beam with End Viscous Damper and its Equivalent SDOF Model

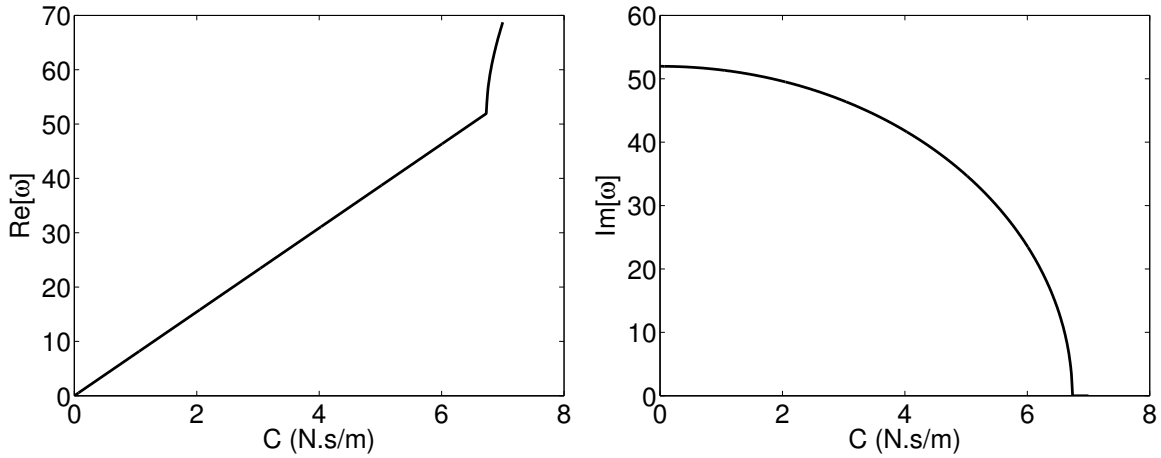

(a) Real Part (b) Imaginary Part

Figure A.2: The Real and Imaginary Parts of the First Eigenvalue